



**UNIVERSIDADE FEDERAL DO PARÁ
INSTITUTO DE GEOCIÊNCIAS
PROGRAMA DE PÓS-GRADUAÇÃO EM GEOLOGIA E GEOQUÍMICA**

DISSERTAÇÃO DE MESTRADO N° 501

**GRANITOIDES COLISIONAIS MESOARQUEANOS DE
OURILÂNDIA DO NORTE (PA): GEOLOGIA,
MICROESTRUTURAL, AFINIDADES PETROLÓGICAS E
IMPLICAÇÕES TECTÔNICAS PARA A PROVÍNCIA CARAJÁS**

Dissertação apresentada por:

LUCIANO RIBEIRO DA SILVA

Orientador: Prof. Dr. Davis Carvalho de Oliveira (UFPA)

**BELÉM
2017**

Dados Internacionais de Catalogação de Publicação (CIP)
Biblioteca do Instituto de Geociências/SIBI/UFPA

Silva, Luciano Ribeiro da, 1991-
Granitoides colisionais mesoarqueanos de Ourilândia do Norte (PA): geologia, microestrutural, afinidades petrológicas e implicações tectônicas para a Província Carajás / Luciano Ribeiro da Silva. – 2017.

xv, 72 f. : il. ; 30 cm

Inclui bibliografias

Orientador: Davis Carvalho de Oliveira

Dissertação (Mestrado) – Universidade Federal do Pará, Instituto de Geociências, Programa de Pós-Graduação em Geologia e Geoquímica, Belém, 2017.

1. Granito – Ourilândia do Norte (PA). 2. Petrologia – Ourilândia do Norte (PA). 3. Geoquímica – Ourilândia do Norte (PA). I. Título.

CDD 22. ed. 553.52098115



**Universidade Federal do Pará
Instituto de Geociências
Programa de Pós-Graduação em Geologia e Geoquímica**

**GRANITOIDES COLISIONAIS MESOARQUEANOS DE
OURILÂNDIA DO NORTE (PA): GEOLOGIA,
MICROESTRUTURAL, AFINIDADES PETROLÓGICAS E
IMPLICAÇÕES TECTÔNICAS PARA A PROVÍNCIA CARAJÁS**

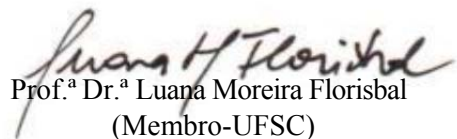
**DISSERTAÇÃO APRESENTADA POR
LUCIANO RIBEIRO DA SILVA**

**Como requisito parcial à obtenção do Grau de Mestre em Ciências na Área de
GEOQUÍMICA E PETROLOGIA.**

Data de Aprovação: 17/ 06 / 2017

Banca Examinadora:


Prof. Dr. Davis Carvalho de Oliveira
(Orientador-UFPA)


Prof. Dr.ª Luana Moreira Florisbal
(Membro-UFSC)


Prof. Dr. José de Arimatéia Costa de Almeida
(Membro-UNIFESSPA)

À família, senseis e amigos.

AGRADECIMENTOS

O autor expressa seus sinceros e profundos agradecimentos a todas as pessoas e entidades que contribuíram para a realização deste trabalho e em especial:

- Ao Programa de Pós-Graduação de Geologia e Geoquímica da Universidade Federal do Pará (UFPA) pelo fornecimento de infraestrutura;
- A Capes pela concessão da bolsa de mestrado;
- Aos convênios VALE-FAPESPA (Edital 01/2010 - ICAFF 053/2011) e INCT/GEOCIAM (Proc. 573733 / 2008-2) pelo suporte financeiro;
- Aos membros do Grupo de Pesquisa Petrologia de Granitoides (GPPG) do Instituto de Geociências da UFPA, pelo suporte técnico-científico durante as diversas fases deste trabalho, em especial a Maria Nattânia dos Santos, Fernando Fernandes, Pablo Leite, Bhrenno Marangoanha, Eleison Garbriel, Jean Machado, Diwhemerson Sousa, Marcela Santos e Rodrigo Santos pelos inúmeros momentos de reflexão e auxílio nas etapas de campo;
- Aos funcionários Cleida e Joelma Lobo da UFPA;
- À minha família, em especial ao meu irmão Brendo Ribeiro e aos meus pais pelas diversas formas de incentivo e companherismo ao longo da confecção deste trabalho;
- À minha namorada Letícia do Carmo pelo apoio nas últimas etapas deste trabalho;
- Aos amigos Rômulo Rosa, José Arimateia Correia, Maicon Silva, Yuri Rafael e Emanuel Aguiar pela ajuda, incentivo e momentos de descontração;
- Por fim, ao professor Davis Carvalho de Oliveira pela oportunidade de realizar este trabalho, com tranquilidade, sob sua orientação e aos professores José de Arimateia, Cláudio Lamarão, Cândido Moura, Paulo Gorayeb, Sergio Valente e Renato Moraes pelo incentivo e ensinamento referente à petrologia e deformação de granitoides.

"O presente pertence a eles, mas o futuro pelo qual sempre trabalhei pertence a mim."

Nikola Tesla

RESUMO

Este estudo investiga a diversidade, origem e significado tectônico dos granitoides mesoarqueanos de Ourilândia do Norte, que ocorrem próximo ao limite entre os domínios Rio Maria e Carajás, no sudeste do Craton Amazônico. Trabalhos anteriores, realizados nesta região, identificaram sanukitoides (~2,87 Ga), (quartzo) dioritos de afinidade BADR (basalto-andesito-dacito-riolito) e leucogranitos indiferenciados. Monzogranitos de afinidade charnokítica seccionam tais unidades. Os novos dados de mapeamento geológico obtidos neste trabalho permitiram definir a natureza e aspectos estruturais dos leucogranitos até então indiferenciados. Assim, foi possível diferenciar três novos grupos de granitoides: (i) biotita monzogranitos (BMzG); (ii) epidoto-biotita granodioritos (EBGd); e (iii) granitoides porfiríticos (Grtp). Com base nestas informações, esta dissertação visa definir a classificação, natureza, processos de formação e aspectos de deformação dessas rochas, e discutir, a partir da integração desses dados com aqueles gerados em trabalhos anteriores, as relações entre plutonismo e deformação para formação e colocação dos granitoides mesoarqueanos de Ourilândia do Norte. Para tanto, foi utilizada uma abordagem integrada de dados de campo, petrografia, microestrutural e geoquímica. Os dados de petrografia mostram que todos os grupos identificados são subdivididos em duas fácies. Aquele de composição BMzG é diferenciado em uma fácie equigranular (BMzGe) e outra heterogranular (BMzGh) e o EBGd em epidoto-biotita granodiorito heterogranular (EBGdh) e titanita-epidoto-biotita granodiorito esparsamente porfirítico (TEBGdep). Esses granitoides compõem dois batólitos separados por uma faixa de sanukitoide e rochas de afinidade BADR. O batólito situado na porção central da área tem forma elipsoidal, com maior eixo orientado na direção ENE-WSW, e o outro, localizado na porção sudeste, é arciforme. Ambos são amplamente dominados por BMzG, com menor ocorrência de lentes de EBGd. O Grtp é individualizado em biotita-hornblenda granodiorito porfirítico (BHGdp) e epidoto-biotita trondjemito porfirítico (EBTdp), e ocorre como corpos menores, espacialmente associados com as rochas de afinidade sanukitoide e BADR, respectivamente. As relações de *mingling* estabeleceram a contemporaneidade entre todos os granitoides de Ourilândia do Norte, incluindo os de assinatura sanukitoide e BADR. Em termos de geologia estrutural, esses plátanos foram afetados por deformação heterogênea. Suas porções centrais representam domínios de menor *strain*, onde mostram foliação magmática de direção principal ENE-WSW e mergulho subvertical, com fraca superposição de deformação em estado sólido. Por outro lado, as bordas desses plátanos são marcadas por zonas de cisalhamento de grande escala, onde foliações miloníticas são tipicamente desenvolvidas, com *trend* subparalelo às bordas e

mergulho subvertical. Os dados meso- e microestruturais indicam que as rochas estudadas são sin- a tardi-tectônicas e foram afetadas por deformação de alta temperatura ($> 500^{\circ}\text{C}$) e baixo esforço diferencial, em regime de transpressão sinistral, controlado predominantemente por cisalhamento puro, indicando que as tramas magmáticas e de estado sólido estão relacionadas a um mesmo evento deformacional. Geoquimicamente, com exceção do EBTdp que tem afinidade Mg-Na, os granitoides de Ourilândia do Norte podem ser agrupados em duas suítes: (i) suíte Fe-K que integra o grupo BMzG e a fácie TEBGdep; e (ii) suíte Mg-K composta por granitoides de afinidade sanukitoide (incluindo EBGdh e BHGdp) e (quartzo) dioritos de afinidade BADR. Ambos os grupos são cárquicos-alcalinos a alcalino-cárquicos e diferem entre si com base em suas relações FeO^t/MgO , Al_2O_3 , K_2O e alguns elementos traços (Sr, Ba, Rb). A origem do BMzGe é atribuída à anatexia de uma crosta TTG (2,92-2,98 Ga). O EBGdh tem afinidade sanukitoide e foi produzido por intenso fracionamento de hornblenda \pm clinopiroxênio. Os granitoides de fácie TEBGdep, BMzGh, BHGdp e EBTdp mostram evidências de *mingling* entre magmas contrastantes, indicando que suas origens requerem interação entre magmas derivados do manto metassomatizado e da crosta. Dados geoquímicos e modelagem foram utilizados para identificar os diferentes processos relacionados à origem e formação destes granitoides: (i) o TEBGdep é enriquecido em HFSE (Ti, Zr e Y) e LILE (Ba e Sr) e foi admitido como produto da fusão parcial de uma fonte mantélica enriquecida, provavelmente em um ambiente de pós-subducção, com participação de magmas crustais; (ii) o BMzGh é gerado pela interação entre magmas de composição TEBGdep (60%) e eBMzG (40%); (iii) o BHGdp é formado pela hibridização entre magmas sanukitoide (80%) e leucomonzogranítico (20%); e (iv) o EBTdp é originado por uma mistura incompleta entre líquido trondjemítico de assinatura TTG (70-80%) e magma de afinidade BADR (20-30%). Portanto, podemos concluir que em $\sim 2,87$ Ga ocorreu um significativo crescimento e retrabalhamento crustal, nas fases finais de estabilização do primeiro ciclo geotectônico registrado na Província Carajás. Isto nos leva a sugerir que todos os granitoides mesoarqueanos de Ourilândia do Norte foram alojados durante a segunda etapa de um modelo tectono-magmático de dois estágios (subducção-colisão): (i) primeiro estágio (2,98-2,92 Ga) - subducção de baixo ângulo com colocação de *slab-melt* e consequente metassomatismo da cunha mantélica; (ii) segundo estágio ($\sim 2,87$ Ga) – ambiente colisional, onde zonas de cisalhamento condicionaram a ascensão e colocação dos magmas, atuando como condutos pré-existentes para o transporte e interação entre magmas mantélicos e crustais.

Palavras-chave: Geoquímica. Microestrutural. Granitoides. Arqueano. Província Carajás.

ABSTRACT

This study investigates the diversity, origin and tectonic significance of the Mesoarchean granitoids of Ourilândia do Norte, emplaced near Rio Maria-Canãä dos Carajás domains boundary, southeastern Amazonian Craton (Brazil). Previous work, done in this region, has identified granitoids of sanukitoid affinity (~ 2.87 Ga), (quartz) diorites of BADR (basalt, andesite, dacite, rhyolite) affinity and undifferentiated leucogranites. In addition there are monzogranites with clinopyroxene, cross-cutting the Mesoarchean granitoids. In this study, new geological mapping data allowed to define the nature and structural aspects of the leucogranites undifferentiated. These data allowed to differentiate three new groups of granitoids, classified as: (i) biotite monzogranites (BMzG); (ii) epitote-biotite granodiorites (EBGd); and (iii) porphyritic granitoids (pGrt). In this respect, this dissertation aims to define the classification, nature, formation processes and deformation aspects of these rocks, and discuss, from the integration of these data with those generated in previous works, the relations between plutonism and deformation for the formation of the Ourilandia do Norte granitoids. For this was used an integrated approach of field, petrography, microstructural and geochemistry data. The petrography data show that the first two groups (BMzG and EBGd) are both subdivided into two facies. The BMzG is differentiated into equigranular (eBMzG) and heterogranular (hBMzG) facies and the EBGd into heterogranular epitope-biotite granodiorite (hEBGd) and sparsely porphyritic titanite-epitote-biotite granodiorites (spTEBGd). These granitoids constitute two batholiths separated by a rock strip of sanukitoid and BADR affinity. The main batholith has an ellipsoidal shape, with the largest axis oriented in the ENE-WSW direction, and other is arc-shape. Both are largely dominated by BMzG rocks, with less occurrence of EBGd lenses. The pGrt is individualized in porphyritic biotite-hornblende granodiorite (pBHGd) and porphyritic epidote-biotite trondhjemite (pEBTd), and occurs as smaller bodies, spatially associated with rocks of sanukitoid and BADR affinities, respectively. The mingling relationships established the contemporaneity between all the Ourilândia do Norte granitoids, including those of sanukitoid and BADR signatures. In terms of structural geology, these plutons were affected by heterogeneous deformation. Their central portions represent lower strain domains, where occurs magmatic foliation of ENE-WSW main direction and subvertical dip, with weak superimposition of solid-state deformation. On the other hand, the borders of these plutons are marked by large-scale shear zones, where milonitic foliations are typically developed, with subparallel trend to the batholith border and subvertical dip. The meso- and microstructural data indicate that the rocks studied are syn- to late-tectonic and were affected by high temperature deformation (> 500 °C) and low

differential stress, in a sinistral transpression regime, predominantly controlled by pure shear, indicating that the magmatic and solid-state fabrics are related to the same deformational event. Geochemically, except the EBTdp facies that has Mg-Na affinity, the Ourilândia do Norte granitoids can be grouped into two suites: (i) Fe-K suite that integrates the BMzG group and the spTEBGd facies; and (ii) Mg-K suite composed of granitoids (including EBGdh and BHGdp) and (quartz) diorites of sanukitoid and BADR affinities, respectively. Both groups are alkali-calcic to calc-alkaline and they differ on the basis of their FeO^t/MgO ratios, Al_2O_3 , K_2O and some trace elements (Sr, Ba, Rb). The origin of the eBMzG is attributed anatexis a 2.92-2.98 Ga old TTG crust. The hEBGd has sanukitoid affinity and could have been produced by intense fractionation of hornblende \pm clinopyroxene. The granitoids of spTEBGd, hBMzG, pBHGd and pEBTd facies show evidence of mingling between contrasting magmas, indicating that their origins require interaction between metassomatized mantle- and crustal derived magmas. Geochemical data and modeling were used to identify the different processes related to the origin and formation of these granitoids: (i) spTEBGd is enriched in HFSE (Ti, Zr and Y) and LILE (Ba and Sr) and was admitted as product of the partial melting of an enriched mantle source, with participation of crustal liquids, probably in a post-subduction setting; (ii) hBMzG is generated by the interaction between magmas of spTEBGd (60%) and eBMzG (40%) composition; (iii) pBHGd is formed by the hybridization between sanukitoid (80%) and leucomonzogranitic (20 %) magmas; and (iv) pEBTd is formed by an incomplete mixture between TTG signature trondhjemite liquid (70-80%) and magma of BARD affinity (20-30%). Therefore, we can conclude that in ~2.87 Ga a significant crustal growth and reworking occurred in the final stages of stabilization of the first geotectonic cycle of Carajás province. This leads us to suggest that all the Ourilândia do Norte Mesoarchean granitoids were emplacement during the second stage of a tectono-magmatic two-stage (subduction-collision) model: (i) first stage (2.98-2.92 Ga) - low-angle subduction with emplacement of slab-melt and consequent mantle wedge metasomatism; (ii) second stage (~ 2.87 Ga) - emplacement of the granitoids studied in a collisional environment, where shear zones conditioned the rise and emplacement of magmas, acting as deep-reaching discontinuities and important conduit for transport and interaction between mantle- and crustal-derived magmas.

Keywords: Geochemistry. Microstructural. Granitoids. Archean. Carajás Province.

LISTA DE ILUSTRAÇÕES

1 INTRODUÇÃO

Figura 1 - Localização e acesso da área de Ourilândia do Norte	2
Figura 2 - Localização da Província Carajás no Cráton Amazônico, compartimentação tectônica da Província Carajás e mapa geológico regional desta com a localização da área de estudo	5
Figura 3 - Mapa de amostragem do mapeamento geológico da área de Ourilândia do Norte.	11

2 DIVERSITY, ORIGIN AND TECTONIC SIGNIFICANCE OF THE MESOARCHEAN GRANITOIDS OF OURILÂNDIA DO NORTE, CARAJÁS PROVINCE (BRAZIL)

Figure 1 - (a) Geochronological provinces of the Amazonian Craton and geological map of the Carajás Province.....	18
Figure 2 - Ourilândia do Norte geological map.	20
Box 1- Synthesis of the field aspects of the Ourilândia do Norte granitoids	21
Figure 3 - General aspects.....	22
Figure 4 - Field relationship.....	23
Figure 5 - Deformation aspects.....	24
Figure 6 - Q-(A+P)-M' and Q-A-P plots.....	27
Box 2 - Mineralogy and microstructural typology of the Ourilândia do Norte granitoids Figure 7 - Microstructural aspects of the granitoids, located in lower strain domains, central portions of the batholiths under study.....	28 29
Figure 8 - Deformation, recovery and recrystallization microstructures of the granitoids studied.....	31
Figure 9 - Tardi- to post-magmatic transformation microstructures.....	32
Figure 10 – Major and minor elements Harker diagrams.....	36
Figure 11 - Trace elements Harker diagrams	37
Figure 12 - Geochemical classification and magmatic series plots	39
Figure 13 - Chondrite-normalized REE patterns and primordial mantle-normalized spider diagrams.....	40
Figure 14 - Petrogenetic aspects and magmatic evolution.....	43

Figure 15 - Binary mixing model for Ourilandia do Norte hybrid granitoids in Chondrite-normalized REE and primordial mantle-normalized multi-elements diagrams	45
Figure 16 - Schematic diagram showing the relation between temperature of deformation and dynamic recrystallization regimes in quartz, feldspars, biotite and amphibole during D1 event.....	47
Figure 17 - Discriminant diagram of tectonic setting.	50
Figure 18 - Flowchart summarizing a two-stage tectono-magmatic model for the origin of the Ourilândia do Norte Mesoarchean Mg-K and Fe-K granitoids	52

LISTA DE TABELAS**2 DIVERSITY, ORIGIN AND TECTONIC SIGINIFICANCE OF THE MESOARCHEAN GRANITOIDS OF OURILÂNDIA DO NORTE, CARAJÁS PROVINCE (BRAZIL)**

Table 1 - Modal compositions of the granitoids of the Ourilândia do Norte area	26
Table 2 - Chemical composition of the Ourilândia do Norte granodiorites-granites	34

SUMÁRIO DEDICATÓRIA	
AGRADECIMENTOS	v
EPÍGRAFE.....	vi
RESUMO.....	vii
ABSTRACT.....	iix
LISTA DE ILUSTRAÇÕES	xi
LISTA DE TABELAS	xiii
CAPÍTULO 1 - INTRODUÇÃO	1
1.1 APRESENTAÇÃO	1
1.2 CONTEXTO GEOLÓGICO-GEOTECTÔNICO REGIONAL	4
1.3 APRESENTAÇÃO DO PROBLEMA	8
1.4 OBJETIVOS	9
1.5 MATERIAIS E MÉTODOS	10
1.5.1 Pesquisa bibliográfica	10
1.5.2 Mapeamento geológico e geologia estrutural.....	10
1.5.3 Petrografia e microestrutural	12
1.5.4 Geoquímica.....	13
CAPÍTULO 2 - DIVERSITY, ORIGIN AND TECTONIC SIGNIFICANCE OF THE MESOARCHEAN GRANITIDS OF OURILÂNDIA DO NORTE, CARAJÁS PROVINCE (BRAZIL).....	15
1 INTRODUCTION	16
2 REGIONAL GEOLOGY	17
3 GEOLOGY AND STRUCTURAL FRAMEWORK.....	19
4 PETROGRAPHY	25
4.1 MODAL COMPOSITION AND CLASSIFICATION	25
4.2 MINERALOGY, MICROSTRUCTURAL ASPECTS AND INTRACRISTALLINE DEFORMATION MECHANISMS	27
5 GEOCHEMISTRY	33
5.1 MAJOR AND TRACE ELEMENTS	33
5.2 CLASSIFICATION AND MAGMATIC SERIES	38
5.3 RARE EARTH AND MULTI-ELEMENTS PATTERNS	41
6 DISCUSSION	41
6.1 PETROGENESIS AND MAGMATIC EVOLUTION	41

6.1.1 Biotite monzogranite	42
6.1.2 Titanite-rich biotite granodiorite	42
6.1.3 Biotite granodiorite and porphyritic granitoids	44
6.2 MICROSTRUCTURAL CONSIDERATIONS.....	46
6.2.1 Deformation temperature	46
6.2.2 Tardi- to post-magmatic transformations	48
6.3 ASCENT AND EMPLACEMENT MECHANISMS AND TECTONIC SIGNIFICANCE	49
7 CONCLUSIONS	53
ACKNOWLEDGEMENTS	54
REFERENCES	54
APPENDIX A. ANALYTICAL PROCEDURES	54
CAPÍTULO 3 - CONSIDERAÇÕES FINAIS	61
REFERÊNCIAS	65

CAPÍTULO 1 - INTRODUÇÃO

1.1 APRESENTAÇÃO

A região de Ourilândia do Norte (Fig. 1) está localizada na parte sudeste do Estado do Pará, porção centro-oeste da Província Carajás (Santos 2003, Vasquez *et al.* 2008). Esta província é considerada o maior núcleo arqueano preservado do Cráton Amazônico (Almeida *et al.* 1981) e tem sido alvo de diversos estudos em função do seu amplo potencial metalogenético. Nas últimas décadas, pesquisadores do Grupo de Pesquisa Petrologia de Granitoides (GPPG), em cooperação com aqueles do Laboratório de Geologia Isotópica (PARA-ISO), ambos vinculados ao Programa de Pós-graduação de Geologia e Geoquímica (PPGG) do Instituto de Geociências (IG) da Universidade Federal do Pará (UFPA), vem desenvolvendo diversos estudos de cunho petrológico e geocronológico nas rochas do embasamento da província, sobretudo naquelas que ocorrem nas porções central do Domínio Rio Maria, principalmente nas áreas de Rio Maria, Xinguara, Marajoara e a leste de Bannach (Macambira & Lafon 1995, Macambira & Lancelot 1996; Althoff *et al.* 2000, Oliveira *et al.* 2009, Almeida *et al.* 2011, 2013) e centro-leste do Domínio Carajás, que abrange as áreas de Canaã dos Carajás (Feio & Dall'Agnol 2012, Feio *et al.* 2012, 2013), Sapucaia (Santos *et al.* 2013b, Teixeira *et al.* 2013) e Água Azul do Norte (Rodrigues *et al.* 2014, Gabriel & Oliveira 2014, Leite-Santos & Oliveira 2014, 2016). No entanto, diversas áreas desta província ainda permanecem pobemente caracterizadas e inseridas no contexto geológico do Complexo Xingu (Silva *et al.* 1974).

Nesse contexto, estudos de mapeamento geológico realizados recentemente pelo GPPG na área de Ourilândia do Norte permitiram um significativo avanço no conhecimento sobre as associações magmáticas que ali ocorrem (Santos *et al.* 2013a, Santos & Oliveira 2016; este trabalho). Santos & Oliveira (2016) mostraram que esta área é marcada por uma ampla ocorrência de granitoides de afinidade sanukitoide, dioritos e quartzo dioritos de afinidade BADR (basalto-andesito-dacito-riolito) e diversos tipos de granitos até então indiferenciados, todos com um padrão deformacional distinto daquele identificado nas demais áreas do Domínio Rio Maria. Além disso esses autores ainda apontaram que todas essas litologias são cortadas por monzogranitos com clinopiroxênio. Na presente pesquisa, novos dados de mapeamento geológico da área de Ourilândia do Norte aliados a estudos petrográficos e geoquímicos, permitiram distinguir pelo menos mais três grupos de granitoides, a saber: (i) biotita monzogranitos; (ii) epidoto-biotita granodioritos; e (iii) granitoides porfiríticos.

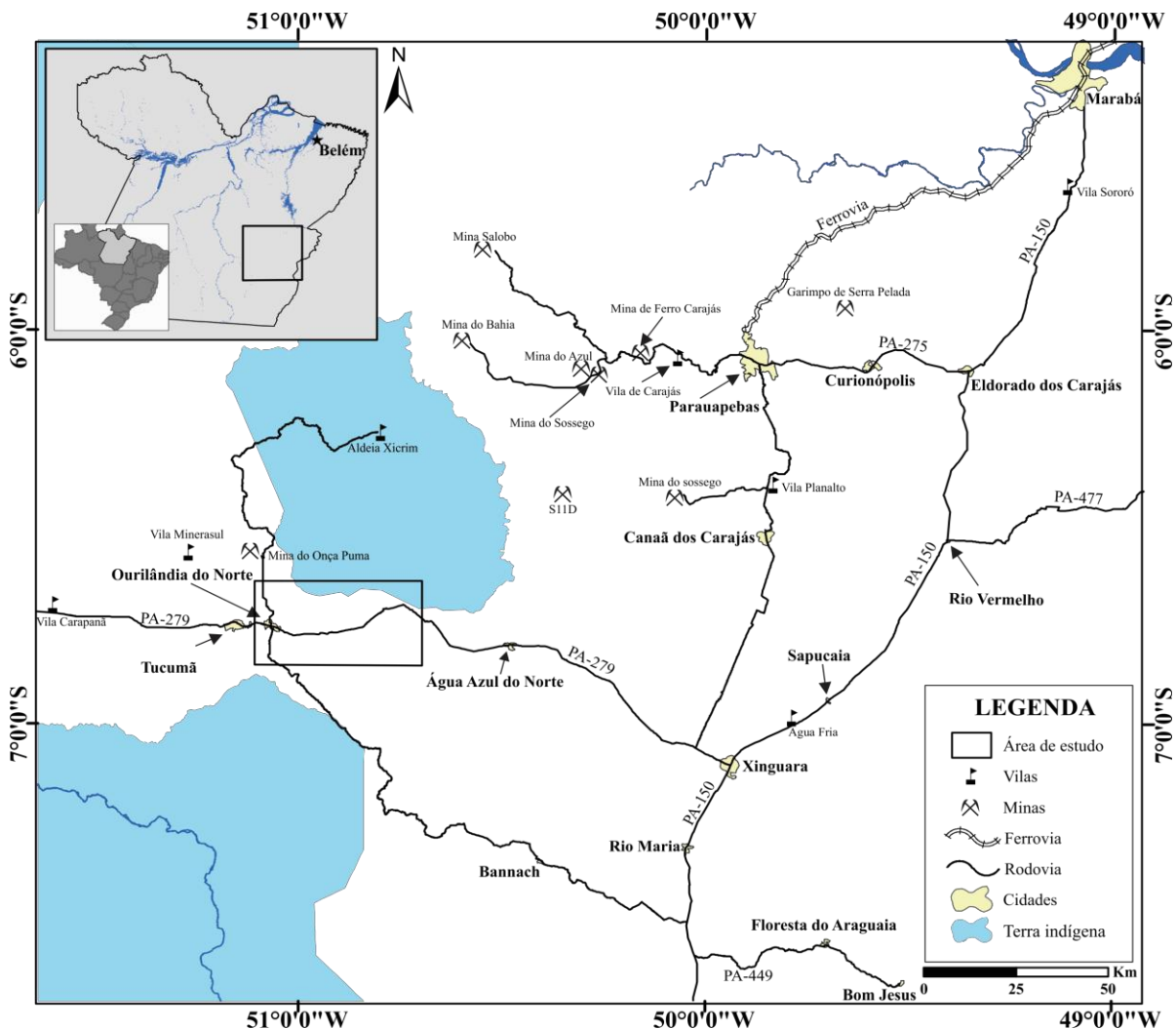


Figura 1 - Localização e acesso da área de Ourilândia do Norte.

Levando-se em consideração de que a área proposta para o desenvolvimento desta dissertação está localizada no limite entre dois domínios tectônicos - Rio Maria e Carajás, a caracterização de sua geologia e da natureza e aspectos deformacionais dos granitoides ali identificados, permitiram um avanço significativo na compreensão dos processos que levaram à formação e estabilização da crosta arqueana dessa região, e que poderão contribuir para um melhor entendimento sobre a zona de interferência entre tais domínios. Para isso, foi necessária a integração das informações obtidas neste estudo com aquelas geradas pelo desenvolvimento da dissertação de Maria Nattânia Sampaio dos Santos (Santos & Oliveira 2016). Tais atividades fazem parte da linha de pesquisa Petrologia e Evolução Crustal desenvolvida pelo GPPG/PPGG e estão vinculadas às metas e objetivos propostos pelos convênios VALE-FAPESPA (Edital 01/2010 - ICAFF 053/2011) e INCT/GEOCIAM (Proc. 573733 / 2008-2).

Os dados obtidos durante o desenvolvimento desta dissertação são apresentados na forma de um artigo científico, sendo que a mesma compreende um capítulo introdutório (Capítulo 1), que aborda os pontos relacionados à localização da área de estudo, o contexto geológico-geotectônico regional da Província Carajás, assim como a apresentação do problema, dos objetivos gerais e específicos e dos materiais e métodos utilizados na pesquisa. O Capítulo 2 (artigo científico) compreende os principais resultados obtidos, onde são apresentados os aspectos geológicos, petrográficos, microestruturais e geoquímicos dos granitoides de Ourilândia do Norte, assim como uma discussão sobre suas afinidades petrológicas e as relações entre plutonismo e deformação – “DIVERSITY, ORIGIN AND TECTONIC SIGNIFICANCE OF THE MESOARCHEAN GRANITOIDS OF OURILÂNDIA DO NORTE, CARAJÁS PROVINCE (BRAZIL)”. Este artigo deverá ser submetido para publicação ao periódico *Journal of South American Earth Sciences* ou outro de classificação similar (Qualis/CAPES). No terceiro e último capítulo, é apresentada uma descrição conjunta dos principais aspectos conclusivos abordados no artigo mencionado acima, buscando-se com isso, fornecer uma visão integrada dos principais resultados e contribuições para a evolução do conhecimento geológico na área de Ourilândia do Norte.

1.2 CONTEXTO GEOLÓGICO-GEOTECTÔNICO REGIONAL

A Província Carajás (Fig. 2), está situada na porção sudeste do Estado do Pará e representa o principal núcleo arqueano preservado do Cráton Amazônico (Almeida *et al.* 1981). Ela é considerada como uma província geocronológica independente por Santos (2003) ou como parte integrante da Província Amazônia Central (Tassinari & Macambira 2004), a qual é subdividida em dois domínios denominados de blocos Carajás e Xingu-Iricoumé (Fig. 2a). Em decorrência de seu enorme potencial metalogenético, a Província Carajás tem sido alvo de diversos estudos geológicos ao longo das últimas décadas, o que resultou na individualização de diversos granitoides a partir do que era considerado como domínio de ocorrência das rochas do Complexo Xingu (Silva *et al.* 1974). Tais pesquisas aliadas a estudos geofísicos e estruturais permitiram que surgissem propostas de sua compartimentação em segmentos crustais tectonicamente distintos (Costa *et al.* 1995, Souza *et al.* 1996, Althoff *et al.* 2000; Dall'Agnol *et al.* 2006, 2013). Inicialmente, Souza *et al.* (1996) subdividiram esta província em Terreno Granito *Greenstone* de Rio Maria (TGGRM), a sul, e a Bacia Carajás (BC), a norte. O primeiro compreenderia as rochas mais antigas e de características ígneas bem preservadas, enquanto que a porção norte manteria um embasamento mesoarqueano, afetado por eventos tectonotermiais de idade neoarqueana, representado por uma vasta sequência vulcanossedimentar e intrusões granitoides. Posteriormente, Vasquez *et al.* (2008) em revisão à geologia do Estado do Pará e seguindo a proposta de Santos (2003), subdividiram a província em dois domínios tectônicos distintos: (i) **Domínio Rio Maria (DRM)**, de idade mesoarqueana, composto por *greenstone belts* do Supergrupo Andorinhas (3,0 e 2,9 Ga) e por granitoides tipo TTG e cárlico-alcalinos alto-K (suítes Xinguara, Guarantã e Rio Maria), colocados entre 2,98 e 2,86 Ga (Oliveira *et al.* 2009, Almeida *et al.* 2011, 2013); e (ii) Domínio Carajás (DC), composto pelos *greenstones belts* de idade neoarqueana que compõem a Bacia Carajás (~2,76 Ga), por rochas indiferenciadas do Complexo Xingu (2,97 – 2,86 Ga) e por granitoides diversos de idade meso- a neoarqueana (3,0 – 2,73 Ga; Feio & Dall'Agnol 2012, Feio *et al.* 2012).

Trabalhos realizados de mapeamento geológico em escala de semi-detalhe por pesquisadores do Grupo de Pesquisa Petrologia de Granitoides (GPPG-UFPA) na porção norte da Província Carajás, mostraram que a área considerada como embasamento da Bacia Carajás, que se estenderia desde a sua borda sul até o limite com o TGGRM, não corresponderia a uma crosta arqueana tectonicamente homogênea, o que levou à adoção das denominações Subomínio Canaã dos Carajás (SCC) e Subomínio Sapucaia (SS) para as

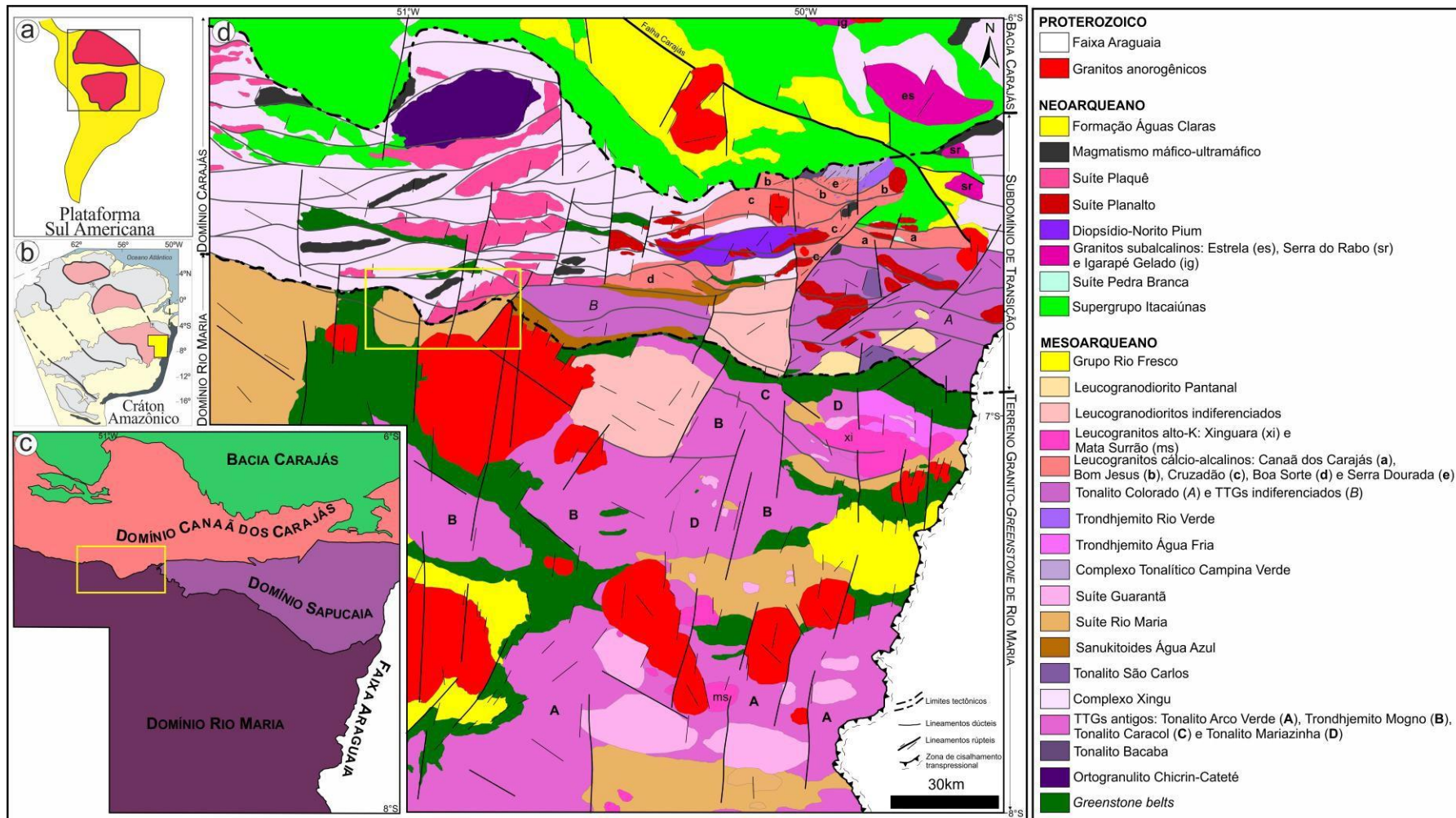


Figura 2 - (a) Localização do Cráton Amazônico na Plataforma Sul Americana (Almeida *et al.* 1981); (b) Localização da Província Carajás no Cráton Amazônico (Tassinari & Macambira 2004); (c) Compartimentação tectônica da Província Carajás segundo Dall'Agnol *et al.* (2013), com a localização da área sob estudo; e (d) mapa geológico regional da Província Carajás (modificado de Oliveira *et al.* 2014) com a localização da área de estudo. Na parte esquerda é mostrado a proposta de compartimentação tectônica de acordo com Vasquez *et al.* (2008) e a direita a proposta de Feio & Dall'Agnol (2012).

porções norte e sul deste segmento crustal da província, respectivamente (Fig. 2c; Dall'Agnol *et al.* 2013). O SCC é caracterizado pela predominância de granitos *stricto sensu* e associações charnockíticas (Suíte Planalto e Diopsídio-Norito Pium), com raras ocorrências de TTG e granitos anorogênicos, enquanto que o SS seria formado por granitoides TTG, sanukitoides e leucogranitos diversos, análogos àqueles identificados no Domínio Rio Maria, sendo, porém, afetados por eventos neoarqueanos.

O **Domínio Rio Maria**, ao sul, é essencialmente Mesoarqueano, e caracterizado por associações *greenstone belt* do Supergrupo Andorinhas de 3,0 a 2,9 Ga (Macambira & Lancelot 1991, Pimentel & Machado 1994, Avelar 1996, Souza *et al.* 2001, Rolando & Macambira 2003, Lafon *et al.* 2000), o qual inclui o Grupo Tucumã (Araújo & Maia 1991). Os granitoides englobam: (a) ***rochas TTG*** de 2,98-2,92 Ga, representados pelo Tonalito Arco Verde, Trondhjemito Mogno e Tonalito Mariazinha (Macambira & Lafon 1995, Rolando & Macambira 2003, Almeida *et al.* 2008, 2011); (b) ***Sanukitoide*** Rio Maria de 2,87 Ga e rochas associadas (Medeiros & Dall'Agnol 1988, Oliveira *et al.* 2009, Santos *et al.* 2013a, Santos & Oliveira 2016); (c) ***leucogranodioritos-granitos de alto Ba-Sr*** representados pelos plútôns Guarantã, Trairão e Azulona, os quais foram agrupados na Suíte Guarantã de 2,87 a 2,86 Ga por Almeida *et al.* (2010); (d) ***leucogranitos potássicos de afinidade cálcio-alcalina***, caracterizados pelo Granito Mata Surrão e afins e datados em 2,87 Ga (Lafon *et al.* 1994, Almeida *et al.* 2013). Tais rochas foram recobertas pelas rochas sedimentares clásticas, transgressivas, do Grupo Rio Fresco (Docegeo 1988). Já no Paleoproterozóico, este terreno foi intrudido por granitos Tipo-A de 1,88 Ga da Suíte Jamon (Dall'Agnol *et al.* 2005, Dall'Agnol & Oliveira 2007). Diques associados a este magmatismo também são frequentes (Rivalenti *et al.* 1998, Silva Jr. 1999, Silva *et al.* 2016).

O **Subdomínio Canaã dos Carajás**, de idade meso- a neoarqueana (3,0-2,73 Ga), é caracterizado pela predominância de granitos cálcico-alcalinos de alto-K e provavelmente representa o embasamento da Bacia Carajás. É formado pelo Ortogranulito Chicrim-Cateté (3,0 Ga), pelas rochas do Complexo Xingu (2,97-2,86 Ga), pelo Diopsídio-Norito Pium (2,74 Ga) e por seis grupos de granitoides, listados a seguir: (i) tonalitos com anfibólito representado pelo Tonalito Bacaba (3,0 Ga) e pelo Complexo Tonalítico Campina Verde (2,87-2,85 Ga); (ii) associação TTG, com baixa expressividade areal, composta pelo Trondhjemito Rio Verde (2,93 Ga); (iii) Granito Canaã dos Carajás cálcico-alcalino de alto-K e com afinidade sódica, datados entre 2,95-2,93 Ga; (iv) granitos cálcico-alcalinos de alto-K, com grande expressividade areal nas áreas geologicamente mais conhecidas do SCC, formados pelos granitos Bom Jesus (sem idade definida), Cruzadão (2,86-2,85 Ga), Serra Dourada (2,85-2,83

Ga) e Boa Sorte (2,86 Ga); (v) Suíte Pedra Branca de idade 2,75; e (vi) Suíte Planalto e rochas charnockíticas associadas, de idade 2,73 Ga (Feio *et al.* 2012, Feio & Dall'Agnol 2012, Feio *et al.* 2013, Santos *et al.* 2013c, Rodrigues *et al.* 2014).

O **Subdomínio Sapucaia**, também de idade meso- e neoarqueana, é dominado por associações TTG similar ao Domínio Rio Maria, mas as rochas mesoarqueanas que o constituem foram intensamente deformadas e seccionadas por granitoides das suítes Vila Jussara e Planalto. Nesse sentido, no SS temos: (i) associações TTG representadas pelo Trondhjemito Colorado (2,87 Ga) e Trondhjemito Água Fria (2,86 Ga); (ii) tonalito com anfibólio composto pelo Tonalito São Carlos; (iii) granodioritos de alto-Mg formados pelos granodioritos Água Ázul e Água Limpa, colocados em 2,87 Ga; (iv) granitos cálcico-alcalinos alto Ba-Sr representados pelos leucogranodioritos Pantanal e Nova Canadá; e (v) granitos cálcico-alcalinos alto-K representados pelos leucogranitos Xinguara e Velha Canadá (Santos *et al.* 2013b, Teixeira *et al.* 2013, Silva *et al.* 2014, Gabriel & Oliveira 2014, Oliveira *et al.* 2014, Leite-Santos & Oliveira 2016).

No Paleoproterozóico (1,88 Ga), a Província foi intrudida por granitos Tipo-A das suítes Jamon (plútons Redenção, Musa, Jamon e Bannach), Serra dos Carajás (plútons Central e Rio Branco) e Velho Guilherme (maciços Central, Cigano, Pojuca e Rio Branco) - Dall'Agnol *et al.* (2005) e Dall'Agnol & Oliveira (2007), e diques associados (Rivalenti *et al.* 1998; Silva Jr. 1999; Silva *et al.* 2016).

1.3 APRESENTAÇÃO DO PROBLEMA

Nas últimas décadas a realização de diversas etapas de trabalho de campo, aliado aos estudos petrográficos, geoquímicos e geocronológicos, contribuíram para a individualização de várias unidades da Província Carajás, anteriormente associadas ao Complexo Xingu. Apesar do avanço do conhecimento científico nesta província, diversas áreas ainda são pobemente caracterizadas e permanecem inseridas neste complexo. Nesse contexto, pesquisas recentes realizadas pelo GPPG permitiram um significativo avanço no conhecimento das associações magmáticas e aspecto estrutural do embasamento arqueano da área de Ourilândia do Norte.

Santos & Oliveira (2016) definiram nessa região os granitoides de afinidade sanukitoide, dioritos e quartzo dioritos de afinidade BADR e granitos indiferenciados, além de apontar a ocorrência de monzogranitos com clinopiroxênio, cortando os demais granitoides. Nesta dissertação, o mapeamento geológico em escala de semi-detalhe (~1:50.000) realizado na área de Ourilândia do Norte permitiu distinguir pelo menos mais três grupos de granitoides arqueanos representados por biotita monzogranitos; epidoto-biotita granodioritos e granitoides porfiríticos. Assim, abaixo são listados alguns problemas que foram esclarecidos com o objetivo de propor um modelo de evolução tectono-magmática para a região de Ourilândia do Norte:

- i. Indefinição da posição estratigráfica dos granitoides identificados nesta dissertação com os demais granitoides da área;
- ii. Incerteza sobre classificação, afinidades petrológicas, origem, evolução magmática, aspectos estruturais e ambiente de formação dos granitoides estudados;
- iii. Indefinições dos mecanismo de ascensão e colocação e história de deformação das rochas de Ourilândia do Norte; e
- iv. Dúvida sobre o real significado desta área no contexto dos domínios Rio Maria e Carajás. Seria este uma possível extensão do Domínio Rio Maria afetado por eventos neoarqueanos (Subomínio Sapucaia) ou uma crosta retrabalhada com evolução geológica semelhante ao Subomínio Canaã dos Carajás?

1.4 OBJETIVOS

Este trabalho tem como objetivo geral definir a classificação, natureza, processos de formação e aspectos de deformação dos biotita monzogranitos, epidoto-biotita granodioritos e granitoides porfiríticos da área de Ourilândia do Norte, além de discutir, a partir da integração desses dados com aqueles de trabalhos anteriores, as relações entre plutonismo e tectonismo para origem, ascensão e colocação dos magmas geradores dessas rochas. Para isso, foram atingidos os seguintes objetivos específicos:

- Individualização e classificação petrográfica das rochas identificadas neste trabalho;
- Caracterização das microestruturas magmáticas e de deformação, transformações tardia pós-magmáticas e dos mecanismos de deformação intracristalina que afetaram essas rochas;
- Definição de tipologia, série magmática e ambiente de formação para os granitoides estudados;
- Comparação das rochas estudadas com granitoides de áreas adjacentes da Província Carajás, contribuindo para um melhor entendimento de suas afinidades petrológicas;
- Realização de modelagem geoquímica para auxiliar na discussão sobre petrogênese e evolução magmática dessas rochas;
- Estimativa da temperatura e intensidade do campo diferencial que atuaram durante o fim da deformação cristal-plástica que afetou essas rochas;
- Elaboração de mapa geológico em escala de semi-detalhe (~1:50.000) para a área de Ourilândia do Norte, a partir de dados de mapeamento geológico, fotointerpretação de imagens de radar, petrografia, microestrutural e geoquímica, visando uma melhor delimitação dos corpos e suas fácies, além de traçar as estruturas dúcteis e rúpteis de grande escala;
- Discussão sobre a evolução do nível de erosão e sobre o significado tectônico das estruturas dúcteis e rúpteis identificadas e fotointerpretadas na área.
- Caracterização do limite entre os domínios Rio Maria e Carajás (Vasquez *et al.* 2008) de acordo com os resultados obtidos.

1.5 MATERIAIS E MÉTODOS

1.5.1 Pesquisa bibliográfica

Consistiu do levantamento bibliográfico de livros, relatórios, artigos, dissertações e teses sobre a Província Carajás (Silva *et al.* 1974, Araújo & Maia 1991, Costa *et al.* 1995, Souza *et al.* 1996, Pinheiro & Holdsworth 1997, Althoff *et al.* 2000, Dall'Agnol *et al.* 2006, Vasquez *et al.* 2008, Docegeo 1988, Oliveira *et al.* 2009, 2010, 2011, Almeida *et al.* 2010, 2011, 2013, Feio & Dall'Agnol 2012, Feio *et al.* 2012, 2013, Ronaib & Oliveira 2013, Santos *et al.* 2013a, 2013b, 2013c, Dall'Agnol *et al.* 2013, Teixeira *et al.* 2013, Rodrigues *et al.* 2014, Silva *et al.* 2014, Gabriel & Oliveira 2014, Oliveira *et al.* 2014, Leite-Santos & Oliveira 2016, Teixeira 2015, Santos & Oliveira 2016, Santos 2017, Dall'Agnol 2017), complementado pela leitura de diversos artigos, com temas relacionados à geologia de terrenos arqueanos, voltados principalmente para a petrogênese, evolução magmática e ambiente geodinâmico (Condie 1993, Sylvester 1994, Matin 1994, Frost *et al.* 1998, Champion & Smithies 2001, 2003, Moyen *et al.* 2003a, Heilimo *et al.* 2010, Laurent *et al.* 2014a, 2014b). Adicionalmente, foram consultados atlas, livros e artigos visando aprofundar os conhecimentos do autor sobre geoquímica de rocha total (Ragland 1989, Rollinson 1993, Gill 2010), além do reconhecimento de fases primárias e secundárias (Mackenzie *et al.* 1982, Best 2003, Vernon 2004), meso- e microestrutural de granitoides e estilos de colocação de magmas (Hibbard 1987, Peterson *et al.* 1989, Blenkinsop 2000, Moyen *et al.* 2003b, Vernon 2004, Passchier & Trouw 2005, Trouw *et al.* 2010, Fossen 2012, Neves 2012, Florisbal 2012).

1.5.2 Mapeamento geológico e geologia estrutural

Primeiramente, foram integrados em ambiente SIG (Sistema de Informação Geográfica) um conjunto de mapas litogeofísicos, confeccionados a partir da fotointerpretação de imagens aeromagnetométricas e aerogamaespectrométricas, e de lineamentos extraídos a partir de Modelo Digital de Terreno (*Shuttle Radar Topography Mission - SRTM*), com resolução espacial interpolada para 15 m (banda C). Esses dados aliados aos estudos de campo, petrografia, microestrutural e geoquímica foram de fundamental importância para a confecção do mapa geológico da área de Ourilândia do Norte, em escala de semi-detalhe (~1:50.000). O mapeamento geológico dessa região foi realizado em três etapas durante os períodos de 18-26/10/2010, 18-27/10/2013, e 23-25/07/2014 (com participação do autor deste trabalho apenas nesta última etapa), somando um total de 197 pontos, que visaram a descrição

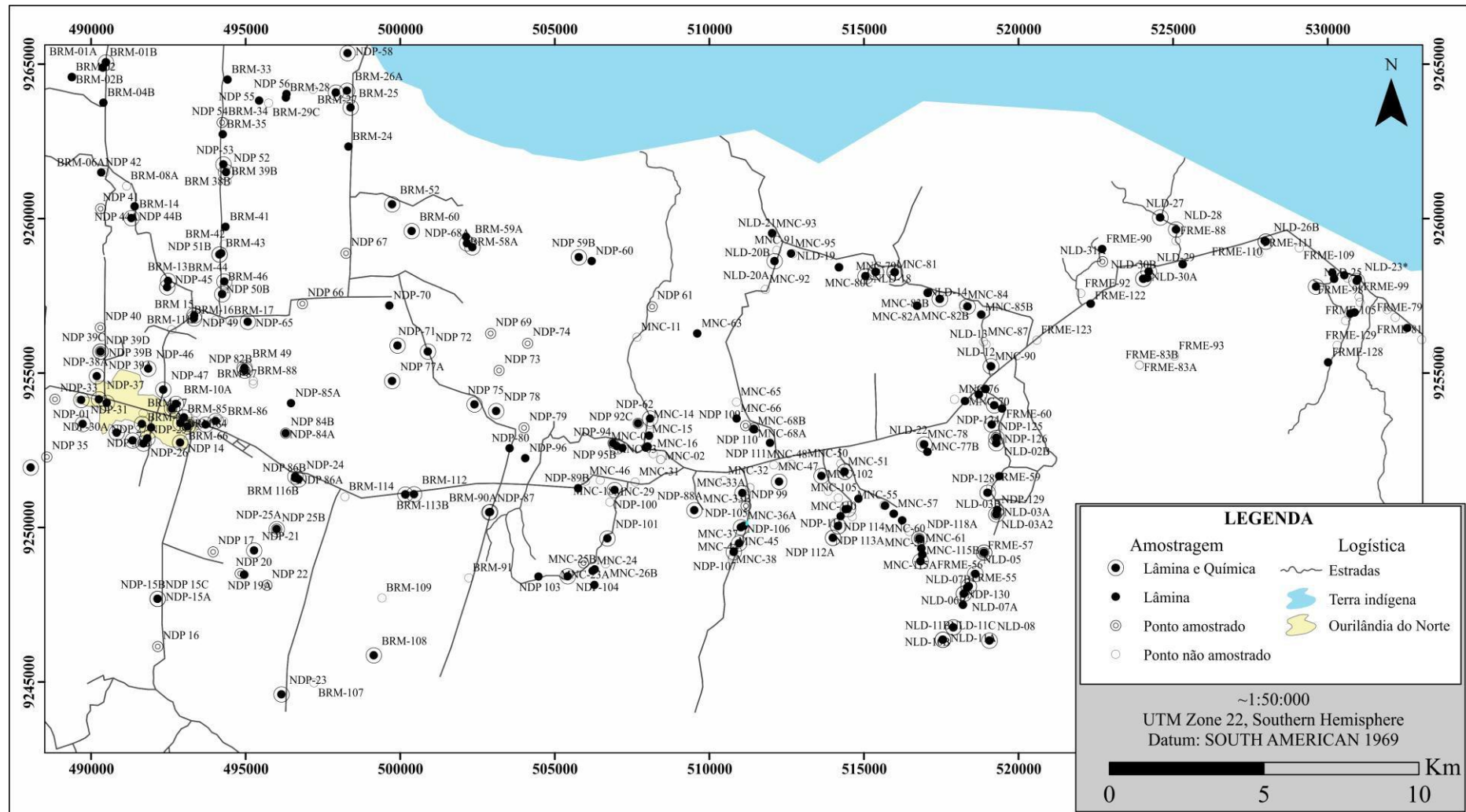


Figura 3 – Mapa de amostragem referente às três etapas de mapeamento geológico realizadas na área de Ourilândia do Norte.

de afloramentos e relevo, com destaque para os aspectos litológicos e estruturais, o que possibilitou diversas observações das relações de contato entre os granitoides estudados e suas rochas encaixantes. Durante o mapeamento, houve uma coleta sistemática de amostras de mão, réplica, lâmina e geoquímica, todas devidamente identificadas e etiquetadas, totalizando 293 amostras, das quais 85 compõem este trabalho (Fig. 3). Adicionalmente, foram mensurados os valores de susceptibilidade magnética das diversas litologias a partir de susceptibilímetro de modelo SM-30, fabricado pela *ZH Instruments*. Para a localização desses pontos foi utilizado um aparelho GPS (*Global Position System*) com precisão de ~3 m.

Em termos de geologia estrutural, vale a pena ressaltar que os dados de foliação não foram coletados com a devida discriminação dos tipos de foliação (magmática ou tectônica, ou ainda uma superposta pela outra), além disso, não foram coletadas amostras orientadas e os dados de lineação, quando observadas, não foram mensurados. Entretanto, mesmo diante dessa escassez de atitudes mesoestruturais, as análises de fotografias de campo e de imagens de radar, combinadas com os estudos microestruturais nos permitiram inferir a história deformacional dessas rochas. Nesse contexto, para uma melhor compreensão da evolução estrutural interpretada para esses granitoides, será necessário aprofundar os estudos de mapeamento estrutural e/ou confecção de painéis em afloramentos chaves, com o objetivo de melhorar a aquisição de atitudes estruturais, tanto planares quanto lineares, assim como realizar a coleta de amostras orientadas.

1.5.3 Petrografia e microestrutural

A princípio as amostras de mão foram descritas e agrupadas com base na composição mineralógica e nos aspectos texturais. Seguido da confecção de lâminas polidas ou delgadas na Oficina de Laminação do Instituto de Geociências da UFPA, com secções de corte aproximadamente perpendicular à foliação da rocha. Em escala microscópica, a descrição das lâminas permitiu um reagrupamento das amostras de mão de acordo com as proporções dos minerais essenciais e varietais, enquanto que a análise mineralógica quantitativa foi adquirida a partir da contagem modal de 2000 pontos, em 54 lâminas das diversas variedades de granitoides estudados, distribuídos numa malha de 0,4 mm de espaçamento em contador de pontos automático do software *Hardledge* (versão *Worsktation 1.3.6.1111; ENDEPER*) e utilizando os princípios de Chayes (1956) e Hutchison (1974). Durante a análise modal, os minerais secundários foram contabilizados como seus minerais primários formadores, visando reconstituir a mineralogia ígnea dessas rochas. Esses dados foram descritos em texto corrido e

plotados nos diagramas de classificação Q-A-P e Q-A+P-M (Streckeisen 1976, Le Maitre 2002), conforme estabelecido pela IUGS (*International Union of Geological Sciences*).

Em termos microestruturais, foi realizado um reconhecimento detalhado da mineralogia e das diversas microestruturas formadas tanto durante a cristalização magmática (Mackenzie *et al.* 1982, Blenkinsop 2000, Best 2003, Vernon 2004, Passchier & Trouw 2005), quanto durante a recristalização e alteração (Hibbard 1987, Peterson *et al.* 1989, Blenkinsop 2000, Best 2003, Vernon 2004, Passchier & Trouw 2005, Trouw *et al.* 2010). A análise das microestruturas primárias observadas nessas rochas foi essencial para auxiliar na interpretação sobre suas origens e evoluções magmáticas, ao passo que, a identificação das microestruturas de deformação e dos mecanismos de deformação intracristalina nos permitiram inferir a relação entre as deformações magmáticas/submagmáticas e de estado sólido que afetaram essas rochas, além de estimar as condições de temperatura atuantes durante as fases finais desta deformação cristal-plástica. A análise das transformações tardias pós-magmáticas nos permitiu inferir as condições de alteração deutérica em que essas rochas foram submetidas.

1.5.4 Geoquímica

Foram tratadas 56 amostras representativas dos granitoides identificados neste trabalho: (i) 31 amostras do grupo biotita monzogranito; (ii) 18 amostras do grupo epidoto-biotita granodiorito; (iii) 07 do grupo de granitoides porfiríticos. Além disso, embora não utilizadas neste trabalho, foram adquiridas as composições de 04 amostras de enclaves, relacionados ao grupo EBGd, 03 de enclaves maficos e 01 de epidoto-biotita tonalito. As amostras foram trituradas, pulverizadas, homogeneizadas e quarteadas no Laboratório de Preparação de Amostras (OPA) do Instituto de Geociências da UFPA e as análises químicas foram realizadas pela ACME *Analytical Laboratories* Ltda. (Vancouver, Canadá), onde os conteúdos de elementos maiores e menores (SiO_2 , Al_2O_3 , Fe_2O_3^t , MgO , CaO , Na_2O , TiO_2 , Cr_2O_3 , P_2O_5 , PF) foram analisados por ICP-ES (*Inductively Coupled Plasma Emission Spectroscopy*) e os elementos traços (Zn, Cu, Pb, Ba, Be, Cs, Ga, Hf, Nb, Rb, Sn, Sr, Ta, Th, U, W, Zr, Bi) e terras raras (La, Ce, Pr, Nd, Sm, Eu, Gd, Tb, Dy, Ho, Er, Tm, Yb e Lu) por ICP-MS (*Inductively coupled plasma mass spectrometry*).

Para a geração dos diagramas desse trabalho, inicialmente foi confeccionada uma planilha no Excel®, com os cálculos dos diversos parâmetros geoquímicos, em que as transformações de óxidos para proporção molar, porcentagem catiônica e de Fe_2O_3^t em FeO^t foram realizadas a partir de proporção estequiométrica. Além das amostras deste trabalho,

essa planilha também integra um banco de dados para comparação, com 256 amostras, representativas de diversas unidades granitoides da Província Carajás, a saber: leucogranitos alto-K (Almeida *et al.* 2013, Feio & Dall'Agnol 2012, Rodrigues *et al.* 2014, Leite-Santos & Oliveira 2016), leucogranodiorito-granitos alto Ba-Sr (Almeida *et al.* 2013, Teixeira *et al.* 2013, Ronaib & Oliveira 2013, Leite-Santos & Oliveira 2016) e associações granodiorito-tonalíticas de afinidade sanukitoide (Santos & Oliveira 2016). Em sequência, foram realizados diversos testes a partir da confecção de vários diagramas utilizando o *software* GCDkit® versão 2.2 e subsequente seleção daqueles que de fato foram inseridos neste trabalho, baseado nos princípios recomendados em Ragland (1989), Rollinson (1993) e Gill (2010). Nesse contexto, as composições dos granitoides estudados foram plotadas em: (i) diagramas de Harker para melhor compreender a evolução composicional dentro de cada grupo e possíveis relações entre eles; (ii) diagramas de classificação (O'Connor. 1965; Barker 1979, Debon & Le Fort 1983) e séries magmáticas (Shand 1943, Nockolds & Allen 1953, Peccerillo & Taylor 1976, Barker & Arth 1976, Frost *et al.* 2001) afim de aperfeiçoar nossa compreensão sobre as afinidades geoquímicas dessas rochas; (iii) diagramas ETRs (Elementos Terras Raras) e multielementos, normalizados para condrito (Evensen *et al.* 1978) e manto primitivo (Taylor & McLennan 1985), respectivamente; e (iv) diagramas selecionados (Moyen *et al.* 2003a, Heilimo *et al.* 2010, Larurent *et al.* 2014a) para auxiliar os anteriores na discussão sobre a petrogênese e evolução magnética. Adicionalmente, foram utilizados estudos de modelagem geoquímica de elementos traços para melhor entender os processos que formaram essas rochas.

CAPÍTULO 2

DIVERSITY, ORIGIN AND TECTONIC SIGNIFICANCE OF THE MESOARCHEAN GRANITOIDS OF OURILÂNDIA DO NORTE, CARAJÁS PROVINCE (BRAZIL)

Luciano Ribeiro da Silva^{1,2} (lucianor@ufpa.br), Davis Carvalho de Oliveira^{1,2} (davis@ufpa.br),
Maria Nattânia Sampaio dos Santos² (nattania@ufpa.br)

¹Graduate Program in Geology and Geochemistry (GPGG), Institute of Geosciences (IG), Federal University of Pará (UFPA), Post office box 8608, CEP-66075-110, Belém, Pará, Brazil.

² Group of Research on Granitoids Petrology (GPGP), IG, UFPA, Brazil.

Abstract:

This study investigates the diversity, origin and tectonic significance of the Ourilândia do Norte Mesoarchean granitoids, emplaced near Rio Maria-Canãa dos Carajás domains boundary, southeastern Amazonian Craton (Brazil). In this area, previous works has identified sanukitoids (~ 2.87 Ga), (quartz) diorites of BADR affinity and undifferentiated leucogranites, with charnockites cross-cutting the other granitoids. New geological mapping data allowed to differentiate three new groups of granitoids: (i) biotite monzogranites (BMzG); (ii) epitote-biotite granodiorites (EBGd); and (iii) porphyritic granitoids (pGrt). Thus, this paper aims to define their classification, nature, formation processes and deformation aspects, and discuss the relations between plutonism and deformation for the Ourilandia do Norte granitoids. The petrographic data showed that each one of these groups can be subdivided into two facies. The BMzG is differentiated into equigranular (eBMzG) and heterograngular (hBMzG) and the EBGd into heterograngular (hEBGd) and sparsely porphyritic (spTEBGd). These granitoids constitute two batholiths separated by a rock strip of sanukitoid and BADR affinities. Both are largely dominated by BMzG rocks, with less occurrence of EBGd lenses. The pGrt is individualized in porphyritic granodiorites (pBHGd) and trondhjemites (pEBTd), which occur as smaller bodies. Structurally, the central portions these plutons represent lower strain domains, while their borders are marked by large-scale shear zones, where occur magmatic and milonitic fabrics of ENE-WSW main direction and subvertical dip, respectively. The meso- and microstructural data indicate that the rocks studied are syn- to late-tectonic and were affected by high temperature deformation (> 500 °C) and low differential stress, in a sinistral transpression regime, indicating that both fabrics are related to the same deformational event. Geochemically, except the EBTdp that has Mg-Na affinity, the Ourilândia do Norte granitoids can be grouped into two suites: (i) Fe-K suite formed by BMzG and spTEBGd; and (ii) Mg-K suite composed for sanukitoids (including hEBGd and pBHGd) and (quartz) diorites of BADR affinity. The origin of the eBMzG is attributed to anatexis of a 2.92-2.98 Ga old TTG crust. The hEBGd has sanukitoid affinity and was produced by intense fractionation of hornblende ± clinopyroxene. The granitoids of spTEBGd, hBMzG, pBHGd and pEBTd facies show mingling evidence between contrasting magmas, indicating that their origins require interaction between metassomatized mantle- and crustal derived magmas. Geochemical data and modeling were used to identify their different formation processes: (i) spTEBGd is enriched in HFSE (Ti, Zr and Y) and LILE (Ba and Sr) and it was admitted as product of the partial melting of an enriched mantle source, with participation of crustal liquids; (ii) hBMzG is generated by the interaction between spTEBGd (60%) and eBMzG (40%) magmas; (iii) pBHGd by hybridization between sanukitoid (80%) and eBMzG (20 %); and (iv) pEBTd by mixture between trondhjemitic (70-80%) and BARD-affinity (20-30%) liquids. Therefore, in ~2.87 Ga a significant crustal growth and reworking occurred in the final stages of stabilization of the first geotectonic cycle of Carajás province, where all the Ourilândia do Norte Mesoarchean granitoids were emplacement during the second stage of a tectono-magmatic two-stage (subduction-collision) model: (i) first stage (2.98-2.92 Ga) - low-angle subduction with emplacement of slab-melt and mantle wedge metasomatism; (ii) second stage (~ 2.87 Ga) - collisional environment, where shear zones conditioned the rise and emplacement of the Ourilândia do Norte magmas.

Keywords: Geochemistry; Microstructural; Granitoids; Archean; Carajás province.

1. Introduction

The continental crust has been continuously extracted from the mantle, with a consequence of the Earth's cooling and differentiation, but growth rates and mechanisms have changed over geological time and at least 50% of the present-day continental volume was formed prior to 2.5 Ga (Taylor & McLennan, 1985, 1995; Kramers & Tolstikhin, 1997; Belousova et al., 2010; Dhuime et al., 2011; Guitreau et al., 2012). Thus, the end of the Archean has long been regarded as a period of fundamental geodynamic changes (Taylor & McLennan, 1995; Condie & O'Neill, 2010; Laurent et al., 2014a). The Archean terranes worldwide are composed primarily of three contrasting lithologies: (i) the so-called "grey gneisses", composed by a complex, deformed and often migmatitic assemblage, geochemically defined as TTG (tonalite-trondhjemite-granodiorite) suites; (ii) the greenstone belts formed by supracrustal, meta-volcanic and meta-sedimentary rocks commonly metamorphosed under greenschist to amphibolite facies; and (iii) high-K granitoid plutons, usually emplaced in a late context, intruding into the two older lithologies. These rocks cover a wide compositional range and can be subdivided into three main groups: high-K calc-alkaline, slightly peraluminous, biotite-bearing leucogranites; metaluminous Mg- and K-rich rocks from the sanukitoid suite; and calc-alkaline hybrid granitoids commonly enriched in Ba and Sr or with assimilation of sodic material. These granitoids generally represent the last Archean geological event in every craton worldwide and appear to be related to final stabilization of the Archean cratonic lithosphere. Although this event is diachronous from one craton to another, it occurred between 3.0 and 2.5 Ga ago on a planetary scale (Condie, 1981; Martin, 1994; Sylvester, 1994; Frost et al., 1998; Champion & Smithies, 1999; Moyen et al., 2003a; Oliveira et al., 2009; Heilimo et al., 2013; Almeida et al., 2011, 2013; Laurent et al., 2014a).

The Carajás province is the largest and best preserved Archean segment of the Amazonian craton, in northern Brazil, and comprises the Rio Maria (RMD), Sapucaia (SD) and Canaã dos Carajás (CCD) domains (Fig. 1; Vasquez et al., 2008; Dall'Agnol et al., 2013). The granitoid magmatism and evolution of the Mesoarchean RMD have been more extensively studied. It is formed mainly by greenstone belts, TTG suites, sanukitoid affinity granodiorites, high Ba-Sr leucogranodiorite-granites and potassic leucogranites (Althoff et al., 2000; Souza et al., 2001; Leite et al., 2004; Oliveira et al., 2009; Almeida et al., 2011, 2013). The Meso- to Neoarchean CCD represents the basement of the Neoarchean Carajás basin and remains poorly characterized. The best known areas of this domain show lithologic associations distinct from RMD and they are dominated by potassic granites and granulitic and charnockitic rocks, with subordinate TTG series (Feio & Dall'Agnol, 2012; Feio et al., 2012, 2013; Santos et al., 2013c; Cunha et al., 2016). The SD is considered an extension of the RMD affected by Neoarchean events that gave rise to the Carajás basin (Gabriel & Oliveira, 2014; Leite-Santos & Oliveira, 2016; Dall'Agnol et al., 2016; Santos, 2017).

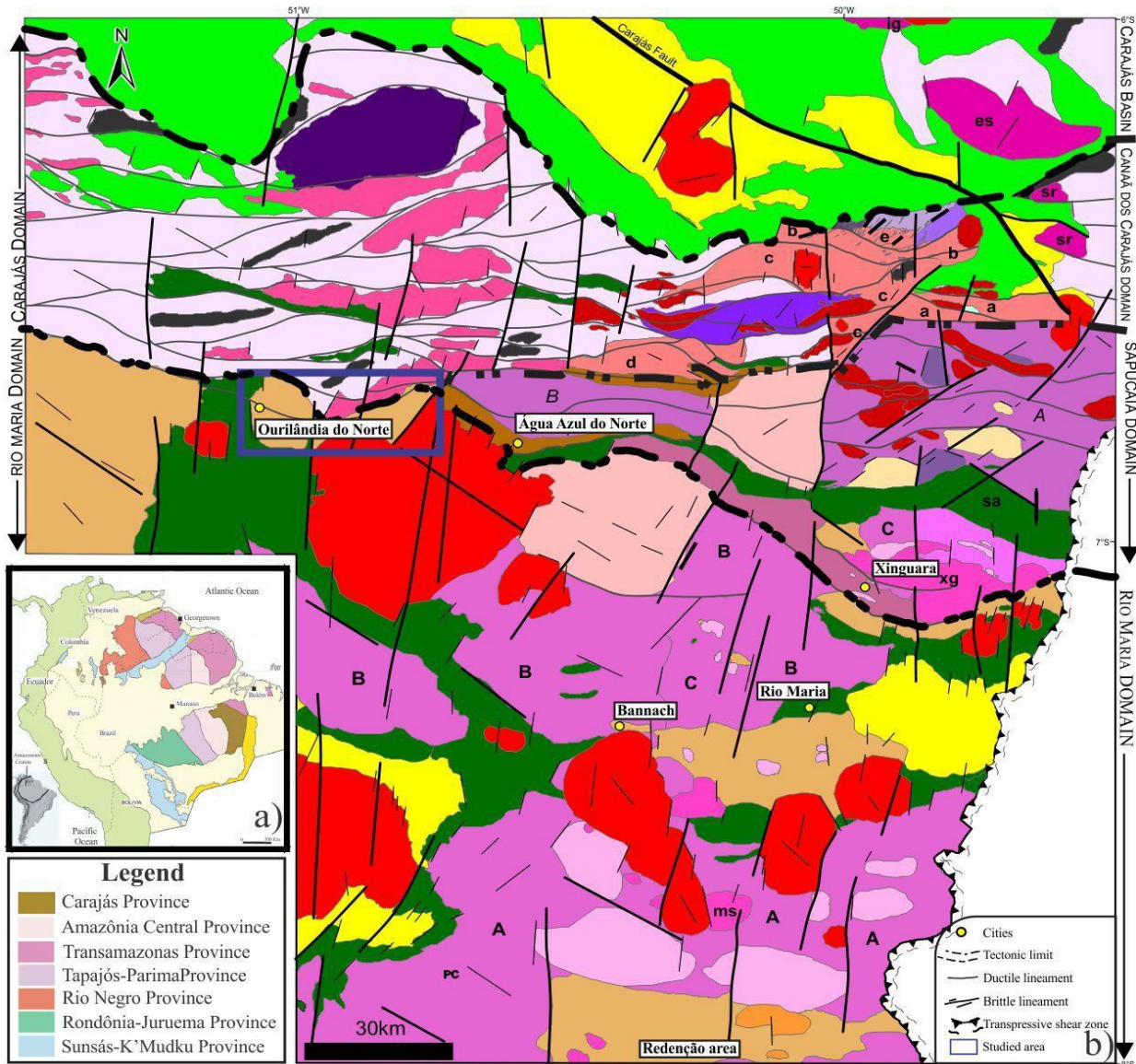
The Ourilândia do Norte area is located in the central-west portion of the Carajás province, straddling the RMD-CCD border. It is predominantly formed by 2.87 Ga old Mesoarchean granitoids of sanukitoid affinity, (quartz) diorites of BADR (Basalt-Andesite-Dacite-Rhyolite) affinity, undifferentiated leucogranites, and younger intrusion of clinopyroxene-bearing monzogranite (Santos et al., 2013a; Santos & Oliveira, 2016). As a result of the present study, the geological mapping performed in the Ourilândia do Norte area distinguished at least three more groups of Mesoarchean granitoids: (i) biotite monzogranites; (ii) epidote-biotite granodiorites; and (iii) porphyritic granitoids. Accordingly, this paper aims to define: (i) the field relationships and structural framework of these rocks, from geologic and photointerpretation data; (ii) the petrographical and geochemical classifications; (iii) the magmatic and deformation fabrics and microstructures; and (iv) the relationships between plutonism and deformation for the origin, emplacement and tectono-magmatic evolution of the Ourilândia do Norte granitoids.

2. Regional geology

The Carajás Province (Fig. 1) is the main preserved Archean domain of the Amazonian Craton (Almeida et al., 1981). Santos (2003) considers it to be an independent geochronological province, while Tassinari & Macambira (2004) interpret it as to be part of the Central Amazon province, which is subdivided into two blocks (Carajás and Xingu-Iricoumé) (Fig. 1a). A new configuration initially proposed by Souza et al. (1996), and revised by Santos (2003) and Vasquez et al. (2008), subdivided the province into two distinct tectonic domains: the Mesoarchean Rio Maria domain (3.0-2.86 Ga) and Meso- to Neoarchean Carajás domain (3.0 – 2.75 Ga). Geophysical data suggest that the border between the two domains coincides with a regional ~E-W trending discontinuity, extending from the southern Xinguara region on the eastern border of the province to São Félix do Xingu on the western border. Dall'Agnol et al. (2013), using an integrated approach for geophysical and geological data, showed that the CD does not correspond to a tectonically homogeneous Archean crust, which led to the designation of the names Canaã dos Carajás and Sapucaia subdomain for its northern and southern portions, respectively (Figure 1b).

The RMD is composed of greenstone belt sequences of the Andorinhas supergroup (3.0 and 2.9 Ga) and four granitoids suites, emplaced between 2.98 and 2.86 Ga (Althoff et al., 2000; Oliveira et al., 2009; Almeida et al., 2011; 2013; Ronaib & Oliveira, 2013). These include: (i) TTG associations represented by Arco Verde, Caracol and Mariazinha tonalities and Mogno trondhjemite, formed during two main magmatic events 2.96 ± 0.2 Ga and 2.93 ± 0.1 Ga ago; (ii) the 2.87 Ga Rio Maria sanukitoid suite, consisting primarily of epidote-hornblende-bearing granodiorite, with associated mafic and intermediate rocks forming enclaves or, locally, layered rocks; (iii) the 2.87 Ga Guarantã suite formed by high Ba-Sr calc-alkaline leucogranodiorite-granites; and (iv) the 2.87–2.86 Ga potassic leucogranites of calc-alkaline affinity, represented by Xinguara and Mata Surrão granites and small stocks, where biotite is the only varietal phase and epidote may be an important accessory phase. These rocks are weakly deformed, showing a WNW-ESE planar fabric (magmatic and tectonic), and intruded by 1.88 Ga Paleoproterozoic anorogenic granites (Barbosa et al., 1995; Paiva Jr. et al., 2011).

The CCS is dominated by 2.87-2.85 Ga high-K calc-alkaline granites (Boa Sorte, Bom Jesus, Cruzadão and Serra Dourada granites) and 2.74 Ga enderbite-charnokite-granites (Planalto suite and Pium diopside-norite) with rare occurrences of TTG (Rio Verde trondhjemite 4– 2.93 Ga), amphibole-bearing tonalite represented by Bacaba tonalite (3.0 Ga) and Campina Verde tonalitic complex (2.87 to 2.85 Ga), sodium leucogranites of calc-alkaline affinity (Canaã dos Carajás granite – 2.93 Ga) and 1.88 Ga anorogenic plutons (Feio et al., 2012, 2013; Santos et al., 2013c; Rodrigues et al., 2014). The SS is dominated by Mesoarchean TTG associations similar to those of the Rio Maria domain, but these were intensely deformed and intruded by granite plutons during the Neoarchean. It consists of TTG (Colorado and Água Fria trondhjemites), amphibole-bearing tonalite (São Carlos tonalite), Água Azul and Água Limpa sanukitoids composed mainly of porphyritic granodiorites, high Ba-Sr calc-alkaline leucogranodiorite-granites (Pantanal and Nova Canadá), and neoarchean high-K calc-alkaline and A-type granites represented by the Velha Canadá and Vila Jussara suites, respectively (Santos et al., 2013b; Teixeira et al., 2013; Silva et al., 2014; Gabriel & Oliveira, 2014; Leite-Santos & Oliveira, 2014, 2016; Dall'Agnol et al., 2016). The structural pattern identified in the SS and CCS is marked by moderate-to-strong heterogeneous deformation when compared to Rio Maria. Both domains are composed of E-W oriented plutonic bodies, which show E-W magmatic and tectonic foliations and subvertical dip.



LEGEND

Araguai Belt
Anorogenic granites
Carajás Basin
Águas Claras formation
Subalkalines granites: Estrela (es), Igarapé Gelado (ig) granites
Mafic-ultramafic magmatism
Itacaiúnas supergroup
Xingu complex
Canaã dos Carajás Domain
Plaquê suite
Pedra Branca suite
Pium diopside-dorite
Subalkalines granites: Planalto suite
Campina Verde tonalitic complex
Calei-alkalines granites: Canaã dos Carajás (a), Bom Jesus (b), Cruzadão (c), Boa Sorte (d) e Serra Dourada (e)
Rio Verde trondhjemite
Xingu complex
Chirrim-Cateté ortogranulite
Bacaba tonalite
Greenstone belts

Sapucaia Domain

Subalkalines granites: Planalto suite
Undifferentiated leucogranodiorites
Pantanal leucogranodiorite
Água Fria trondhjemite
Xinguara granite
TTG: Colorado trondhjemito (A) and Undifferentiated TTG (B)
Sanukitoides: Água Azul and Água Limpa granodiorites
Mariazinha tonalite
São Carlos tonalite
Caracol tonalite
Sapucaia greenstone belts

Rio Maria Domain

Rio Fresco Grup
Potassic leucogranites: Mata Surrão (ms) granite
Guarantã suite
Rio Maria suite
Rancho de Deus granite
Older TTG: Arco Verde tonalite (A), Mogno trondhjemite (B) and Mariazinha tonalite (C)
Andorinhas supergroup

Figure 1 - (a) Geochronological provinces of the Amazonian Craton ([Santos, 2003](#); [Vasquez et al., 2008](#)); and (b) Geological map of the Carajás province, with location of the studied area. Modified from [Dall'Agnol et al. \(2013\)](#). In the left part is shown the tectonic compartmentation according to [Vasquez et al. \(2008\)](#) and in the right part is shown the proposal of [Dall'Agnol et al. \(2013\)](#).

3. Geology and structural framework

Recent studies have resulted in significant advances in knowledge about the magmatic associations and structural aspects of the Mesoarchean crustal segment of Ourilândia do Norte (Fig. 2; Santos et al., 2013a; Santos & Oliveira, 2016), previously mapped as the Xingu complex, Rio Maria and Plaque suites (Vasquez et al., 2008). Santos & Oliveira (2016) recently defined high-Mg granitoids of sanukitoid affinity, correlated to the Rio Maria suite (RMS), (quartz) diorites of BADR affinity and undifferentiated leucogranites. Moreover, they identified small bodies of clinopyroxene-bearing monzogranite cross-cutting the other granitoids. In this study, the semi-detailed scale (~1:50,000) geological mapping performed in the Ourilândia do Norte area distinguished at least three additional groups of Archean granitoids, all separated into two facies (Box 1; Fig. 2 and 3), as follows: (i) **biotite monzogranite** (BMzG) showing even-grained (eBMzG) and heterograngular (hBMzG) textures, with subordinate granodiorite; (ii) **epidote-biotite granodiorite** (EBGd), heterograngular (hEBGd) and sparsely porphyritic (spTEBGd); and (iii) **porphyritic granitoids** (pGrt), porphyritic epidote-biotite trondhjemite (pEBTd) and porphyritic biotite-hornblende granodiorite (pBHGd).

The geological map of the area shows that the BMzG rocks are predominant and constitute two composite batholiths with minor occurrence of EBGd rock lenses separated by a strip constituted of RMS sanukitoids with subordinated BADR-affinity rocks (Fig. 2). Field relationships suggest that both are intrusive in high-Mg granitoids and in those undifferentiated from the Xingu complex, where the main pluton, located in the northern part of the area, is ellipsoidal with dimensions of ~37x8 Km and its major axis shows a ENE-WSW trend. A second arc-shaped pluton in the southeastern portion is intruded by Paleoproterozoic Seringa granite. The eBMzG variety is predominant throughout these two batholiths, while the hEBGd and spTEBGd facies have a subordinate spatial distribution and occur as E-W lenses within these larger leucogranitic bodies. The hBMzG rocks shows a closed spatial relationship with those of spTEBGd variety. In turn, the porphyritic granitoids (pEBTd and pBHGd) occur as small bodies associated with the BADR-affinity diorites and RMS high-Mg granitoids, respectively. The pEBTd variety was mapped as a E-W lens with dimensions of ~2x1 Km situated in the central portion of the area, while the pBHGd variety form two larger stocks with dimensions of ~7x4 Km and ~7x2 Km, separated by a strip of RMS granitoids in the southwestern part of the map.

The representative rocks of the EBGd and pGrt groups exhibit a large number of mafic enclaves, which are elongated according to regional foliation (Fig. 4a and 4g), similar to those commonly observed in the RMS granitoids. Granites from the BMzG group show ambiguous cross-cutting relationships with the granodiorites (EBGd). In this respect, rocks from the hBMzG facies frequently exhibit rounded hEBGd and spTEBGd enclaves (Fig. 4c and 4d), often with mingling features, suggesting low viscosity contrast between these rocks (e.g. Fig. 4b, 4c, 4d and 4f). On the other hand, the common occurrence of eBMzG veins cross-cutting EBGd rocks (e.g. Fig. 4a) indicates that the BMzG magma is slightly or partially younger than those that gave rise to the granodiorites (hEBGd and spTEBGd). However, it cannot be ruled out that these melts may have coexisted during the accommodation processes.

The field observations, petrography, photointerpretation [Shuttle Radar Topography Mission (SRTM) image interpolated to 15 m, C-band] and microstructural (see section 4.2) data allowed to define the structural framework of the Ourilândia do Norte granitoids. Although these rocks show well-preserved igneous features, they are affected by heterogeneous deformation defined by magmatic or mylonitic foliation of ENE-WSW main trend and subvertical dip (Fig. 2), where the fabrics are subparallels to the main axis of the bodies and concordant with the regional deformation pattern. The local variation in the intensities and orientations of these fabrics can be seen in the stereograms of the Fig. 2.

The lower strain domains occur predominantly in the central parts of the batholiths and commonly show (S_0) magmatic foliations marked by the alignment of biotite ±hornblende crystals,

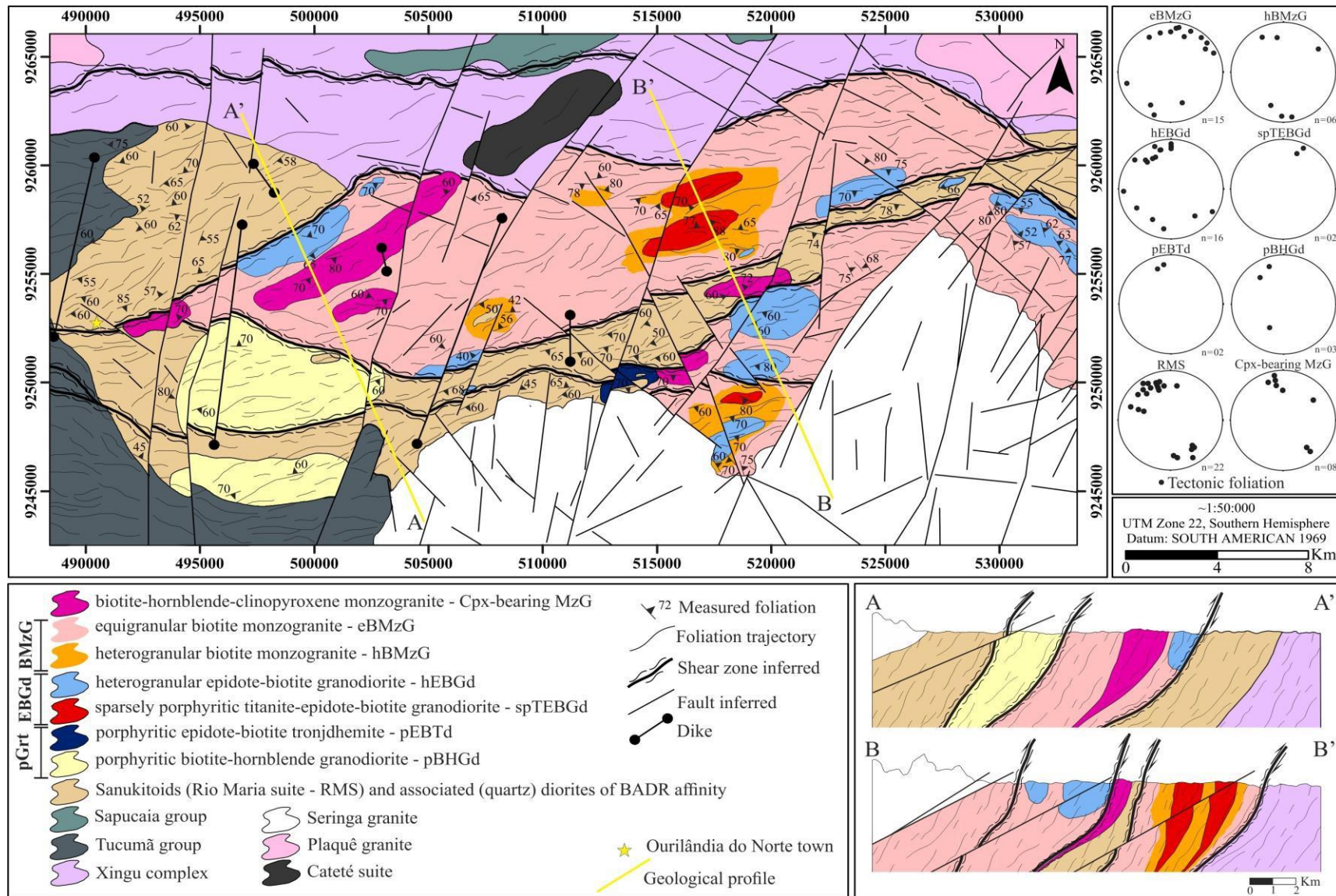


Figure 2 - Ourilândia do Norte geological map and location of the A-A' and B-B' schematic geological profiles shown in the lower right portion. In the upper right portion is displayed equal-area (Schmidt-Lambert) stereographic projections with the main attitude of measured foliation.

Box 1 - Synthesis of the field aspects of the granitoids studied. Colour index according Le Maitre (2002). Legend: M' = Colour Index; and RMS = Rio Maria Suite.

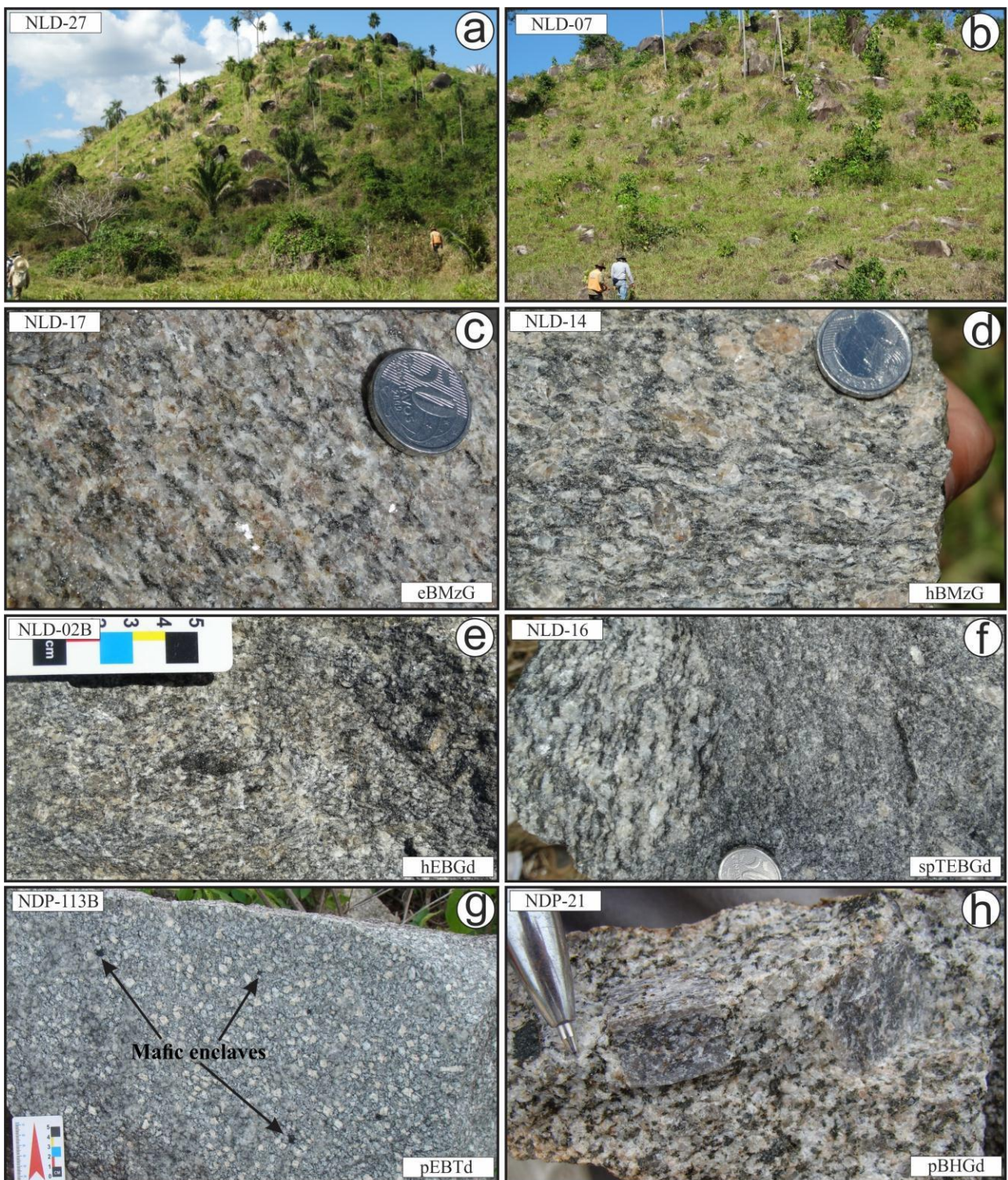


Figure 3 - General aspects of the granitoids under study. (a) and (b) these rocks commonly outcrop as rolled or in situ blocks. The granites supporting mound relief and granodiorites dominate the more razed portions of the area; (c) even-grained biotite monzogranite (eBMzG), show spaced foliation defined by the alignment of biotite; (d) heterograniular biotite monzogranite (hBMzG), showing mylonitic foliation defined by feldspar porphyroclasts contoured by biotite and stretched quartz; (e) heterograniular epidote-biotite granodiorite (hEBGd), exhibiting partially digested mafic enclave; (f) sparsely porphyritic titanite-epidote-biotite granodiorite (spTEBGd) show digested biotite tonalite xenolith; (g) porphyritic epidote-biotite trondhjemite (pEBTd), displaying small mafic microgranular enclaves and (h) porphyritic hornblende-biotite granodiorite (pBHGd), with centimetric feldspar phenocrysts.



Figure 4 - Field relationship of the granitoids studied. (a) injections of eBMzG composition cross-cutting the hEBGd. Note the mafic to intermediate enclaves, oriented according to the foliation; (b) straight contact between hBMzG and spTEBGd, suggesting low viscosity contrast; (c) and (d) rounded or slightly angular enclaves of spTEBGd composition in hBMzG, indicating material partially digested within the host granitoid; (e) compositional banding between hBMzG and hEBGd, indicating low viscosity contrast; (f) spTEBGd displaying digested enclave (hBMzG composition?); and (g) spTEBGd shows angular enclave of mafic composition and digested xenoliths of biotite tonalitic composition, suggesting higher viscosity contrast between these rocks.

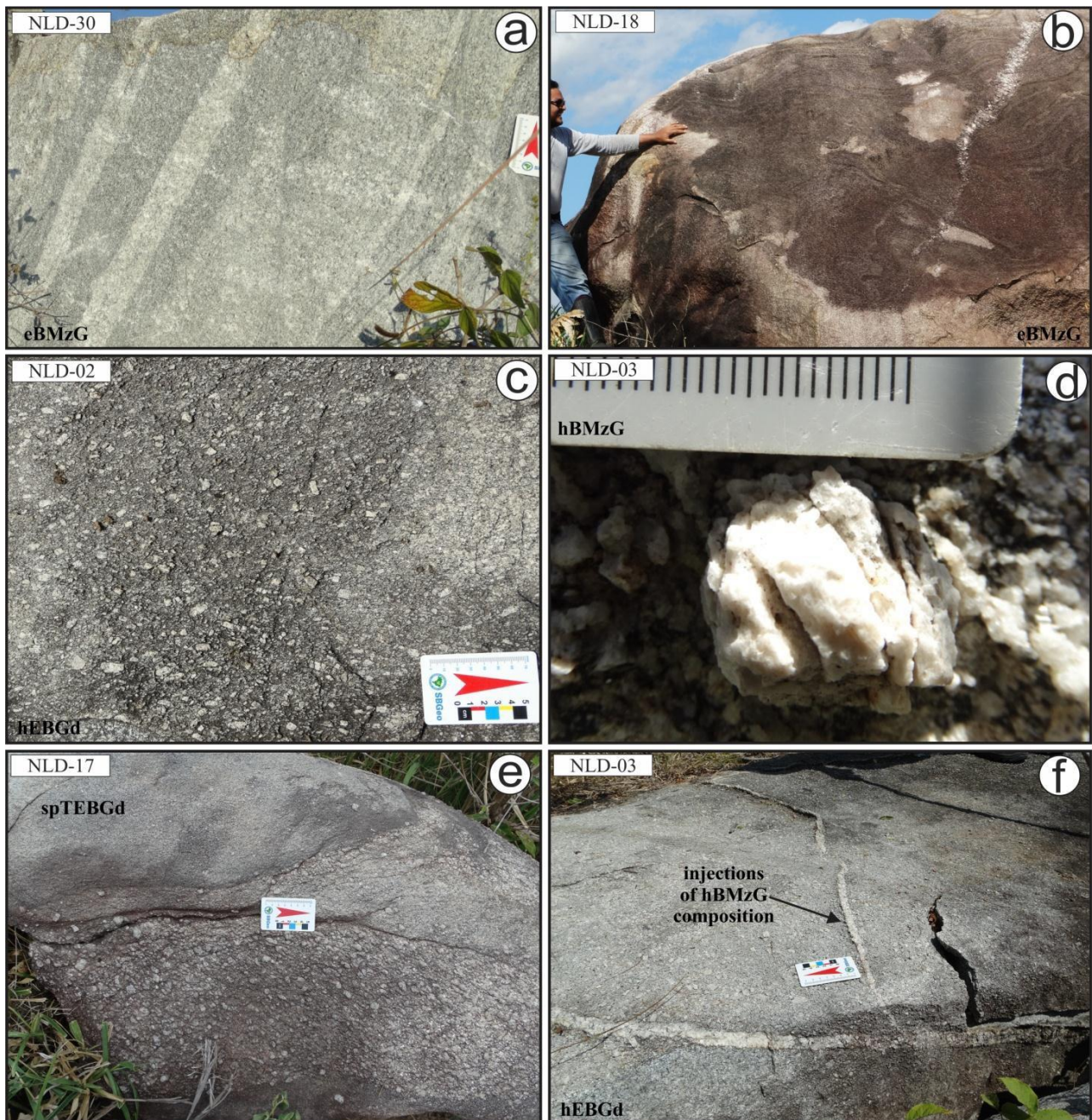


Figure 5 - Deformation aspects of the granitoids under study. (a) Primary compositional banding in rocks of the eBMzG facies shows magmatic fault, healed by melt (Neves, 2012); (b) complex folds observed in primary planar fabric; (c) magmatic foliation defined by aligned euhedral feldspar phenocrysts (Paterson et al., 1989); (d) alkali feldspar fenocristal shows deformation feature; (e) heterograniular granite (hBMzG) cross-cutting the rocks of spTEBGd facies. Note the presence of well-developed magmatic foliation in the hBMzG and sinuous contacts with the spTEBGd, indicating low viscosity contrast between them; e (f) fractures filled by granitic material in rocks of hEBGd facies.

euhedral feldspars and stretched quartz aggregates, indicating the presence of magmatic defomation for these rocks (e.g. Fig. 5c; Paterson et al., 1989). On the other hand, the higher strain domains show (S_1) proto- to mylonitic foliation (e.g. Fig. 3d) and are located primarily near the pluton borders, defining an anastomosed geometry and suggesting that these batholiths are limited by large-scale shear zones (see geological map and sections of the Fig. 2). This mylonitic foliation is defined by rounded or augen feldspar porphyroclasts, contoured by biotite and quartz aggregates, where S-C fabric occasionally may occur (e.g. Fig. 3d and 8a). In addition, it is worth mentioning that eBMzG rocks often show magmatic banding (Fig. 5a), wherein both bands are mineralogically

similar, but the darker ones are biotite-enriched. This compositional banding commonly develops disharmonic and complex folds (e. g. Fig. 5b).

The structural history of the Carajás region was registered on the undifferentiated Mesoarchean granitoids of the Xingu complex from the occurrence of oblique lineation, and kinematic indicators which suggest a regime of high temperature sinistral transpression with partitioning of deformation producing linked systems of ductile strike-slip and thrust dominated shear zones (Araújo and Maia, 1991; Pinheiro and Holdsworth, 1997). For the Ourilândia do Norte region the kinematic indicators and local variation in intensity and orientation of the fabric suggest that the deformation was predominantly controlled by pure shear, under conditions of high temperature and low differential stress. Such information is reinforced by microstructural observations (see section 4.2).

4. Petrography

4.1. Modal composition and classification

Meso- and microscopic petrographic analysis coupled with modal compositional data performed on 54 polished or thin sections (2000 points per section from a mesh of 0.4 mm counted in Endeeper Hardedge software; Table 1) enabled individualization and classification (Fig. 6; Le Maitre, 2002) of the aforementioned varieties (see Box 1). The **BMzG** rocks are divided into equigranular leuco- to biotite monzogranite (**eBMzG**) and heterograngular biotite monzogranite (**hBMzG**), which are predominantly hololeucocratic with color index M' , ranging from 1.6 to 11.7% and from 5.4 to 13.6%, respectively. Their essential mineralogy is composed of quartz (22.7-41.2%), plagioclase (27.10-48.80%) and alkali feldspar (12.4-39.6%). Biotite represents the single varietal mineral from both the **eBMzG** (0.6-9.9%) and **hBMzG** (3.7-10.7%) varieties and the primary accessory phases are epidote, titanite, apatite, zircon, allanite and opaque minerals, whereas the secondary accessories are chlorite, muscovite, epidote and titanite.

Granitoids from the **EBGd** group were differentiated into heterograngular epidote-biotite granodiorite (**hEBGd**) and sparsely porphyritic titanite-epidote-biotite granodiorite (**spTEBGd**), the former with scarce tonalite and monzogranite. The **hEBGd** rocks are holo- to leucocratic ($M'=2.9\text{-}18.8\%$) and the **spTEBGd** are leucocratic ($M'=13.7\text{-}19.9\%$). They are essentially composed of quartz (19.6-38.9%), plagioclase (29.7-56.4%) and alkali feldspar (3.1-24.5%). Biotite (2.8-17.4%) and epidote (0.1-2.8%) are common varietal minerals, while hornblende (0.2-1.0%) and titanite (1.2-2.4%) are important accessory phases in the **hEBGd** and **spTEBGd** varieties, respectively. Other minor primary phases comprise allanite, apatite, zircon and magnetite and the secondary mineral paragenesis is represented by chlorite, muscovite, epidote, biotite and titanite.

Rocks from the **pGrt** group are classified into two facies: porphyritic epidote-biotite trondhjemite (**pEBTd**) and porphyritic biotite-hornblende granodiorite (**pBHGd**). The **pEBTd** facies is formed by hololeucocratic ($M'=4.2\text{-}8.7\%$) trondhjemite, while the **pBHGd** facies is composed of holo- to leucocratic ($M'=7.6\text{-}15.7\%$) granodiorite, with subordinate monzogranite and quartz monzonite. In these varieties, quartz content varies from 24.6-32.2% and 13.5-30.2%, plagioclase from 62.1 to 65.1% and 33.8 to 64.5% and alkali feldspar 0.9 to 1.1% and 9.1 to 25.9%, respectively. Epidote (0.8-1.9%) and hornblende (3.9-12.0%) occur as varietal minerals in the **pEBTd** and **pBHGd** varieties, respectively, whereas biotite is common in both, with higher modal content in the former (2.4-6.3%) than the latter (0.1-2.0%). Their primary accessory phases are titanite, apatite, zircon and opaque minerals, while post-magmatic mineral assemblage consists of chlorite, muscovite, epidote, biotite and titanite.

Table 1 -Modal compositions of the granitoids under study (2000 points from 54 polished or thin sections; Le Maitre, 2002).

Group	Biotite monzogranite - BMzG																				hBMzG									
Facies	MzG	MzG	Gd	MzG	Gd	MzG	LMzG	LGd	LMzG	LMzG	LMzG	LMzG	LMzG	LMzG	LMzG	LMzG	LGd	Gd	Gd	MzG	MzG	Gd	MzG	MzG	MzG	MzG	MzG	MzG		
Litology	NLD	NLD	NLD	NLD	NDP	NLD	NLD	NLD	NLD	NLD	NDP	NLD	NLD	NLD	NLD	NDP	NDP	NDP	NDP	NDP	NDP									
Samples	04B	06B	25	30B	127	29	07B	10A	8	30A	17B	27	11B	118	18	17C	89B	5	117B	03A	14	20A	16B	11C	91	92B	117A			
Minerals (%)																														
Quartz	25.40	30.35	28.40	34.55	27.75	28.35	32.90	28.95	34.85	33.70	39.20	34.45	31.25	24.65	37.05	32.65	30.95	32.60	30.05	30.15	41.20	28.60	35.73	29.50	35.25	22.75	32.95			
Plagioclase	40.65	29.20	42.55	32.95	42.80	27.45	38.95	38.20	48.80	34.25	27.20	32.10	36.80	40.10	32.60	30.20	27.80	47.25	39.70	40.45	27.10	31.70	40.10	35.15	35.25	43.85	39.35			
Microcline	21.80	31.80	19.65	23.95	23.05	37.75	22.55	28.80	12.40	27.50	30.20	29.90	29.20	32.75	27.90	35.45	39.55	19.05	16.65	18.90	21.40	30.45	15.34	26.95	21.05	27.10	22.10			
Hornblende	-	-	-	-	-	-	-	-	-	-	-	-	-	-	-	-	-	-	-	-	-	-	-	-	-	-	-			
Biotite	9.90	7.90	6.95	6.90	5.20	5.10	3.90	3.85	3.40	3.35	2.25	2.15	2.25	1.60	1.45	0.80	0.60	0.60	10.70	8.50	8.80	6.55	5.96	6.80	5.55	4.80	3.65			
Epidote	0.05	Tr	1.05	0.35	0.30	0.15	0.20	Tr	Tr	0.10	0.30	0.60	Tr	0.20	0.15	0.05	0.65	0.05	0.35	1.00	0.10	0.30	0.91	Tr	1.70	0.15	0.35			
Muscovite	0.15	0.05	0.80	0.65	0.25	0.90	-	Tr	Tr	0.25	0.35	0.45	Tr	0.05	0.15	-	0.05	-	-	0.20	0.40	0.10	0.16	Tr	0.40	0.05	0.20			
Titanite	0.85	0.50	Tr	Tr	0.15	0.10	0.10	Tr	Tr	0.15	0.05	Tr	Tr	0.20	0.25	0.05	Tr	Tr	0.15	0.15	0.50	0.64	0.10	0.15	0.10	0.75				
Allanite	0.10	0.05	-	-	0.05	-	-	-	-	-	-	-	-	-	-	-	0.05	0.10	-	0.15	0.10	0.20	0.30	Tr	0.15	Tr	0.20	0.10		
Apatite	0.20	Tr	0.45	0.30	0.05	Tr	0.30	Tr	0.05	0.45	Tr	0.10	Tr	Tr	0.05	Tr	0.05	Tr	Tr	0.10	0.15	0.35	0.16	0.35	0.05	Tr	Tr			
Zircon	0.15	Tr	0.10	0.05	Tr	Tr	0.05	Tr	Tr	0.15	Tr	Tr	Tr	Tr	Tr	0.05	Tr	Tr	Tr	Tr	0.05	Tr	0.15	0.05	Tr	0.20	Tr	Tr		
Opalines	0.75	0.15	0.05	0.30	0.40	0.20	1.05	0.20	0.50	0.15	0.45	0.25	0.50	0.45	0.35	0.75	0.25	0.45	-	0.40	0.50	1.00	0.96	1.00	0.35	1.00	0.55			
Σfelsic	87.95	91.40	91.40	92.10	93.85	94.45	94.40	95.95	96.05	95.70	96.95	96.90	97.25	97.55	97.70	98.25	98.35	98.90	86.40	89.70	90.10	90.85	91.32	91.60	91.95	93.75	94.60			
A+P	62.45	61.00	62.20	56.90	65.85	65.20	61.50	67.00	61.20	61.75	57.40	62.00	66.00	72.85	60.50	79.85	67.35	66.30	56.35	59.35	48.50	62.15	55.44	62.10	56.30	70.95	61.45			
Color index (M')	11.65	8.60	8.05	7.55	6.10	5.55	5.25	4.05	3.90	3.75	3.05	3.00	2.75	2.45	2.20	1.70	1.60	1.10	13.60	10.15	9.75	8.65	8.47	8.05	7.80	6.25	5.40			
Quartz	28.92	33.23	31.35	37.77	29.65	30.30	34.85	30.18	36.29	35.31	40.29	36.32	32.14	25.28	37.97	33.22	31.49	32.96	34.78	33.68	45.94	31.52	39.19	32.20	38.51	24.16	34.91			
K-feldspar	24.81	34.81	21.68	26.19	24.62	40.36	23.89	30.01	12.90	28.81	31.29	31.31	30.02	33.60	28.60	36.07	40.23	19.26	19.26	21.11	23.85	33.55	16.82	29.42	22.98	29.30	23.41			
Plagioclase	46.28	31.96	46.96	36.03	45.73	29.35	41.26	39.82	50.81	35.88	28.41	32.36	37.84	41.13	33.42	30.72	28.28	47.78	45.96	45.21	30.22	34.93	43.99	38.38	38.51	46.54	41.68			
Group	Epidote-biotite granodiorite - EBGd																		Porphyritic granitoids - pGnt											
Facies	hEBGd												spTEBGd				pEBTd		pBHGd											
Litology	Gd	Gd	Gd	TnL	Gd	MzG	Gd	TnL	Gd	Gd	MzG	Gd	MzG	Gd	MzG	LGd	LGd	Gd	Gd	Gd	Td	Td	MzG	Gd	Gd	Gd	QMzD			
Samples	NDP	NDP	NDP	NLD	NDP	NLD	NLD	NLD	NLD	NLD	NDP	NDP	NLD	NDP	NLD	NDP	NLD	NLD	NDP	NDP	NDP	NDP	NDP	NDP	NDP	NDP	NDP	NDP		
Minerals (%)	126	100	101	02B	130	124	07A	04A1	06A	10B	128A	71	03B	70	23	68	26A	15B	16C	17A	113B	115	23	87	25A	21	84A			
Quartz	29.25	35.65	34.00	25.85	33.00	32.80	19.65	26.15	25.70	28.65	22.15	19.95	19.95	23.45	33.45	26.75	38.90	31.90	29.45	22.20	24.60	32.20	24.40	24.64	19.90	30.15	13.50			
Plagioclase	38.05	37.10	39.35	50.15	40.00	33.70	45.55	56.35	39.75	44.45	39.90	56.35	44.30	48.05	38.20	48.50	44.40	29.65	46.35	51.85	65.05	62.10	33.80	52.33	56.45	39.79	64.45			
Microcline	13.90	9.85	9.95	6.50	11.85	18.50	19.65	3.10	20.25	13.50	24.35	10.45	24.45	19.40	22.50	21.65	13.40	17.25	5.65	11.40	0.95	1.10	25.90	9.10	13.45	20.75	13.65			
Hornblende	0.90	1.00	0.15	-	0.20	0.45	-	0.15	-	-	-	-	-	-	-	-	-	-	-	-	-	-	0.80	12.05	10.60	8.85	6.65	3.90		
Biotite	17.40	14.80	13.70	15.10	14.35	13.55	14.00	13.65	10.95	13.15	11.10	8.30	10.10	5.75	4.60	2.10	2.80	14.50	12.55	6.65	6.30	2.40	0.05	2.00	0.60	1.55	1.95			
Epidote	0.40	1.30	2.30	0.85	0.35	0.80	0.20	0.25	2.85	Tr	2.10	1.85	0.65	1.40	0.25	0.60	0.10	1.05	2.80	1.55	1.90	0.80	1.55	0.44	0.20	0.10	0.75			
Muscovite	-	-	-	0.85	-	-	-	-	-	-	-	-	-	-	-	0.40	Tr	0.35	-	-	0.10	0.10	-	-	-	-	-	-		
Titanite	0.05	0.30	0.35	0.35	0.10	0.10	0.45	0.15	0.15	0.25	0.25	1.10	0.30	1.25	0.10	0.25	0.05	2.20	1.20	2.40	0.55	0.20	Tr	0.78	0.30	0.55	0.95			
Allanite	0.05	-	0.20	-	0.10	0.10	0.05	-	0.10	-	Tr	0.35	-	-	0.20	-	-	0.70	0.45	0.40	-	-	-	-	-	-	-			
Apatite	Tr	Tr	Tr	0.25	0.05	Tr	0.35	0.20	0.25	Tr	0.15	0.05	0.15	0.40	0.25	0.15	Tr	1.00	0.75	0.70	0.50	0.20	0.20	Tr	Tr	Tr	0.20	0.70		
Zircon	Tr	Tr	Tr	0.10	Tr	Tr	0.10	Tr	Tr	Tr	Tr	0.15	0.10	0.25	Tr	Tr	Tr	0.25	0.05	0.05	0.05	0.20	Tr	Tr	Tr	Tr	Tr	0.10		
Opalines	-	-	-	-	-	-	-	-	-	-	-	-	-	-	-	0.05	0.05	Tr	-	1.50	0.75	2.70	-	-	2.05	0.11	0.25	0.25	0.05	
Σfelsic	81.20	82.60	83.30	83.35	84.85	85.00	84.85	85.60	85.70	86.60	86.40	86.75	88.70	90.90	94.55	96.90	97.05	78.80	81.45	85.55	90.70	95.40	84.10	86.07	89.80	90.70	91.60			
A+P	51.95	46.95	49.30	56.65	51.85	52.20	65.20	59.45	60.00	57.95	64.25	66.80	68.75	67.45	60.70	70.15	57.80	46.90	52.00	63.25	66.00	63.20	59.70	61.43	69.90	60.54	78.10			
Color index (M')	18.80	17.40	16.70	16.30	15.10	15.00	14.70	14.20	14.05	13.40	13.45	11.60	11.05	8.45	5.20	2.95	2.95	19.95	17.75	13.70	8.75	4.20								

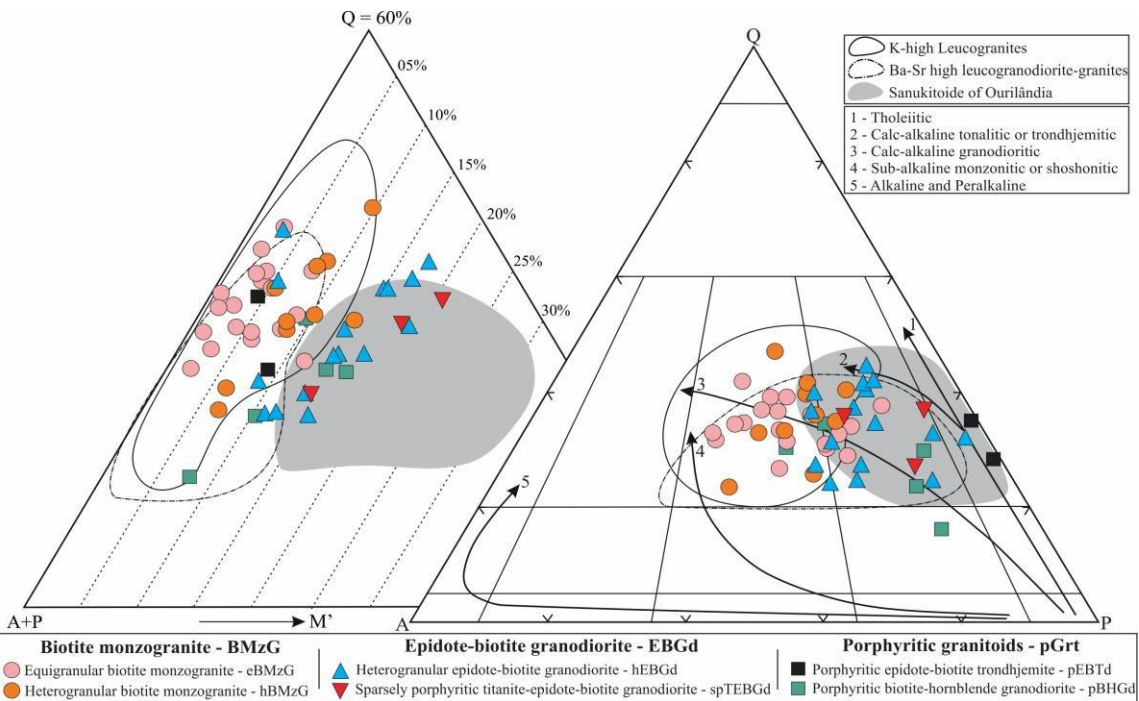


Figure 6 - Q-(A+P)-M' and Q-A-P plots for petrographic classification of the granitoids studied (Le Maitre, 2002). Granitic series and their evolutionary trends from Lameyre & Bowden (1982) and Bowden (1984). Fields for the comparison: K-high leucogranites and Ba-Sr high leucogranodiorite-granites (Almeida et al. 2013); and Rio Maria Sanukitoid Suite of the Ourilândia do Norte area (Santos & Oliveira 2016).

4.2. Mineralogy, microstructural aspects and intracristalline deformation mechanisms

Although the rocks from the different varieties of granitoids identified in this study show some mineralogical and textural differences, they display many petrographic similarity under the microscope, enabling a general description of the microstructural typology of their mineral assemblages (Box 2). The Fig. 7 shows the microstructural aspects of representative samples of the different varieties, collected in the lower strain domains, located in the central portions of the batholiths, whereas Fig. 8 illustrates the deformation microstructures in the higher strain domains, near the batholith borders. The Fig. 9 displays the tardi- to post-magmatic transformation microstructures, common in both higher and lower strain domains.

In the central parts of the plutons, the Ourilândia do Norte granitoids show well-preserved igneous features, where feldspar (Pl_1 and Kfs_1) and mafic (Bt_1 , Hbl_1 and primary accessory) crystals show typical igneous textures, for instance hypidiomorphic equigranular plagioclase and alkali feldspar crystals (e.g. 7a), oscillatory zoning in idiomorphic plagioclase crystal (e.g. 7c) and idiomorphic to hypidiomorphic hornblende and biotite crystals (e.g. 7b, 7k and 7l). However, even the less deformed or undeformed rocks display strain features, such as alkali feldspar phenocryst with intragranular microfractures filled by minerals of the matrix, which indicates deformation in the presence of melt (e.g. 8d; Vernon, 2004). Primary quartz (Qtz_1) crystals often occur as reliquiar cores in core-mantle microstructures, show weak to moderate undulatory extinction, intracrystalline deformation bands and lobated to sutured grain boundary shapes. The mantle is represented for medium- to fine-grained recrystallized quartz (Qtz_2) crystals with sutured or straight grain boundary shapes. In quartz, this sutured shape indicate that the deformation was controlled by high temperature grain boundary migration (GBM) and subgrain rotation (SGR) mechanisms, which suggests high deformation temperature and low differential stress (Hirth & Tullis, 1992). On the other hand, the straight shape evidence grain boundary area reduction (GBAR), responsible by granoblastic polygonal microstructure formation (Blenkinsop, 2000; Passchier & Trouw, 2005).

The batholiths are limited by large-scale shear zones and their borders are marked by development of milonitic foliation characterized by rounded or augen feldspar porphyroclasts, contoured by recrystallized biotite and quartz aggregates (e.g. Fig. 8a). The primary feldspar (Pl_1

Box 2 - Mineralogy and microstructural typology of the Ourilândia do Norte granitoids.

Mineralogy	Microstructure and texture terms are used as synonyms		
Plagioclase	Pl ₁	- Medium to coarse-grained (<8.0 mm), idiomorphic to hypidiomorphic primary crystals; - In spTEBGd, pEBTd and pBHGd varieties it also represents centimetric (0.5-3.0 cm) phenocrysts; - Lobate to sutured or less often straight grain boundary shapes;	- Partially transformed for Ms ₂ and Ep ₂ (saussuritization); - Normal and oscillatory zoning; - Deformation twins; - Soft to moderate undulatory extinction;
	Pl ₂	- Very fine- (<0.1 mm; xenomorphic) to fine-grained (<1.0 mm; hypidiomorphic) subgrains and new grains; - Sutured to lobate grain boundary shapes;	- Straight grain boundary shapes; - Granoblastic polygonal microstructure; - No or gentle undulatory extinction;
	Pl ₃	- Fine-grained (<1.0 mm), idiomorphic to hypidiomorphic solid inclusions within Kfs ₁ ; - Partially transformed for Ms ₂ e Ep ₂ (saussuritization);	- Preferred orientation can occur (magmatic flow?); - No or gentle undulatory extinction;
	Pl ₄	- Fine-grained (<0.5 mm), xenomorphic crystals; - Defines myrmekite texture, together with Qtz ₄ ;	- Associated with the Pl ₁ -Kfs ₁ boundary; - Grows in lobes or colonies replacing Kfs ₁ ;
	Kfs ₁	- Medium to coarse-grained (<8.0 mm), predominantly hypidiomorphic primary crystals; - Lobate to sutured or less often straight grain boundary shapes; - String-type perthitic microstructure;	- Poikilitic microstructure; - Deformation twins; - Soft to moderate undulatory extinction; - Subordinated recrystallization;
	Kfs ₂	- Very fine- (<0.1 mm; xenomorphic) to fine-grained (<1.0 mm; hypidiomorphic) subgrains and new grains; - Sutured to lobate grain boundary shapes;	- Straight grain boundary shapes; - Granoblastic polygonal microstructure; - No or soft undulatory extinction;
	Kfs ₃	- Fine-grained (<1.0 mm), xenomorphic, interstitial primary crystals; - Lobate to straight grain boundary shapes;	- String-type perthitic microstructure; - Deformation twins; - Soft to moderate undulatory extinction;
	Qtz ₁	- Medium to fine-grained (< 3.0 mm), xenomorphic to hypidiomorphic primary crystals; - Bt ₁ , Ttn ₁ , Zrn, Ap and Op solid inclusions;	- Soft to moderate undulatory extinction; - Intracrystalline deformation bands; - Moderate to strong recrystallization;
	Qtz ₂	- Fine-grained (<1.0 mm), xenomorphic to idiomorphic, subgrains and new grains; - Can produce elongated polycrystalline aggregates; - Sutured to lobate grain boundary shapes;	- Straight grain boundary shapes; - Granoblastic polygonal microstructure; - No or soft undulatory extinction;
	Qtz ₃	- Fine-grained (<1.0 mm), xenomorphic or rounded solid inclusions in Kfs ₁ ;	- Curved grain boundary shapes; - No undulatory extinction;
Quartz	Qtz ₄	- Vermicular grain shape giving rise myrmekite texture, together with Pl ₄ ;	- Very fine-grained (<0.1 mm); - Associated with the Pl ₁ -Kfs ₁ boundary;
	Qtz ₅	- Very fine-grained (<0.1 mm), xenomorphic crystals; - Grows, together with Bt ₄ and Ttn ₂ , along the Hbl cleavage;	- Irregular grain boundary shapes; - No undulatory extinction;
	Bt ₁	- Fine-grained (<1.0 mm) hypidiomorphic primary crystals; - Preferred orientation of single crystal or cluster; - Straight to Sutured grain boundary shapes;	- Ttn ₁ , Zrn, Ap and Op solid inclusions; - Partially transformed for Chl and Ttn ₃ ; - Soft to moderate undulatory extinction;
	Bt ₂	- Fine-grained (<0.5 mm), idiomorphic subgrains and new grains - Preferred orientation of cluster often occur;	- Straight grain boundary shapes; - No or gentle undulatory extinction;
	Bt ₃	- Fine-grained (<0.5 mm), predominantly idiomorphic solid inclusions in Kfs ₁ or Pl ₁ ;	- Preferred orientation parallel to major axis of the host crystal (magmatic flow?);
Biotite	Bt ₄	- Very fine-grained (<0.1 mm), xenomorphic crystals; - Grows, together with Qtz ₅ and Ttn ₂ , along the Hbl cleavage	- Irregular grain boundary shapes; - No undulatory extinction;
	Ep ₁	- Very fine-grained (<0.5 mm), idiomorphic to hypidiomorphic primary crystals;	- Zoning can occur; - No or gentle undulatory extinction;
	Ep ₂	- Fine-grained (<1.0 mm), xenomorphic neocrystals, associated, together with Ms ₂ , the calcic plagioclase saussuritization;	- Straight or irregular boundary shapes; - No undulatory extinction;
	Ep ₃	- Very fine-grained (<0.1 mm), xenomorphic crystals - Reaction rim surrounding allanite crystals;	- Irregular grain boundary shapes; - Corona microstructure, with Aln core;
Epidote	Ep ₄	- Very fine-grained (<0.1 mm), hypidiomorphic clinzoisite crystals (only in spTEBGd);	- Straight or irregular boundary shapes; - No undulatory extinction;
	Ms ₁	- Fine-grained (<0.5 mm), idiomorphic to hypidiomorphic primary crystals;	- Straight or irregular boundary shapes; - No or gentle undulatory extinction;
	Ms ₂	- Very fine- (<0.1 mm, sericite) to fine-grained (<1.0 mm) xenomorphic neocrystals, associated, together with Ep ₂ , the calcic plagioclase saussuritization;	- Irregular grain boundary shapes; - Grows often along the cleavage; - No undulatory extinction;
Muscovite	Ttn ₁	- Fine-grained (<1.0 mm), predominantly hypidiomorphic primary crystals;	- Straight or irregular boundary shapes; - No undulatory extinction;
	Ttn ₂	- Very fine-grained (<0.01 mm), hypidiomorphic crystals; - Grows, together with Qtz ₅ and Bt ₄ , along the Hbl cleavage;	- Irregular grain boundary shapes; - No undulatory extinction;
	Ttn ₃	- Very fine-grained (<0.01 mm), hypidiomorphic neocrystals; - Grows, together with Chl, along the Bt ₁ cleavage;	- Irregular grain boundary shapes; - No undulatory extinction;
	Ttn ₄	- Very fine-grained (<0.1 mm), xenomorphic crystals;	- Reaction rim or corona, with Op core;
Titanite	Hbl	- Fine-grained (<1.5 mm), idiomorphic to hypidiomorphic primary crystals (only in pBHGd and hEBGd facies); - Partially transformed to Qtz ₅ , Bt ₄ and Ttn ₂ ;	- Twinning can occur; - Soft to moderate undulatory extinction; - Straight or irregular boundary shapes;
	Ap, Aln, Zrn e Op	- Very fine-grained (<0.1 mm), idiomorphic to hypidiomorphic primary crystals; - Commonly occur associate with Bt ₁ or Hbl;	- Straight or irregular boundary shapes; - No undulatory extinction; - No recrystallization;
Varietal and Accessories	Chl	- Fine-grained (<0.1 mm), xenomorphic neocrystals; - Epitaxial Grows, together with Ttn ₂ , along the Bt ₁ cleavage;	- Irregular grain boundary shapes; - No undulatory extinction;

Legend: PI = plagioclase; Kfs = K-feldspar; Qtz = quartz; Bt = biotite; Ep = epidote; Ms = muscovite; Ttn = titanite; Hbl = hornblende; Ap = apatite; Aln = allanite; Zrn = zircon; Op = opaques; Chl = chlorite.

and Kfs_1) crystals commonly occur as reliquiar cores in core-mantle microstructures. They present weak undulatory extinction and have irregular to sutured grain boundary shapes. The mantle is represented for very fine-grained recrystallized feldspar (Pl_2 and Kfs_2) crystals or less frequently form coarser subgrains and new grains, with sutured or straight grain boundary shapes (e.g. 8b and

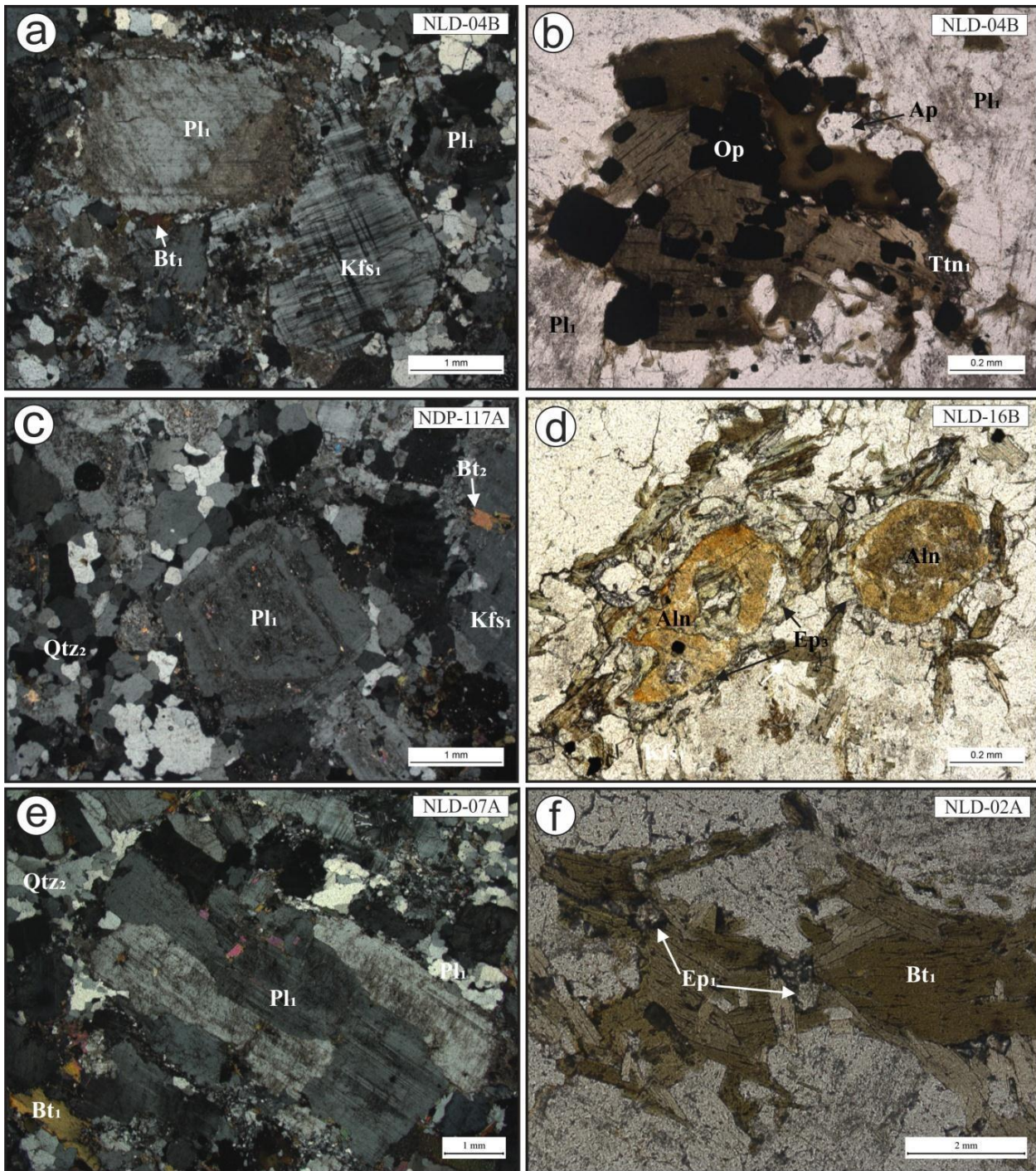


Figure 7 - Microstructural aspects of the granitoids, located in lower strain domains, central portions of the batholiths under study. The photomicrographs show samples of eBMzG variety in (a) and (b), hBMzG in (c) and (d) and hEBGd in (e) and (f). Thus have: (a) plagioclase and alkali feldspar crystals show hypidiomorphic equigranular texture; (b) idiomorphic to hypidiomorphic biotite and opaque crystals; (c) idiomorphic, inequigranular plagioclase crystal exhibiting oscillatory zoning. Note that quartz of the matrix shows granoblastic polygonal microstructure; (d) hypidiomorphic allanite armored by epidote; (e) hypidiomorphic plagioclase crystal display deformation twinning and high temperature recrystallization microstructures, indicating new grain formation in early stage; (f) hypidiomorphic biotite and epidote crystals. Photomicrography (b), (d) and (f) plane-polarized light and (a), (c) and (e) crossed nicois.

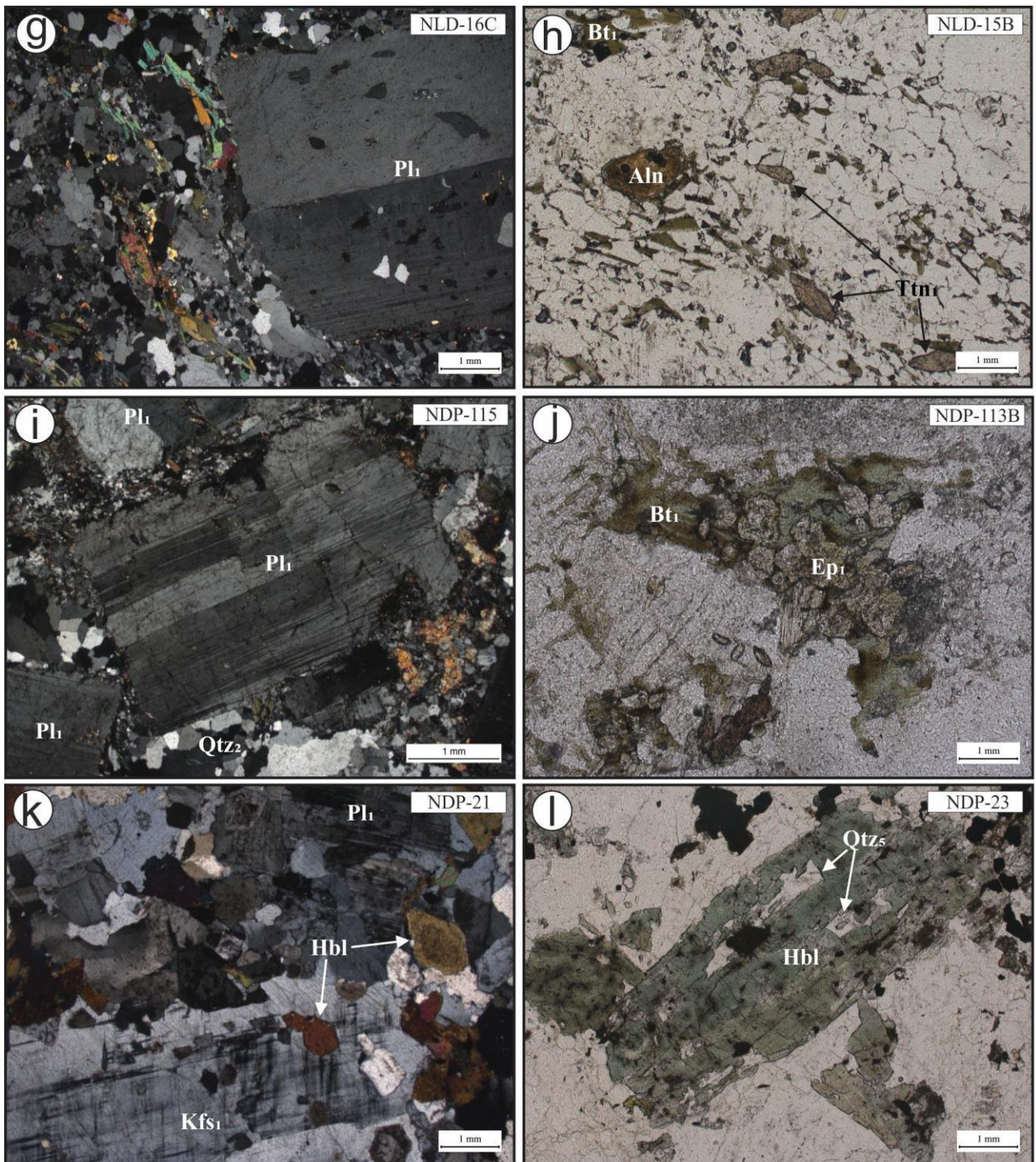


Figure 7 (continued) - Microstructural aspects of the granitoids, located in lower strain domains, central portions of the batholiths under study. The photomicrographs show samples of spTEBGd facies in (g) and (h), pEBTd in (i) and (j) and pBHGd in (k) and (l). Thus have: (g) centimetric, idiomorphic plagioclase phenocryst immersed in fine- to medium-grained matrix. Note that the quartz of the matrix is strongly recrystallized, defining polygonal or sutured granoblastic aggregates. These aggregates combined with titanite and biotite crystals show a foliation of perpendicular direction to the largest axis of the phenocrystal; (h) idiomorphic to hypidiomorphic titanite and allanite crystals; (i) plagioclase phenocrysts display idiomorphic inequigranular texture. Note that the central phenocryst shows deformation twinning and intragranular microcracks, while the quartz of the matrix is strongly recrystallized, defining polygonal or sutured granoblastic aggregates; (j) biotite and epidote primary crystals; (k) centimetric, idiomorphic alkali feldspar phenocryst and idiomorphic hornblende crystals; (l) coarse-grained, idiomorphic hornblende crystals. Photomicrography (h), (j) and (l) in plane-polarized light and (g), (i) and (k) in crossed nicois.

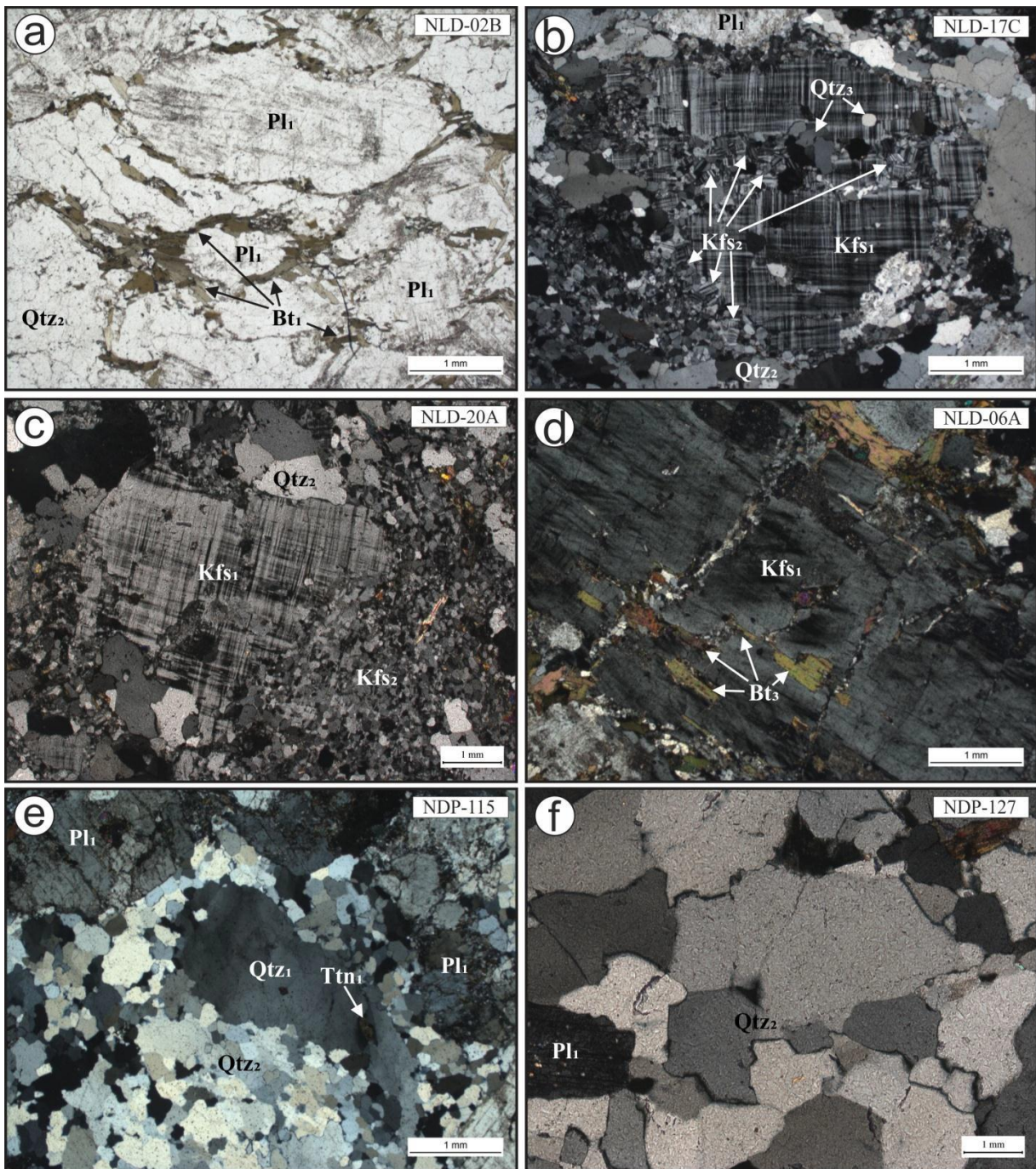


Figure 8 - Deformation, recovery and recrystallization microstructures of the granitoids studied. The samples NLD-20A and NLD-17C are located near the north border of the ellipsoidal shape batholith, in the northern portion of the geological map (Fig. 2); the samples NLD-02B, NDP-115 and NDP-127 are associated with shear zones located near the north border of the arc-shape batholith, in the southern portion of the map; and the sample NLD-06A is located in central domain of the arc-shape batholith. (a) Mylonitic foliation defined by feldspar crystals contoured by biotite and quartz aggregates in rocks of hEBGd facies; (b) core-mantle microstructure in alkali feldspar phenocryst formed by subgrains rotation (SGR) and low temperature grain boundary migration (bulging, BLG) in rocks of the spTEBGd variety; (c) BLG recrystallization in alkali feldspar of sample of the hBMzG facies. Note the presence of granoblastic polygonal microstructure in quartz.; (d) idiomorphic alkali feldspar phenocryst of centimetric size and displaying intragranular microfractures filled by matrix minerals, which indicates deformation in the presence of melt for the granitoids of hEBGd facies. Note the presence of smooth to moderate undulatory extinction; (e) core-mantle microstructure in quartz formed by SGR and high temperature grain boundary migration (GBM), which suggests different dynamic recrystallization regimes for quartz and feldspar; (f) Detail of GBM recrystallization in quartz of granite of the eBMzG variety. The sutured contacts of quartz crystals indicate GBM still in progress and those with straight shape evidence GBAR (grain boundary area reduction) process. Photomicrography (a) plane-polarized light and (b), (c), (d), (e) and (f) crossed nicois.

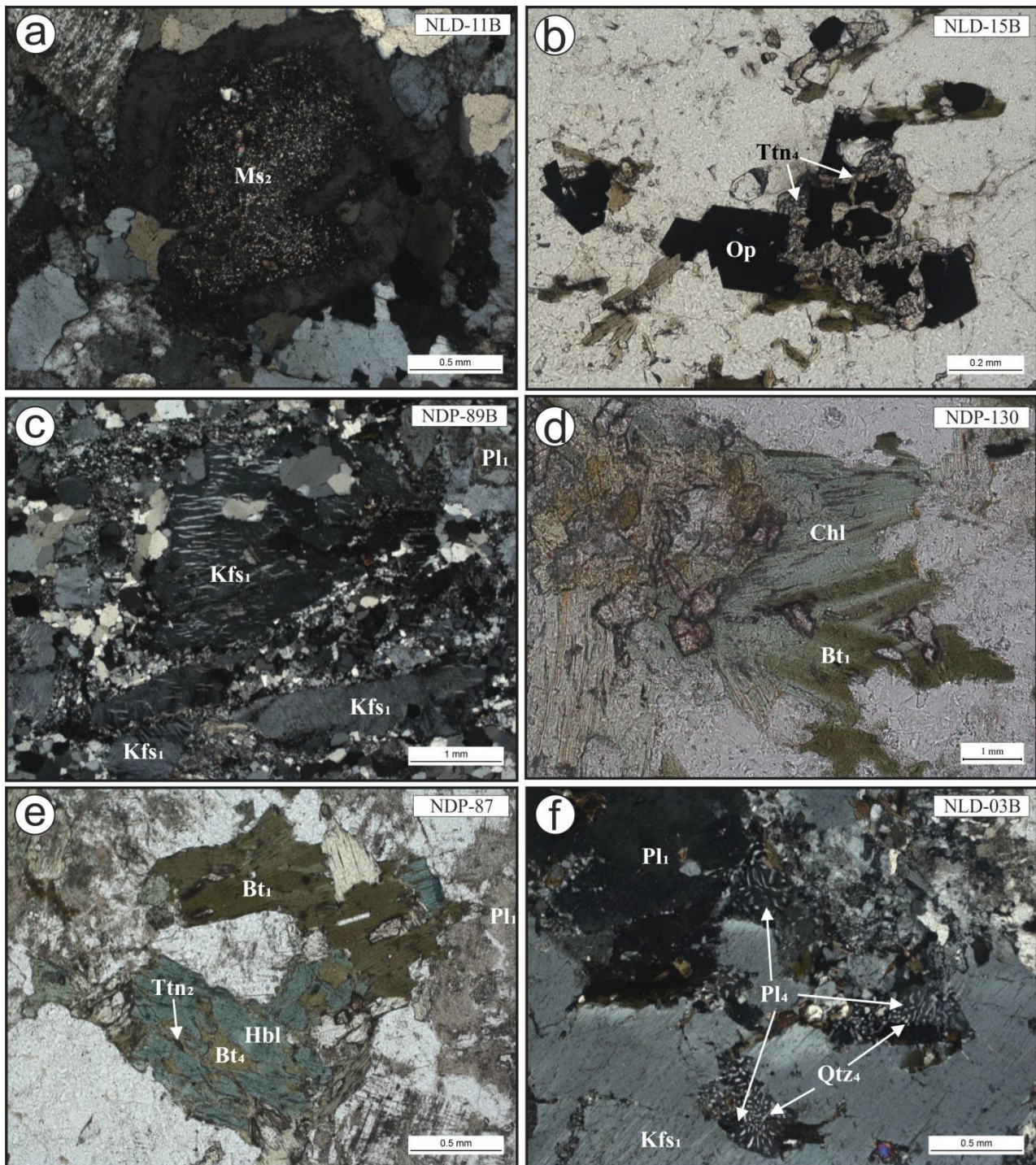


Figure 9 - Tardi- to post-magmatic transformation microstructures of the granitoids under study. (a) saussuritization of the calcic plagioclase, evidencing normal zoning in exemplary of the eBMzG variety; (b) xenomorphic, Fe-Ti oxide crystal armored by titanite in granitoid of the sptEBGd facies; (c) exsolution lamellae in alkali feldspar in specimen of the eBMzG variety.; (d) biotite chloritization commonly observed, in greater or lesser degree of transformation, in all the granitoids of the Ourilândia do Norte area. Note that the growth of chlorite is along the host biotite cleavage; (e) transformation microstructure of hornblende to biotite and titanite in granitoid of the pBHGd variety;(f) myrmekite texture replacing alkali feldspar in rocks of the hEBGd facies. Photomicrography (b), (d) and (e) plane-polarized light and (a), (c) and (f) crossed nicois.

8c). These features indicate that feldspar recrystallization occurred mainly via low temperature grain boundary migration (bulging, BLG) and SGR. In feldspars, these intracrystalline deformation mechanisms mean moderate to high deformation temperature (Passchier & Trouw, 2005). Primary

quartz (Qtz_1) crystals, when present in the more intensely deformed rocks, they are observed as small reliquiar cores in core-mantle microstructures. However, quartz commonly occur as medium-to fine-grained recrystallized (Qtz_2) crystals defining polycrystalline aggregates elongated parallel to the mylonitic foliation (e.g. 8a). The grain boundary shapes of the Qtz_2 crystals generally are sutured or straight (e.g. 8f), which is consistent with high deformation temperature and low differential stress (Hirth & Tullis, 1992). Primary biotite (Bt_1) crystals may be present and often occur chloritized (Fig. 9d). However, due to the higher deformation intensity, the biotite commonly is observed as very fine-grained recrystallized (Bt_2) crystal clusters, with irregular or straight grain boundary shapes. Magmatic (Hbl_1) hornblende, as well as the primary accessory minerals, show predominantly brittle deformational behavior, though Hbl_1 may occur with weak undulatory extinction and subgrain formation.

5. Geochemistry

The geochemical data of the granitoids, summarized in [Table 2](#), comprise 56 whole rock chemical analyses for the different granitoid varieties identified, as follows: (i) 31 samples of the biotite monzogranite group - 23 of eBMzG and 8 of hBMzG facies; (ii) 18 specimens of the epidote-biotite granodiorite - 15 of the hEBGd and 3 of the spTEBGd variety; and (iii) 7 samples of porphyritic granitoids - 2 of the pEBTd group and 5 of pBHGd facies. The analytical methods used for major and trace elements are described in [Appendix A](#). The comparison database contains 256 samples from Carajas Province high-K leucogranites (Almeida et al., 2013; Feio & Dall'Agnol, 2012; Rodrigues et al., 2014; Leite-Santos & Oliveira, 2016) and Carajas Province high Ba-Sr leucogranodiorite-granites (Almeida et al., 2013; Teixeira et al., 2013; Ronaib & Oliveira, 2013; Leite-Santos & Oliveira, 2016), in addition to tonalite-granodiorite associations of sanukitoid affinity from the Ourilândia do Norte area (Santos & Oliveira, 2016).

5.1. Major and trace elements

The granitoids were allocated to three main groups, based on field and petrography criteria (see [Box 1](#) and [Table 1](#)). [Fig. 10](#) and [11](#) show Harker variation diagrams of selected major and trace elements for the different facies of these rocks. Although these varieties may show some common characteristics, their geochemical signatures are distinct. The BMzG rocks are the most evolved of the granitoids identified, where SiO_2 content ranges from 75.9-69.6 wt.% in eBMzG facies to 72.3-69.3 wt.% in the hBMzG. Both varieties display a positive correlation for K_2O and negative for Al_2O_3 , CaO , Fe_2O_3^t , MgO and TiO_2 , with an increase in SiO_2 ([Fig. 10a-f](#)). Despite the wide overlap between the major element contents of these granitoids, the eBMzG variety shows slightly higher K_2O content (5.37-2.47 wt.%) and lower of Al_2O_3 (15.34-12.99 wt.%), CaO (2.22 to 0.87 wt.%), Fe_2O_3^t (3.13 to 0.67 wt.%), MgO (1.05 to 0.07 wt.%) and TiO_2 (0.36 to 0.06 wt.%) compared to hBMzG facies ($\text{K}_2\text{O} = 4.37\text{-}3.83$ wt.%; $\text{Al}_2\text{O}_3 = 14.63\text{-}13.9$ wt.%; $\text{CaO} = 2.09\text{-}1.62$ wt.%; $\text{Fe}_2\text{O}_3^t = 3.40\text{-}2.26$ wt.%; $\text{MgO} = 0.81\text{-}0.47$ wt.%; and $\text{TiO}_2 = 0.44\text{-}0.25$ wt.%). These granites exhibit an increase in Rb and decrease in Ba, Sr, Ni and La with a rise in SiO_2 . The Ba, Sr, Ni and La contents are lower in eBMzG rocks ($\text{Ba} = 1677\text{-}446$ ppm; $\text{Sr} = 824\text{-}127$ ppm; $\text{Ni} = 16.1\text{-}1.6$ ppm; and $\text{La} = 80\text{-}13.7$ ppm) than the hBMzG facies ($\text{Ba} = 1969\text{-}1242$ ppm; $\text{Sr} = 386\text{-}231$ ppm; $\text{Ni} = 14.7\text{-}6.8$ ppm; and $\text{La} = 107\text{-}69.8$ ppm; [Fig. 11a-d](#)). The Rb/Sr and Ba/Sr ratios ([Fig. 11e](#) and [11f](#)) are higher and wider-ranging in the former group ($\text{Rb/Sr} = 1.93\text{-}0.12$; and $\text{Ba/Sr} = 6.72\text{-}1.48$) than the latter ($\text{Rb/Sr} = 0.83\text{-}0.39$; $\text{Ba/Sr} = 6.0\text{-}4.42$). The NLD-05 sample shows depleted anomalous geochemical behavior in K_2O and is enriched in Al_2O_3 , CaO and Na_2O , while the NLD-26A sample exhibits a

Table 2 - Chemical composition of the gneisses studied (major and minor elements are given in percentage and trace in parts per million)

(continued).

Group	Biotite monzogranite - BMzG																				hBMzG							
Facies	eBMzG												hBMzG															
Samples	NLD 04B	NLD 25	NLD 30B	NLD 05*	NLD 06B	NLD 29	NLD 30A	NLD 8	NLD 17B	NLD 27	NDP 07B	NLD 118A	NLD 10A	NLD 18	NDP 89B	NLD 17C	NLD 11B	NLD 16B	NLD 03A	NDP 92B	NDP 93	NLD 11C	NDP 117B	NLD 14	NLD 20A			
SiO ₂	69.56	70.53	71.43	72.04	72.04	72.46	73.05	73.10	73.65	73.66	73.79	73.81	73.92	74.01	74.05	74.33	74.64	74.69	69.30	70.80	71.13	71.20	71.30	71.46	71.60	72.30		
TiO ₂	0.32	0.18	0.31	0.36	0.20	0.20	0.15	0.19	0.13	0.14	0.18	0.17	0.16	0.08	0.11	0.16	0.08	0.14	0.44	0.28	0.33	0.28	0.31	0.25	0.30	0.28		
Al ₂ O ₃	15.31	15.25	14.82	15.95	14.41	14.13	14.53	14.10	14.07	13.96	14.16	13.66	13.93	14.01	13.75	13.75	13.49	13.22	14.50	14.40	14.40	14.63	13.90	14.43	14.00	13.90		
Fe ₂ O ₃	2.74	1.95	2.05	1.04	1.86	1.63	1.21	2.02	1.34	1.44	1.40	1.67	1.37	1.21	1.27	1.52	1.21	1.42	3.40	2.57	2.65	2.54	2.66	2.36	2.54	2.26		
MnO	0.02	0.03	0.03	0.02	0.01	0.03	0.02	0.03	0.03	0.02	0.02	0.01	0.03	0.01	0.03	0.02	0.03	0.01	0.04	0.02	0.02	0.01	0.01	0.05	0.03	0.03		
MgO	0.68	0.74	0.53	0.12	0.44	0.43	0.28	0.43	0.25	0.32	0.27	0.27	0.27	0.25	0.24	0.22	0.18	0.24	0.81	0.57	0.63	0.58	0.60	0.47	0.56	0.47		
CaO	2.22	1.69	1.63	3.34	1.66	1.14	1.35	1.24	1.30	1.35	1.21	1.16	1.17	1.25	1.20	1.10	1.26	1.09	2.09	1.98	1.90	1.62	1.89	1.71	1.83	1.65		
Na ₂ O	4.48	4.19	4.28	5.49	3.71	3.77	4.21	4.13	3.70	3.66	4.18	3.60	3.89	4.04	3.67	3.60	3.72	3.73	3.83	3.94	3.60	3.86	3.73	3.94	3.56	3.67		
K ₂ O	3.30	4.33	4.17	0.70	4.48	4.99	4.44	4.12	4.60	4.57	4.01	4.68	4.45	4.08	4.77	4.77	4.38	4.44	4.05	3.96	4.00	4.37	3.83	4.23	4.18	4.36		
P ₂ O ₅	0.11	0.09	0.13	0.06	0.08	0.06	0.06	0.04	0.04	0.04	0.04	0.03	0.02	0.03	0.04	0.02	0.03	0.17	0.09	0.10	0.08	0.10	0.08	0.09	0.11			
LOI	1.00	0.70	0.40	0.70	0.80	0.90	0.50	0.30	0.70	0.60	0.60	0.70	0.60	0.90	0.70	0.30	0.80	0.80	0.90	1.00	0.90	0.60	1.30	0.70	0.90	0.50		
Total	99.74	99.68	99.78	99.83	99.67	99.76	99.80	99.74	99.81	99.76	99.86	99.77	99.82	99.86	99.82	99.81	99.81	99.81	99.59	99.68	99.66	99.77	99.70	99.68	99.71	99.66		
Ba	1428.00	1334.00	861.00	275.00	1420.00	901.00	800.00	1176.00	598.00	1002.00	771.00	1069.00	653.00	825.00	558.00	1053.00	446.00	877.00	1969.00	1569.00	1690.00	1430.00	1815.00	1242.00	1657.00	1475.00		
Sr	343.80	386.20	292.10	590.40	289.90	241.30	261.10	249.20	197.20	281.40	153.30	167.90	127.50	180.10	182.50	156.60	158.30	151.30	386.60	339.20	311.80	268.00	302.50	231.30	296.70	312.40		
Rb	158.90	116.20	102.80	33.70	149.50	133.80	103.00	175.20	192.40	188.30	211.00	235.20	245.60	223.20	192.50	234.50	170.70	232.80	151.90	151.30	158.80	173.70	157.10	192.20	143.10	152.40		
Zr	13.00	41.00	55.00	130.30	11.00	31.00	30.00	14.00	26.00	32.00	162.20	9.00	140.00	9.00	25.00	156.90	27.00	6.00	48.00	20.00	268.90	236.00	8.00	237.40	48.00	31.00		
Y	11.10	4.10	9.00	17.20	7.60	8.10	4.50	14.60	8.30	8.00	18.20	10.40	21.80	13.40	7.90	11.70	5.90	10.30	22.20	14.90	20.10	15.60	13.80	15.80	15.80	21.20		
Hf	7.50	6.00	4.90	3.50	6.20	5.10	3.90	6.00	3.80	4.80	4.50	5.00	4.10	3.00	4.30	5.50	7.50	4.20	8.00	7.30	6.70	6.00	7.30	6.10	7.00	5.90		
Cr	20.53	13.68	13.68	75.26	13.68	20.53	13.68	13.68	13.68	13.68	13.68	13.68	13.68	13.68	13.68	13.68	13.68	13.68	20.53	13.68	13.68	13.68	13.68	13.68	13.68	13.68		
Ni	9.70	13.90	6.00	8.20	9.40	14.80	5.70	5.50	6.60	5.10	8.30	3.40	4.50	4.10	7.40	1.60	3.00	3.60	14.70	7.90	9.30	7.40	8.50	6.80	18.40	8.80		
Nb	10.40	2.90	5.20	7.10	7.00	5.10	2.60	13.20	5.80	4.50	12.90	8.50	11.90	9.70	4.40	13.40	3.20	9.60	13.60	10.90	8.80	9.10	10.80	8.20	8.50	12.10		
Ta	1.10	1.40	1.00	0.90	1.10	1.70	1.00	2.80	1.50	2.00	1.40	0.90	1.60	2.00	1.80	1.60	0.90	1.10	1.50	1.90	0.70	1.20	1.50	1.10	1.70			
Th	20.50	42.90	29.90	13.40	33.60	36.70	23.10	35.10	38.10	44.60	20.10	38.60	21.70	31.10	29.30	34.10	47.80	30.50	25.50	22.70	22.00	19.50	25.40	22.40	23.50	46.60		
U	2.70	1.10	3.40	1.90	5.30	2.30	3.20	8.50	14.30	8.00	4.50	4.20	4.70	11.90	14.70	8.20	11.0	4.30	3.10	3.90	2.30	3.00	3.80	3.60	1.60	5.30		
Ga	20.70	17.50	19.90	17.70	17.90	17.40	19.60	18.40	18.30	17.40	15.80	17.40	18.80	17.00	16.90	16.50	19.20	19.10	16.60	18.00	19.10	17.80	18.20	18.10				
La	80.00	65.60	49.70	11.90	61.00	68.80	34.30	70.80	41.70	62.00	65.30	51.90	53.40	35.00	31.40	70.10	32.70	36.80	101.40	85.60	89.50	70.20	87.00	117.00	88.40	69.80		
Ce	138.60	98.00	88.80	21.00	101.20	98.00	60.30	118.80	79.50	106.90	112.80	99.00	91.70	59.40	61.50	126.40	59.90	67.40	187.40	145.70	170.00	144.50	148.30	162.90	163.60	128.20		
Pr	14.07	11.68	9.18	2.75	10.22	12.32	6.48	12.68	8.58	11.78	12.66	10.41	9.99	6.01	6.75	13.28	6.76	7.07	20.40	14.79	16.77	14.53	15.42	20.19	17.30	13.38		
Nd	43.50	36.80	30.20	10.10	30.80	40.70	19.40	39.80	27.10	37.20	38.40	32.10	32.60	20.10	23.60	42.10	22.20	22.10	70.30	47.70	55.80	47.00	49.40	60.60	56.60	44.20		
Sm	5.05	4.35	4.98	2.67	3.92	6.06	3.46	4.89	4.87	4.96	6.45	4.47	5.33	2.96	4.22	6.07	3.41	3.60	10.34	6.31	7.31	6.90	6.33	8.12	7.91	7.03		
Eu	0.82	0.66	0.55	0.42	0.59	0.68	0.50	0.53	0.57	0.58	0.72	0.39	0.69	0.47	0.52	0.71	0.51	0.41	1.57	1.00	1.10	0.74	1.08	0.91	1.08	1.14		
Gd	3.98	2.63	3.89	2.33	2.91	4.16	2.55	3.83	3.28	3.43	4.88	3.38	4.77	2.65	3.09	4.17	2.49	2.84	7.91	4.87	5.48	4.65	4.97	5.18	6.36	5.61		
Tb	0.42	0.23	0.47	0.41	0.32	0.41	0.28	0.46	0.38	0.34	0.59	0.40	0.62	0.37	0.34	0.47	0.26	0.36	0.93	0.53	0.61	0.48	0.55	0.67	0.70	0.69		
Dy	2.05	0.88	2.13	2.72	1.61	1.87	1.09	2.43	1.58	1.57	3.26	1.87	3.57	2.10	1.49	2.54	1.20	1.88	4.68	2.59	3.27	2.70	2.71	2.73	3.34	3.57		
Ho	0.38	0.15	0.30	0.58	0.28	0.25	0.16	0.49	0.30	0.22	0.53	0.34	0.63	0.39	0.25	0.42	0.21	0.33	0.79	0.44	0.60	0.42	0.49	0.50	0.58	0.59		
Er	1.05	0.38	0.75	1.77	0.78	0.61	0.38	1.33	0.78	0.64	1.67	0.87	1.94	1.20	0.62	1.31	0.64	0.88	2.22	1.33	1.96	1.37	1.40	1.37	1.34	1.83		
Tm	0.17	0.05	0.09	0.28	0.13	0.08	0.05	0.22	0.13	0.09	0.25	0.14	0.27	0.18	0.10	0.18	0.12	0.13	0.30	0.21	0.31	0.18	0.21	0.20	0.19	0.26		
Yb	1.12	0.37	0.58	1.83	0.85	0.58	0.33	1.49	0.90</																			

Table 2 - Continued.

Group	Biotite monzogranite - BMzG								Epidote-biotite granodiorite - EBGd												Porphyritic granitoids - pGrt											
Facies	eBMzG								hEBGd												spTEBGd				pEBTd				pBHGd			
Samples	NDP 112B*	NLD 23*	NDP 68*	NLD 26A*	NLD 16A*	NDP 100	NLD 11A	NLD 10B	NDP 125	NDP 128	NDP 124	NLD 126	NLD 03B	NLD 06A	NDP 101	NLD 04A	NLD 02B	NLD 07A	NDP 71	NLD 26B	NLD 16C	NLD 15B	NLD 17A	NDP 113B	NDP 115	NDP 87	NDP 84A	NDP 25A	NDP 21	NDP 23*		
SiO ₂	70.60	72.30	73.91	73.09	75.90	66.62	67.52	67.56	67.84	67.94	68.00	68.03	68.20	68.39	68.34	69.04	69.23	69.24	69.29	70.65	66.34	67.65	68.08	71.53	72.66	65.77	66.58	66.88	67.26	67.80		
TiO ₂	0.25	0.22	0.11	0.09	0.06	0.44	0.39	0.39	0.37	0.39	0.38	0.38	0.36	0.37	0.35	0.38	0.36	0.34	0.37	0.34	0.55	0.60	0.54	0.26	0.23	0.41	0.38	0.38	0.36	0.37		
Al ₂ O ₃	14.22	14.16	14.37	15.34	12.99	15.32	14.96	15.18	15.20	15.41	15.18	14.99	15.33	15.18	15.10	15.26	15.55	14.91	15.57	15.55	15.30	15.09	14.90	14.98	14.36	15.74	15.51	15.51	15.65	14.62		
Fe ₂ O ₃	3.13	1.61	0.92	0.90	0.67	3.90	3.37	3.11	3.31	3.09	3.42	3.71	3.24	2.97	3.51	2.54	2.49	2.76	2.22	2.20	4.38	4.02	3.74	1.98	1.74	3.53	3.25	3.13	3.01	3.11		
MnO	0.02	0.02	0.02	0.01	0.01	0.03	0.04	0.03	0.03	0.03	0.03	0.03	0.03	0.03	0.02	0.02	0.02	0.02	0.03	0.05	0.03	0.04	0.01	0.01	0.04	0.04	0.04	0.04	0.05			
MgO	1.05	0.49	0.39	0.27	0.07	2.26	2.14	1.87	1.70	1.84	1.85	1.76	1.73	1.69	1.64	1.80	1.50	1.59	1.04	0.88	1.24	0.93	0.74	1.06	0.99	2.03	1.78	1.75	1.42			
CaO	1.36	1.50	1.51	2.21	0.87	2.89	2.93	2.61	2.42	2.72	2.41	2.44	2.52	2.65	2.91	2.92	2.67	2.43	2.63	2.50	3.03	2.55	2.42	2.55	2.66	3.62	3.43	3.18	3.28	1.83		
Na ₂ O	4.31	3.82	4.77	4.95	3.01	4.54	3.91	4.05	4.01	3.86	3.90	4.22	3.84	4.06	4.36	4.61	4.32	3.96	4.83	5.29	3.84	3.68	3.94	5.48	5.22	4.90	5.01	4.82	5.04	4.53		
K ₂ O	3.88	4.56	3.30	2.47	5.37	2.38	3.43	3.61	3.61	3.21	3.66	2.88	3.64	3.57	2.37	1.81	2.52	3.37	3.10	1.76	3.63	4.28	3.86	1.12	1.01	2.43	2.27	2.79	2.45	4.79		
P ₂ O ₅	0.09	0.08	0.03	0.01	0.01	0.16	0.15	0.14	0.13	0.14	0.13	0.13	0.12	0.12	0.14	0.10	0.12	0.13	0.08	0.28	0.21	0.18	0.08	0.08	0.16	0.14	0.14	0.14	0.15			
LOI	0.70	1.00	0.50	0.40	0.90	1.10	0.80	1.10	1.00	1.10	0.60	1.10	0.70	0.60	0.90	1.20	1.00	0.90	0.50	0.50	0.70	0.40	1.00	0.80	0.90	1.00	1.30	1.00	0.70	0.90		
Total	99.62	99.76	99.83	99.74	99.86	99.65	99.66	99.66	99.63	99.74	99.58	99.68	99.73	99.64	99.64	99.73	99.65	99.70	99.78	99.34	99.44	99.44	99.86	99.87	99.64	99.70	99.66	99.58				
Ba	1568.00	1197.00	869.00	1677.00	524.00	821.00	1333.00	1463.00	1194.00	1173.00	1322.00	889.00	1220.00	1297.00	1147.00	306.00	1011.00	1194.00	1200.00	545.00	3485.00	2877.00	3410.00	170.00	169.00	1456.00	1139.00	1644.00	1171.00	2247.00		
Sr	824.50	348.00	588.50	483.40	137.10	789.20	698.10	756.30	671.70	631.50	634.50	618.30	602.70	723.30	788.40	651.60	598.10	624.30	857.20	571.00	782.70	513.30	585.40	776.70	719.30	965.30	818.90	986.80	985.70	758.10		
Rb	105.90	101.90	74.40	57.20	154.60	124.40	143.90	158.20	186.10	116.80	232.10	205.30	144.60	150.40	134.20	119.30	181.70	171.90	95.30	79.70	126.90	117.70	145.20	62.10	53.90	67.60	72.60	73.10	69.90	159.50		
Zr	132.80	169.60	55.70	75.00	71.20	152.60	125.90	137.50	133.80	132.20	130.80	135.00	110.30	132.60	122.50	147.70	136.10	130.20	114.20	83.70	340.50	455.00	346.40	134.30	114.80	133.70	145.60	131.70	135.90	203.90		
Y	5.10	3.10	2.60	1.50	2.60	8.70	6.30	6.10	5.40	10.80	9.10	13.40	9.40	5.00	5.60	8.40	5.70	8.40	3.30	5.60	22.10	26.70	16.00	6.50	6.90	7.50	6.30	5.70	6.40	7.50		
Hf	4.20	4.70	1.60	2.40	2.50	4.00	3.30	3.50	3.50	4.20	3.20	3.60	3.10	3.80	3.80	4.10	3.80	3.80	3.30	2.30	8.50	11.30	8.40	4.00	3.20	3.60	4.00	3.40	4.00	6.10		
Cr	34.21	13.68	13.68	13.68	13.68	82.10	109.47	88.94	88.94	75.26	129.99	88.94	68.42	68.42	68.42	68.42	75.26	13.68	13.68	20.53	20.53	13.68	34.21	34.21	75.26	61.58	54.73	54.73	54.73			
Ni	16.10	15.70	9.90	31.60	7.00	41.50	45.60	46.20	37.10	39.50	52.60	35.50	37.40	33.70	32.50	44.40	40.20	42.20	10.50	12.10	22.10	11.40	8.80	19.20	15.10	24.40	27.30	20.60	20.70	5.20		
Nb	4.80	2.50	2.00	1.90	1.80	5.50	5.00	4.70	4.20	4.50	4.60	9.80	4.10	6.30	4.70	5.50	7.80	6.30	3.60	4.60	14.70	17.70	14.60	4.80	4.40	3.60	3.90	3.50	3.30	8.90		
Ta	0.40	1.70	0.60	1.70	1.10	0.70	1.00	0.90	0.70	0.80	0.60	1.70	0.70	1.20	0.60	1.00	0.90	1.10	0.40	0.80	1.50	1.50	1.30	0.80	0.50	0.90	0.70	0.60	1.10			
Th	10.80	13.50	8.80	8.40	24.00	7.20	13.10	11.20	10.30	11.30	11.70	12.30	12.50	11.70	8.50	12.50	10.70	14.10	7.70	1.10	30.30	28.50	32.50	12.10	12.80	7.40	6.80	8.30	7.70	27.00		
U	3.30	0.90	3.40	0.20	7.60	1.70	4.60	3.90	2.70	3.50	6.20	4.10	6.40	4.90	3.10	2.50	1.80	6.20	2.70	0.50	2.20	2.60	4.90	1.60	2.20	3.40	2.20	2.20	2.00	5.80		
Ga	21.90	16.60	16.70	16.90	14.00	21.30	22.50	22.60	21.20	20.40	21.30	25.40	19.80	23.90	20.50	23.80	21.90	23.20	19.90	19.60	19.60	18.80	17.50	20.00	19.20	18.70	19.80	17.10				
La	29.40	39.20	13.70	22.60	16.60	23.70	38.90	37.50	27.60	48.00	44.50	65.90	37.80	35.80	29.30	45.10	16.30	35.70	29.80	7.10	124.80	124.60	115.80	27.60	38.00	31.20	30.30	32.00	28.80	51.90		
Ce	57.00	53.60	27.90	39.30	31.40	47.90	69.00	65.60	59.10	71.70	84.90	94.30	69.50	66.40	58.90	83.60	45.20	62.40	59.40	12.50	223.60	241.60	199.10	56.90	74.50	64.10	61.00	65.30	59.00	115.50		
Pr	6.72	6.26	2.66	4.02	3.82	5.52	8.29	7.70	5.80	9.36	9.40	12.40	7.54	7.18	6.60	9.48	3.63	7.45	6.29	1.65	24.03	24.09	20.72	6.61	8.29	7.04	7.03	6.95	6.54	12.12		
Nd	25.80	21.00	9.50	14.30	13.40	21.70	29.10	27.40	20.50	34.20	35.50	44.50	27.80	25.90	24.20	33.50	12.60	26.80	23.10	6.40	83.10	81.20	66.90	25.30	33.00	27.10	25.40	25.40	24.60	44.40		
Sm	4.29	2.45	1.38	1.44	2.03	3.63	4.46	4.05	3.42	5.44	5.55	6.73	4.26	3.99	3.65	4.64	1.97	4.25	3.30	1.67	11.40	11.41	8.95	4.55	5.14	4.74	4.36	4.51	4.05	6.89		
Eu	0.99	0.71	0.37	0.36	0.47	0.94	0.97	0.99	0.93	1.24	1.35	1.43	1.09	0.97	0.93	0.72	0.51	0.93	0.81	0.52	2.09	1.92	1.92	0.97	1.36	1.20	1.06	1.12	1.01	1.63		
Gd	2.91	1.58	1.07	0.97	1.23	2.66	3.05	2.83	2.22	3.78</																						

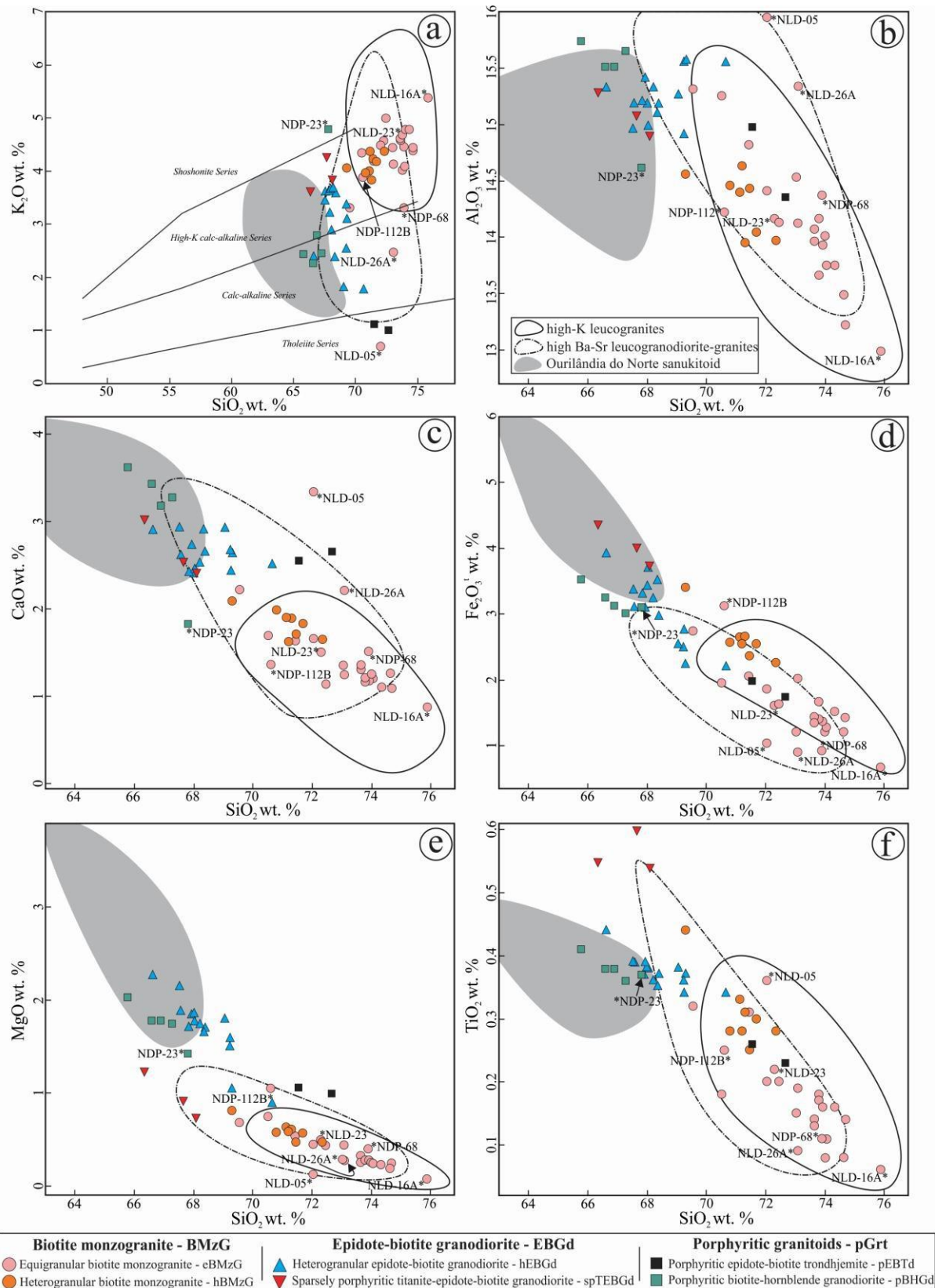


Figure 10 – Major and minor elements Harker diagrams for the Ourilândia do Norte granitoids. (a) K_2O vs. SiO_2 (Peccerillo & Taylor 1976); (b) Al_2O_3 vs. SiO_2 ; (c) CaO vs. SiO_2 ; (d) $Fe_2O_3^t$ vs. SiO_2 ; (e) MgO vs. SiO_2 ; and (f) Na_2O vs. SiO_2 . Data source of the fields for comparison: (i) Carajás Province high-K leucogranites (Almeida et al. 2013; Feio & Dall'Agnol 2012; Rodrigues et al. 2014; Leite-Santos & Oliveira 2016); (ii) Carajás Province high Ba-Sr leucogranodiorite-granites (Almeida et al. 2013; Teixeira et al. 2013; Ronaib & Oliveira 2013; Leite-Santos & Oliveira 2016); and (iii) Ourilândia do Norte tonalite-granodiorite associations of sanukitoid affinity (Santos & Oliveira 2016).

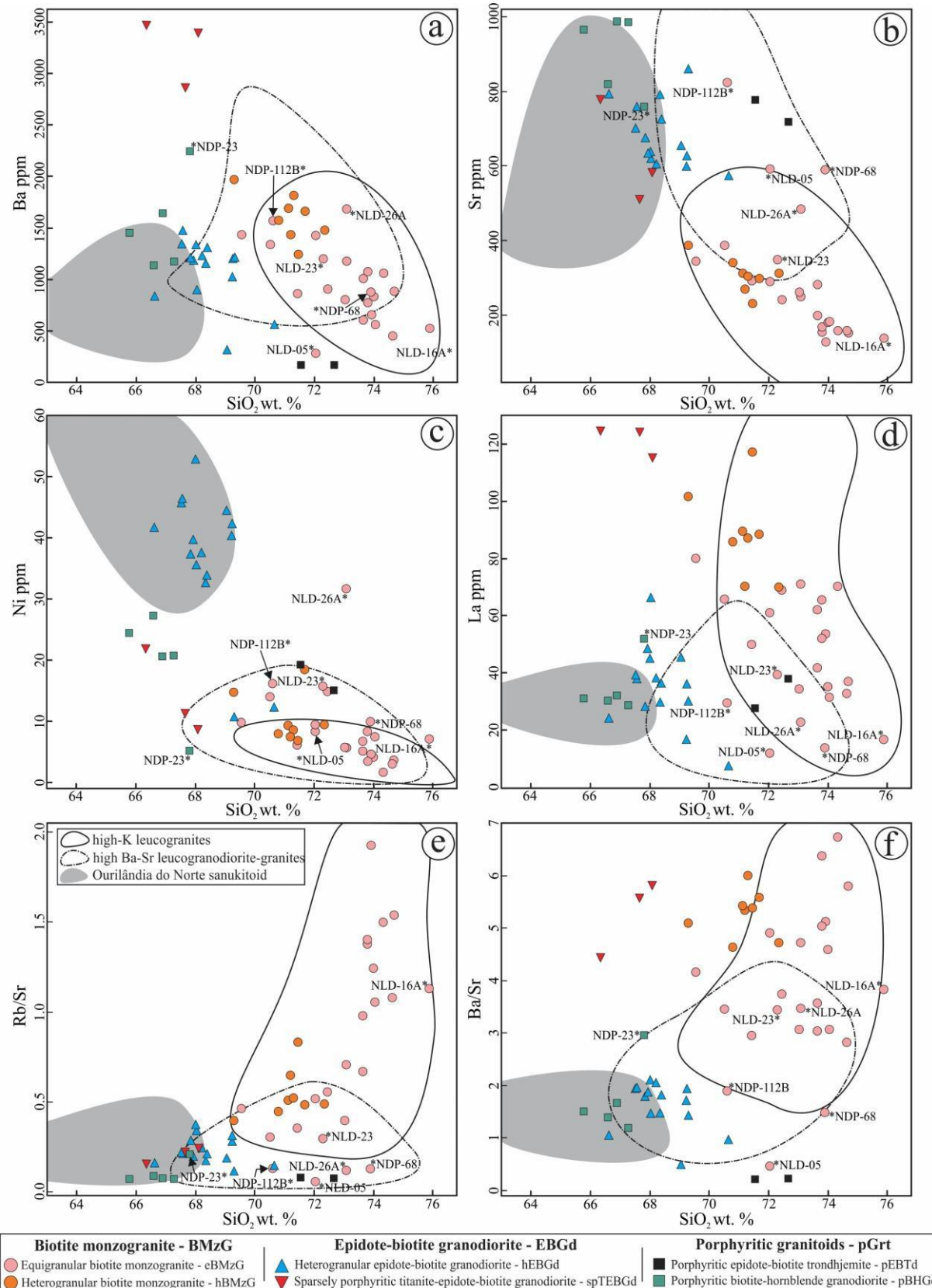


Figure 11 - Trace elements Harker diagrams for the Ourilândia do Norte granitoids. (a) Ba vs. SiO_2 . (b) Sr vs. SiO_2 . (c) Rb vs. SiO_2 (d) Rb/Sr vs. SiO_2 . (e) Ba/Sr vs. Sr. (f) Ba vs. Sr. Data source of the fields for comparison: (i) Carajás Province high-K leucogranites (Almeida et al. 2013; Feio & Dall'Agnol 2012; Rodrigues et al. 2014; Leite-Santos & Oliveira 2016); (ii) Carajás Province high Ba-Sr leucogranodiorite-granites (Almeida et al. 2013; Teixeira et al. 2013; Ronaib & Oliveira 2013; Leite-Santos & Oliveira 2016); and (iii) Ourilândia do Norte tonalite-granodiorite associations of sanukitoid affinity (Santos & Oliveira 2016).

higher mean Ni content (32 ppm) compared to eBMzG (14.8-1.6).

The granitoids of the EBGd group are clearly less evolved than those of the BMzG group, which can be denounced by significantly lower K₂O content, as well as higher Al₂O₃, CaO, Fe₂O₃^t, MgO, TiO₂, Sr and Ni content and Rb/Sr ratio (Fig. 11). The hEBGd and spTEBGd varieties are compositionally distinct and can be easily distinguished from Harker diagrams, where they exhibit a negative correlation for Al₂O₃, CaO, Fe₂O₃^t and MgO with increasing SiO₂, in non-colinear trends. The granitoids of the hEBGd facies display a scattered trend and are more enriched in SiO₂ (70.65-66.62 wt.%), Al₂O₃ (15.57-14.90 wt.%), CaO (2.93-2.41 wt.%) and MgO (2.26-0.88 wt.%) and slightly depleted in K₂O (3.66-1.76 wt.%), Fe₂O₃^t (3.90-2.20 wt.%) and TiO₂ (0.44-0.34 wt.%) when compared to those of the spTEBGd variety, whose SiO₂ content ranges from 68.08 to 66.34 wt.%, whereas those of Al₂O₃, CaO, MgO, K₂O, Fe₂O₃^t and TiO₂ vary between 15.30 and 14.90 wt.%, 3.03 and 2.42 wt.%, 1.24 and 0.74 wt.%, 4.28 and 3.63 wt.%, 4.38 and 3.74 wt.% and 0.60 and 0.54 wt.%, respectively (Fig. 10a-f). In these granitoids, Ba, Sr, Ni and La decresase and Rb increases with a rise in SiO₂ (Fig. 11); however, for samples with the same SiO₂ content, the granitoids of the hEBGd facies are more enriched in Sr (857-571 ppm) and Ni (52-10 ppm) and depleted in Ba (1463-306 ppm) and La (65-71 ppm) in relation to those of the spTEBGd variety (Ba = 3485-2877 ppm; Sr = 782.7-513.3 ppm; Ni = 22.1-8.8 ppm; and La = 124.8-115.2 ppm; Fig. 11a-d). The Rb/Sr ratio values (Fig. 11e) for the rocks of both varieties overlap, but are wider-ranging in the hEBGd facies samples (Rb/Sr = 0.37-0.11) than those of the spTEBGd facies (Rb/Sr = 0.25-0.16). Ba/Sr ratio values (Fig. 11f) are lower for hEBGd facies rocks (Ba/Sr = 2.08-0.47) than those of the spTEBGd variety (Ba/Sr = 5.83-4.45).

The granitoids that constitute the pGrt group are compositionally distinct and can be readily differentiated from Harker diagrams, where SiO₂ contents range from 72.66 to 70.60 wt.% in the pEBTd and 67.80 to 65.77 wt.% in the pBHGd varieties (Fig. 10). The less evolved character of the pBHGd variety is also evidenced by higher contents of Al₂O₃ (15.74-14.62 wt.%), CaO (3.62-1.83 wt.%), Fe₂O₃^t (3.53-3.01 wt.%), MgO (2.03-1.42 wt.%) and TiO₂ (0.41-0.36 wt.%), compared to those of the pEBTd variety (Al₂O₃ = 14.98-14.22; CaO = 2.66-1.36; Fe₂O₃^t = 3.13-1.74 wt.%; MgO = 1.06-0.99 wt.%; and TiO₂ = 0.26-0.23 wt.%) – Fig. 10a-f. In this regard, the former is more enriched in Ni (27-5 ppm), Sr (987-758 ppm) and Ba (2247-1139 ppm) than the rocks with the highest SiO₂ content in this group (Ni = 19-15 ppm; Sr = 824-719 ppm; Ba = 1568-170 ppm), and both varieties show higher Ni and Sr content than those of the BMzG group, with similar Sr and lower Ni and Ba in relation to the EBGd group, hEBGd and spTEBGd varieties, respectively (Fig. 11a-c). The La (52-27 ppm) and K₂O (3.88-1.01 wt.%) contents and Rb/Sr (0.21-0.07) and Ba/Sr (2.96-0.23) ratios are similar in both facies of the pGrt group and clearly lower than those of the BMzG and spTEBGd varieties (Fig. 10a and 11d-f). The NDP-23 sample is anomalously enriched in K₂O and Ba and depleted in Al₂O₃, CaO, and Ni.

5.2. Classification and magmatic series

In the P-Q cationic classification (Fig. 12a; Debon & Le Fort, 1983) and normative feldspar triangle (Fig. 12b; O'Connor, 1965; fields of Barker, 1979) diagrams, the BMzG and EBGd rocks plot predominantly in the (monzo) granite and granodiorite fields, respectively, which is consistent with modal analysis data. Based on these diagrams, the pEBTd and pBHGd (pGrt group) samples tend to reproduce the classification obtained from modal analysis (Fig. 6).

With the exception of the pEBTd variety, all the granitoids studied display affinity with the calc-alkaline series in the K-Na-Ca diagram [Fig. 12c; Nockolds & Allen (1953); trend defined by Barker & Arth (1976)]. On the other hand, in the K₂O vs. SiO₂ diagram (Fig. 10a; Peccerillo & Taylor, 1976), the granites of the BMzG group and the spTEBGd variety can be assigned to a high-K calc-alkaline series, while hEBGd and pBHGd rocks show affinity with the calc-alkaline to high-K calc-alkaline series and the pEBTd variety with the tholeitic series (Fig. 10a).

In the Shand (1943) diagram, the BMzG samples plot in the peraluminous field, with

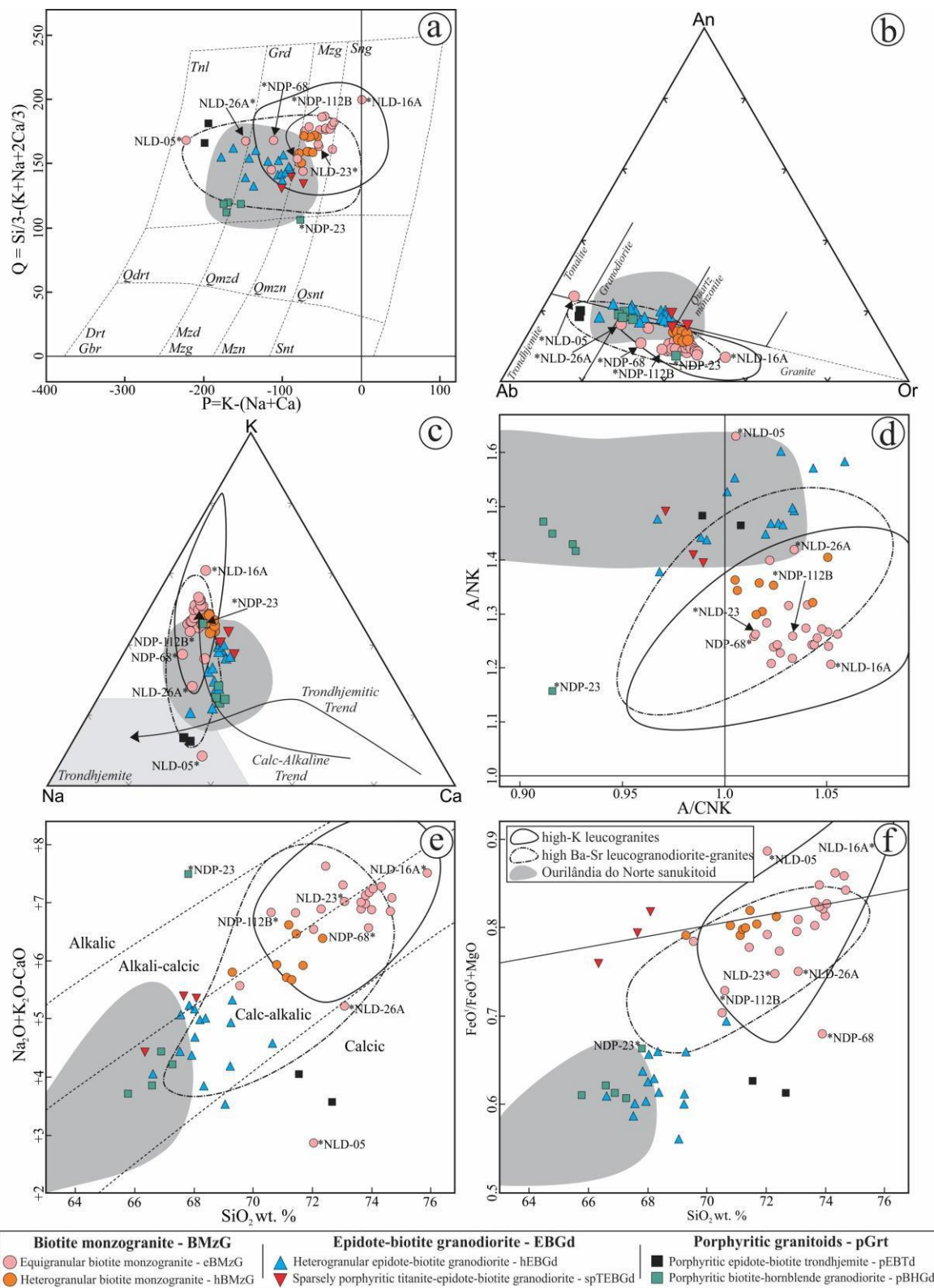


Figure 12 - Geochemical classification and magmatic series plots for the Ourilândia do Norte granitoids. (a) P–Q diagram (Debon & Le Fort 1983); (b) Normative feldspar triangle (O’Connor 1965; fields of Barker 1979); (c) K–Na–Ca diagram, calc-alkaline trend defined by Nockolds & Allen (1953) and trend and field trondhjemite defined by Barker & Arth (1976). (d) A/CNK [$\text{Al}_2\text{O}_3/(\text{CaO}+\text{Na}_2\text{O}+\text{K}_2\text{O})$]mol vs. SiO_2 diagram (Shand 1943); (e) $\text{Fe}^*/\text{FeO} + \text{MgO}$ vs. SiO_2 (Frost et al. 2001); and (f) $\text{Na}_2\text{O}+\text{K}_2\text{O}-\text{CaO}$ (MALI) vs. SiO_2 diagram (Frost et al. 2001). Data source of the fields for comparison: (i) Carajás Province high-K leucogranites (Almeida et al. 2013; Feio & Dall’Agno 2012; Rodrigues et al. 2014; Leite-Santos & Oliveira 2016); (ii) Carajás Province high Ba-Sr leucogranodiorite-granites (Almeida et al. 2013; Teixeira et al. 2013; Ronaib & Oliveira 2013; Leite-Santos & Oliveira 2016); and (iii) Ourilândia do Norte tonalite-granodiorite associations of sanukitoid affinity (Santos & Oliveira 2016).

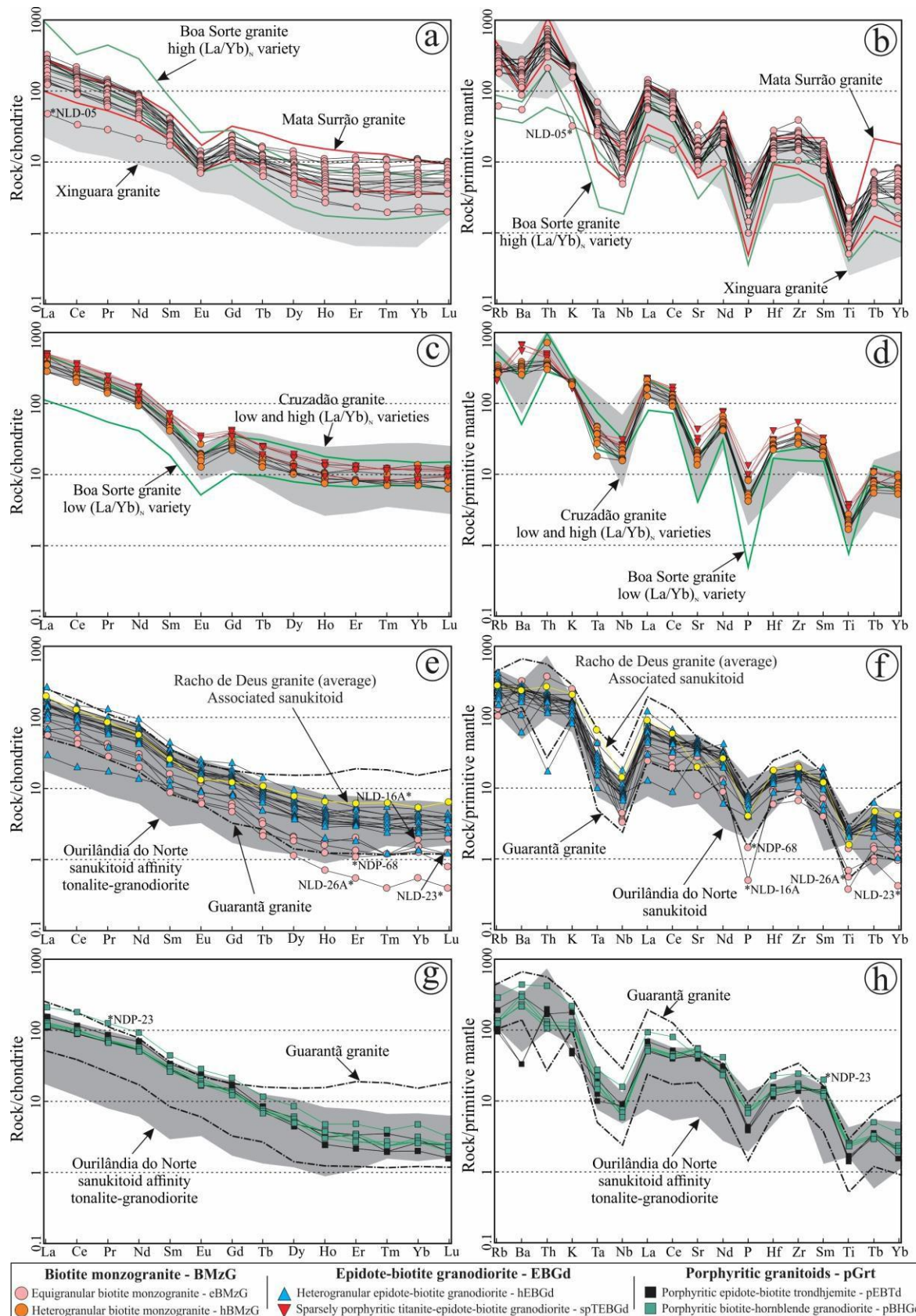


Figure 13 - Chondrite-normalized (Evensen et al., 1978) REE patterns and primordial mantle-normalized (Taylor & McLennan, 1985) spider diagrams. (a) and (b) eBMzG facies; (c) and (d) hBMzG and spTEBGd varieties; (e) and (f) hEBGd group; (g) and (h) pEBTd and pBHGd facies. Data source of the fields for comparison: Xingura, Mata Surrão and Gurantã granites (Almeida et al. 2013); Boa Sorte granite (Rodrigues et al., 2014); Cruzadão granite (Feio & Dall'Agnol, 2012); Velha Canadá granite (Leite-Santos & Oliveira, 2016); Ourilândia do Norte tonalite-granodiorite associations of sanukitoid affinity (Santos & Oliveira, 2016).

A/CNK values [molecular ratio of $\text{Al}_2\text{O}_3/(\text{CaO}+\text{Na}_2\text{O}+\text{K}_2\text{O})$] ranging between 1.06 and 1.01, whereas the hEBGd and pEBTd varieties are meta- to peraluminous, with A/CNK values varying from 1.06 to 0.97, and the spTEBGd and pBHGd rocks are strictly metaluminous, with A/CNK values varying from 0.99 to 0.97 and 0.93 to 0.92, respectively (Fig. 12d). The MALI (alkali-lime index = $\text{Na}_2\text{O}+\text{K}_2\text{O}-\text{CaO}$) vs. SiO_2 diagram (Fig. 12e; Frost et al., 2001) shows that the granites of the BMzG group and the spTEBGd variety have calc-alkalic to alkali-calcic affinity, while the remaining granitoids present overall calc-alkalic character, except pEBTd rocks, which display a calcic tendency. According to the iron index diagram (Fig. 12f; Frost et al., 2001), the BMzG and spTEBGd varieties range from magnesian to slightly ferroan, with Fe^* [$\text{FeO}^\text{t}/(\text{FeO}^\text{t}+\text{MgO})$] values between 0.90 and 0.70, whereas hEBGd and porphyritic granitoid (pEBTd and pBHGd) samples plot in the magnesian field with significantly lower Fe^* values (0.69-0.56) than previously reported.

5.3. Rare earth and multi-elements patterns

Trace element concentrations (Table 2) are reported in chondrite-normalized REE patterns and primitive mantle-normalized multi-element diagrams (Fig. 13). The varieties belonging to the BMzG group show slightly distinct rare earth and multi-element patterns. Granites from the eBMzG facies have moderately fractionated rare earth element (REE) patterns (Fig. 13a), defined by relative enrichment in light REEs (LREE) and depletion in heavy REEs (HREE), as indicated by values of the $(\text{La/Yb})_\text{N}$ ratios ranging from 169.4 to 18.60. These rocks also exhibit a moderate negative Eu anomaly ($\text{Eu/Eu}^*=0.60-0.31$) and smooth concave shape in HREE, which may suggest amphibole fractionation during their magmatic evolution. The NLD-05 sample shows an anomalous pattern with marked LREE impoverishment and the lowest $(\text{La/Yb})_\text{N}$ (4.39) ratio. In the primitive mantle normalized spidergram, these granites display moderate to strong negative Ba-Nb-Ta-Sr-P-Ti anomalies (Fig. 13b). On the other hand, rocks from the hBMzG facies exhibit a less fractionated REE pattern with values of the $(\text{La/Yb})_\text{N}$ ratios of 57.64-29.08 and weakly negative Eu anomaly ($\text{Eu/Eu}^*=0.59-0.40$) – Fig. 13c. In addition, these granitoids display less pronounced negative Nb-Ta-Sr-P-Ti anomalies than those of the eBMzG facies (Fig. 13d).

The granitoids that constitute the EBGd group exhibit significantly distinct REE and multi-element patterns, whereas those of the spTEBGd variety are similar to the hBMzG granitoids, although they show lower $(\text{La/Yb})_\text{N}$ ratios (55.04-40.63), a much weaker negative Eu anomaly ($\text{Eu/Eu}^*=0.74-0.65$), fewer negative Nb-Ta-Sr-P-Ti anomalies and a slightly positive Ba anomaly (Fig. 13d). In turn, the hEBGd variety, as well as samples of the pGrt group (pEBTd and pBHGd varieties), are markedly impoverished in overall REE content ($\sum \text{REE} = 235.08$ to 34.01 ppm and 241.45 to 127.92 ppm), with nearly constant $(\text{La/Yb})_\text{N}$ ratios (91.43 to 11.15 and 60.13 to 38.81, respectively) and slightly negative to absent Eu anomalies ($\text{Eu/Eu}^*=1.10$ to 0.79 and 1.01 to 0.79, respectively) - Fig. 13e,g. Furthermore, the hEBGd, pEBTd and pBHGd varieties display moderately negative Nb-Ta-P-Ti and slightly positive Ba and Sr anomalies (Fig. 13f,h). Martin et al. (2005) suggest that moderate negative Nb-Ta-Ti anomalies indicate the presence of amphibole and/or iron and titanium oxides as residual phases, whereas P and Th are related to low apatite and zircon content, respectively. The NLD-16, NLD-23 and NDP-68 samples show ambiguous behavior and are akin to granites from the eBMzG facies; however, their REE pattern is similar to those of the hEBGd variety and pGrt group, with a concave shape in HREE (Fig. 13e).

6. Discussion

6.1. Petrogenesis and magmatic evolution

According to Almeida et al. (2013), the three most common types of Mesoarchean granites of calc-alkaline affinity exposed in the Rio Maria domain are potassic leucogranites (Xinguara and Mata Surrão granites), the leucogranodiorite-granite group (Guarantã suite and similar rocks) and

amphibole-biotite monzogranites (Rancho de Deus granite). An association of high-Mg diorite-granodiorite ± granite was collectively termed the Rio Maria sanukitoid suite (Oliveira et al., 2009; Santos & Oliveira, 2016). In contrast to this terrane, the Canaã dos Carajás domain is broadly dominated by high-K leucogranites (e.g. Cruzadão and Boa Sorte granites). Geochemical modelling suggests that the three granite groups cannot be derived from a common precursor magma (Almeida et al., 2013; Feio & Dall'Agnol, 2012). In Figs. 10, 11, 12 and 13, the major and trace element contents of the granitoid group samples identified in the Ourilândia do Norte area are compared to the compositions of these three granite groups and sanukitoid rocks.

The Mesoarchean Ourilândia plutons consist of granodiorites and monzogranites with subordinate trondhjemites. Petrography and whole-rock major and trace element compositions of these granitoids are similar to those of collisional “magnesio-potassic”(Mg-K) and “ferro-potassic”(Fe-K) suites. Both Mg- and Fe-rich groups are alkali-calcic to calc-alkaline and differ in their FeO^t/MgO ratio, Al_2O_3 , K_2O and some trace elements (Sr, Ba, Rb). The origin of the Mg-K suites is better understood, which requires only metasomatized mantle (Heilimo et al., 2010; Laurent et al., 2014a; Santos and Oliveira, 2016). In contrast, there is no consensus about the petrogenesis of the Fe-K associations, with models ranging from melting of juvenile lower crust (Duchesne et al., 2010), old felsic crustal lithologies (Tagne-Kamga, 2003), metasomatized mantle (Ferré et al., 1998) or two contrasted sources involving enriched sub-continental lithospheric mantle and asthenospheric mantle (Laurent et al., 2014b).

6.1.1. Biotite monzogranite

The eBMzG and hBMzG rocks (BMzG group) have high *Fe and low Mg# values (Figs. 12f and 14a), and can be assembled into the Fe-rich or Fe-K group. They exhibit modal and geochemistry compositions akin to Archean potassic calc-alkaline leucogranites identified in other areas of the Carajás province that are interpreted as the product of crustal anatexis of TTG-type rocks in the plagioclase stability zone (<1.0 GPa) (Almeida et al., 2013; Feio & Dall'Agnol, 2012), as evidenced by their moderate to pronounced negative Eu and Sr anomalies (Fig. 13a,c). In addition, the major element compositions of these granites are consistent with those of experimental melts derived from tonalites (Fig. 14c). The BMzG granitoids show internal compositional variation, suggesting that their magmas evolved through fractionated crystallization controlled by plagioclase (Fig. 14d), K-feldspar and biotite (Fig. 14e).

Despite the fact that the hBMzG variety shows compositional similarity to eBMzG rocks, their REE and multi-element patterns reveal greater affinity with those of the spTEBGd variety (Fig. 13c,d). The field relationships and the slightly less evolved aspect of the hBMzG variety in relation to eBMzG rocks suggest that the generation of hBMzG rocks likely involves some degree of mixing between eBMzG and spTEBGd magmas. This hypothesis is reinforced by the spatial distribution of these granitoids, which are mingled synplutonically (Fig. 4b,f), and the presence of oscillatory zoning in the plagioclase of the hBMzG variety (Fig. 7c). A model based on binary mixing can be seen through normalized REE and multi-element diagrams, suggesting a mixture of 60% spTEBGd (NLD-15B sample) and 40% eBMzG (NLD-18 sample) to explain the origin of the hBMzG granites (Fig. 15a,b).

6.1.2. Titanite-rich biotite granodiorite

The presence of varietal titanite combined with high LILE and REE content, and the slightly fractionated patterns with moderate negative Eu anomaly, indicate that spTEBGd rocks had a felsic parental magma. However, the large number of microgranular mafic enclaves (Fig. 4g) and the high modal content of mafic minerals ($M' = 8.45\text{--}19.95\%$) suggest that a mafic component likely participated in the origin of these rocks. The discriminant diagram of trace elements (Fig. 14b)

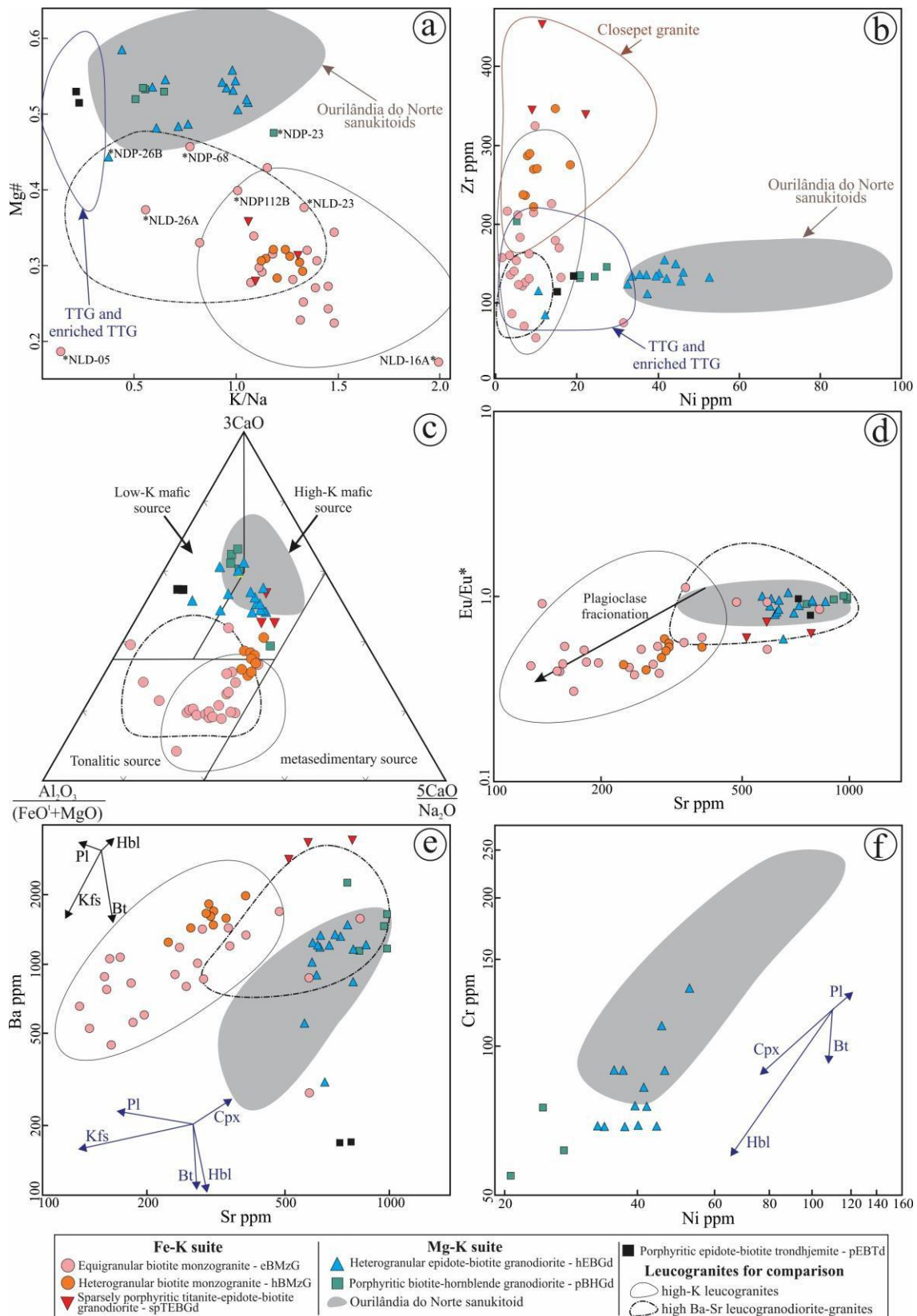


Figure 14 - Petrogenetic aspects and magmatic evolution of the Ourilândia do Norte granitoids. (a) Mg# ($MgO/(MgO+FeO^t)_{mol}$) vs. K/Na (Moyen et al., 2003a); (b) Zr vs. Ni with closepet granite and TTGs fields for comparison (Moyen et al., 2003a); (c) Petrogenetic classification diagram with fields determined from major-element compositions of experimental studies (Laurent et al., 2014a); (d) Eu/Eu* vs. Sr; (e) Ba vs. Sr; and (f) Cr vs. Ni. Distribution coefficients are mainly from Rollison (1993) for granitic composition (black vector) and Villemant et al. (1981) for mafic composition (blue vector). Abbreviations: Pl = plagioclase, Kfs = alkali feldspar, Bt = biotite, Cpx = clinopyroxene e Hbl = hornblende.

shows that spTEBGd samples have a clear affinity with Closepet-type granites (denominated high-Mg and high-K granites) from the Dharwar Craton (Moyen et al., 2003a). These rocks exhibit several petrographic [granodiorites, highly porphyritic, with large (2–5 cm) K-feldspar phenocrysts and abundant accessory minerals including titanite] and geochemical [LILE enriched (such as K, Ba and Sr), moderate MgO, Cr and Ni, high HFSE (such as Ti, Zr and Y) and REE contents] similarities. In addition, large, dioritic to monzonitic enclaves with rare K-feldspar phenocrysts, are found within the spTEBGd, which are analogous to those considered comagmatic from Closepet-type granites (Jayananda et al., 1995). Thus, to explain the moderate LILE enrichment ($Ba + Sr < 1000$ ppm) of the mafic enclaves associated with Ourilândia granitoids, their mafic parent magma would be generated at shallow depths from a fluid-metasomatized mantle (fluid-assisted flux melting) in a subduction environment (Santos & Oliveira, 2016).

Close compositional similarities between spTEBGd and Closepet-type granites strongly suggest a petrogenetic analogy (high- Ti and Ba magmas), which can be formed by partial melting of an enriched mantle source (Moyen et al., 2003a) or high-K mafic source (Fig. 14c; Laurent et al., 2014a). Subsequent melting of this enriched mantle (probably in a post-subduction setting) gave rise to uncommon high-HFSE, Mg, REE and K magmas. As demonstrated for the Closepet Granite (Dharwar Craton), a hot mantle-derived magma can induce continental crust melting and mix with the anatetic products (Moyen et al., 2003a).

6.1.3 Biotite granodiorite and porphyritic granitoids

In contrast to the Fe-K granitoid group, the hEBGd and porphyritic granitoid (pEBTd and pBHGd) varieties have low Fe^* and high $\#Mg$ values, showing remarkable sanukitoid affinity (Mg-K suite) (Figs. 12f and 14a,b). The granodiorite rocks (hEBGd and pBHGd) are more enriched in MgO, Ni and Sr and more depleted in FeO, K_2O , TiO_2 , Ba and HREE, when compared to their spTEBGd counterparts, and resemble only those most impoverished in SiO_2 (< 70 wt.%) from the high Ba- and Sr-enriched leucogranodiorite-granite group (Guarantã suite) of the Carajás province (see aforementioned diagrams). Accordingly, considering that the proposed model to explain the origin of the Guarantã suite granitoids involves mixing between a Ba- and Sr-enriched granite magma and trondhjemite liquids, generating rocks with a wide variation in SiO_2 content (68.20 to 73.14 wt%) (Almeida et al., 2013), it is assumed a minimum or no participation of magma akin to TTG rocks in the hEBGd and pBHGd granitoid genesis. The normalized REE and multi-element patterns show the chemical affinity between them and Rancho de Deus granite (Fig. 13e-h), an amphibole-bearing monzogranite generated by fractional crystallization and differentiation of sanukitoid magmas enriched in Ba and Sr (Almeida et al., 2013), which may further indicate their petrogenetic links with sanukitoid magmas.

The behavior of some major (e.g. MgO, Fe_2O_3 and TiO_2) and compatible trace (e.g. Ni and Cr) elements from the hEBGd and pBHGd sample groups does not represent collinear trends, suggesting the existence of distinct parental liquids and/or different processes responsible for their origin and evolution. The hEBGd samples form linear continuous trends with Rio Maria sanukitoids, overlapping the field relative to its more evolved rocks, which strongly suggests that these rocks are ultimately related through fractional crystallization processes. The Rayleigh mineral fractionation modeled for the Cr-Ni vector diagram (Fig. 14f) indicates that the hEBGd variety could have been produced by intense fractionation of hornblende \pm clinopyroxene and biotite during the evolution of the Rio Maria sanukitoid, justifying its greater impoverishment in HREE compared to Rancho de Deus granite. Furthermore, the Eu/ Eu^* vs. Sr diagram (Fig. 14d) shows that during the evolution of the Mg-K rock groups, the Eu/ Eu^* ratio remained constant with increasing Sr contents, which is not compatible with plagioclase fractionation. Despite the fact that the pBHGd variety shows affinity with these petrological features, its rocks are distinguished from those of the hEBGd group for presenting a slightly less evolved character which are more depleted in SiO_2 and K_2O and enriched in CaO, even though Ni and Cr content are contradictorily lower in a context of

magmatic evolution by fractional crystallization of the sanukitoid magma. Thus, the frequent presence of partially digested microgranular mafic enclaves suggest a more complex process to explain the ambiguous geochemical features of the pBHGd rocks (Fig. 3h). A petrogenetic model that combines this geochemical behavior and textural aspects is shown through normalized REE

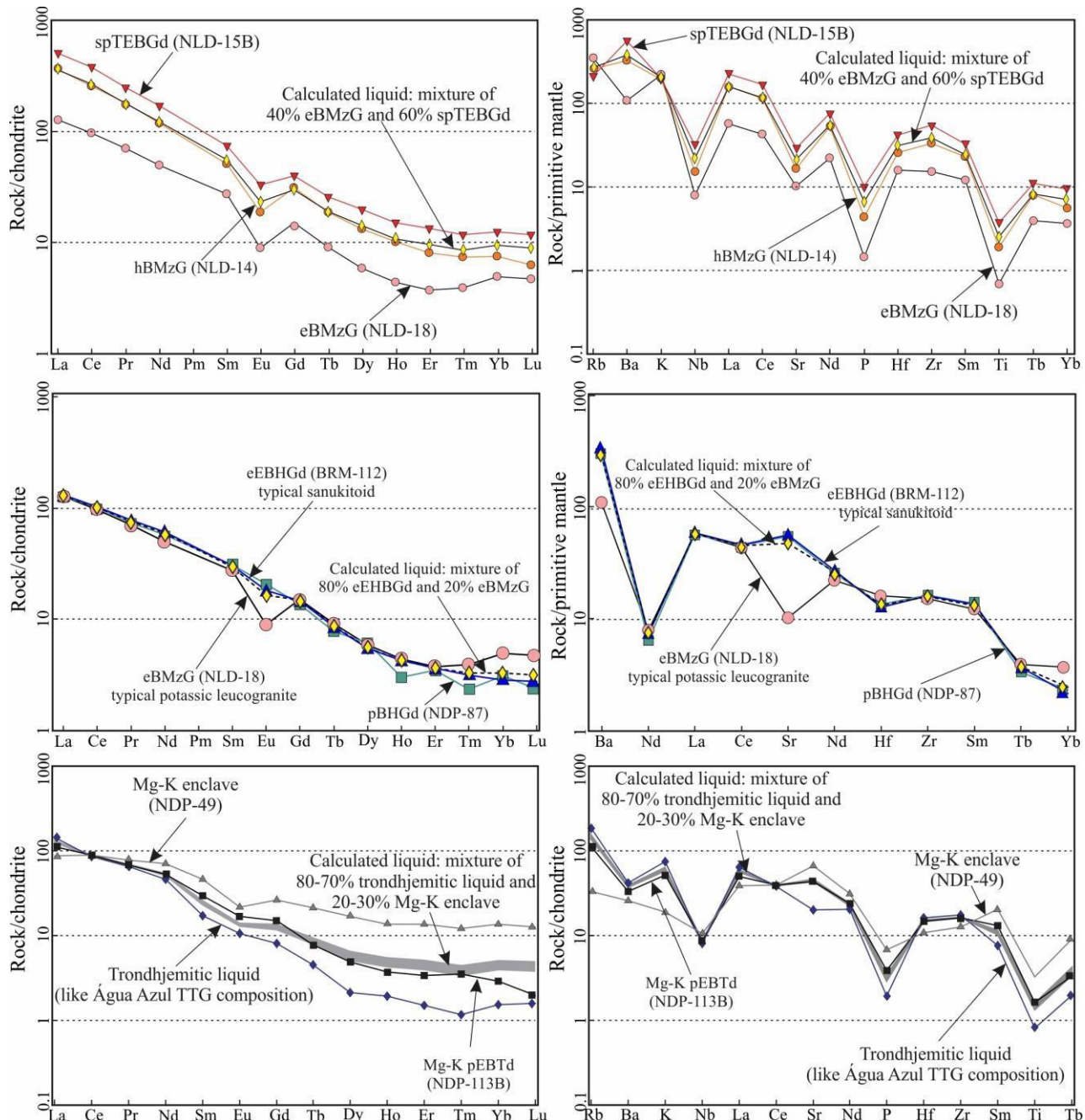


Figure 15 - Binary mixing model for Ourilandia do Norte hybrid granitoids in Chondrite-normalized (Evensen et al., 1978) REE and primordial mantle-normalized (Taylor & McLennan, 1985) multi-elements diagrams. The calculations were performed using the $X_M = X_A \cdot f + X_B \cdot (1-f)$ equation, wherein X_A and X_B are the concentration of trace elements in the end members of the mixing, X_M is the content of trace element in the calculated mixture and f an index described by $A/(A+B)$. (a) and (b) model for the origin of the hBMzG granites (NLD-14 sample) from the mixture of 60% spTEBGd (NLD-15B sample) and 40% eBMzG (NLD-18 sample); (c) and (d) model for the formation of pBHGd rocks (NDP-87 sample) from the mixture of 80% eHBGd (BRM-112 sample) and 20% eBMzG (NLD-18 sample); and (e) and (f) model for the formation of trondhjemite (NDP-113B sample) from the mixture of 70-80% TTG-type melt (trondhjemitic liquid like TTG of the Água Azul do Norte area; the EDC-10 sample was used for modeling) and 20-30% mafic enclave (NDP-49 sample).

and multi-element diagrams (Fig. 15c,d), which depict the results of the binary mixture, modelling between 80% sanukitoid (BRM-112 samples) and 20% leucogranite (NLD-18) to explain the origin of the pBHGd variety.

The chemical composition of the trondhjemite variety (pEBTd) is very similar to that of typical TTG granitoids; however, they are slightly more enriched in Sr, #Mg and Ni. Their textural features resemble those identified in the other porphyritic variety (Fig. 3g). The small, scattered, equant subrounded mafic microgranular enclaves (blob of coeval magma that has sharp contact with its host) are the most common heterogeneities present in the pEBTd rocks. Thus, within a model in which mafic rocks have mingled and mixed synplutonically with granitic rocks, we hypothesize that the Ourilândia do Norte Mg-Na granitoids (pEBTd) likely derived from incomplete mixing of 70-80% TTG-type liquid, akin to 2.93 Ga Água Azul do Norte trondhjemite (Santos, 2017), and 30-20% mantle-derived magma (Fig. 15e,f) represented by diorite enclaves generated from a fluid-metasomatized mantle at shallower depths (Santos & Oliveira, 2016). This model contends that 2.87 Ga trondhjemite liquid would be the product of partial melting of a low-K mafic source (Fig. 14c; Laurent et al., 2014a), under the base of thickened metavolcanic piles, caused by the ascension mantle-derived magmas and consequent crust underplate (Almeida et al., 2013, Oliveira et al., 2011). The mingling relationships established the contemporaneity between all the Ourilândia do Norte granitoids, including those of sanukitoid and BADR (enclaves) signatures, suggesting that significant crustal growth and recycling occurred during the final phases of stabilization of the first Mesoarchean orogenic cycle registered in the Carajás province.

6.2. Microstructural considerations

6.2.1. Deformation temperature

Laboratory experiments and observation of naturally deformed minerals have generated a large amount of information about the temperature and pressure conditions under which these minerals were deformed and recrystallized, mainly quartz, feldspars and micas (Tullis, 1983; Tullis & Yund, 1985, 1987; Kronenberg et al., 1990; Hirth & Tullis, 1992; Kohlstedt et al., 1995; Blenkinsop, 2000; Vernon, 2004; Passchier & Trouw, 2005). The creep microstructures and intracrystalline deformation mechanisms identified in Ourilândia do Norte granitoids allowed to investigate the effects of temperature and strain rate on the structural control of magma emplacement by regional deformation. The deformation history of these rocks is represented by a sequence of submagmatic to subsolidus microstructures resulting from intracrystalline plasticity: (i) undulatory extinction in primary crystal; (ii) deformation bands; (iii) subgrains; (iv) new grains; (v) core-and-mantle microstructure; (vi) undulatory extinction in new grains; (vii) subgrain formation from new grains; and (viii) granoblastic polygonal microstructure in quartz ± feldspars. All primary phases exhibit intragranular microcracks. The occurrence of intragranular microfractures in feldspars filled by residual minerals petrographically continuous with the igneous groundmass indicate deformation in the presence of melt (e.g. 8d; Blenkinsop, 2000; Vernon, 2004). Furthermore, the coexistence of deformation and melt can be ratified by the occurrence of biotite and primary accessory crystals trapped within the feldspar microfractures (Bouchez et al., 1992; Blenkinsop, 2000; Passchier & Trouw, 2005).

Temperature is not the only factor that determines deformation behavior in quartz, since it also depends strongly on strain rate, differential stress and the presence of water in the lattice and along grain boundaries (Kronenberg, 1994; Luan & Paterson, 1992; Gleason & Tullis, 1995; Kohlstedt et al., 1995; Post et al., 1996). The quartz crystals of the three granitoid groups indicate that their dynamic recrystallizations occurred mainly by subgrain rotation (SGR) and high temperature grain boundary migration (GBM) (Fig. 8e and 8f), followed by grain boundary area reduction (GBAR), which is illustrated by the granoblastic polygonal microstructures and suggests post-deformation static recrystallization. These observations indicate that quartz recrystallization

was controlled by regime 3 of Hirth & Tullis (1992) and occurred at higher temperatures ($>500^{\circ}\text{C}$, Fig. 16) and lower strain rate, differential stress and dislocation density. This recrystallization regime is characterized by core-and-mantle microstructures, which often define a planar fabric. Paterson et al. (1989), Blenkinsop (2000) and Vernon (2004) indicate that GBM recrystallization in quartz, although not proving deformation in the presence of melt, may suggest continuity between magmatic and high-temperature solid-state deformation. Stipp et al. (2002) report that at higher temperatures (above 700°C), the rapid recovery and recrystallization of quartz give rise to new grains with strain-free appearance, which is commonly observed in the Ourilândia granitoids.

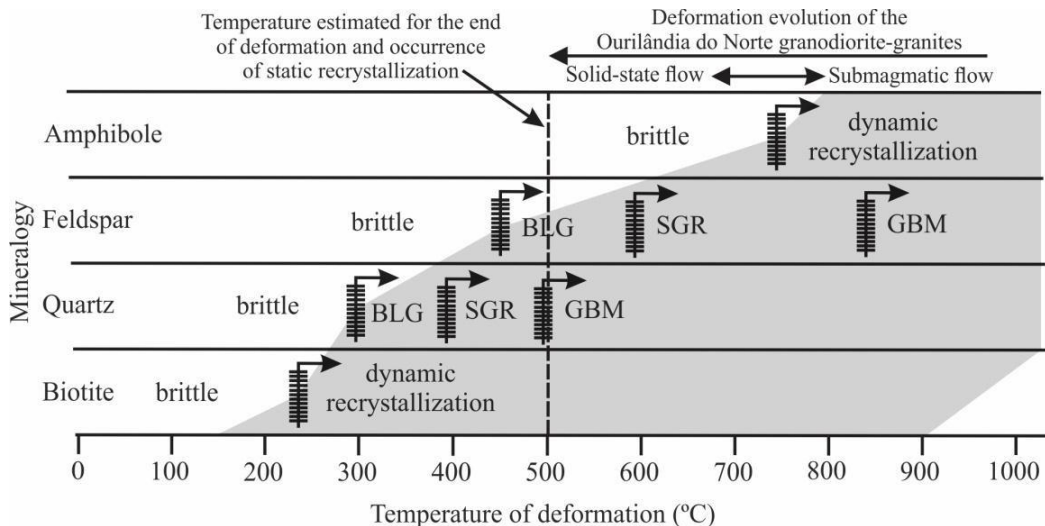


Figure 16 - Schematic diagram showing the relation between temperature of deformation and dynamic recrystallization regimes in quartz, feldspars, biotite and amphibole during D1 event [modified from Passchier & Trouw (2005)]. The gray field is the temperature spectrum for the occurrence of dynamic recrystallization in each mineral. Legend: BLG = bulging or low temperature grain boundary migration; SGR = subgrain rotation; GBM = high temperature grain boundary migration.

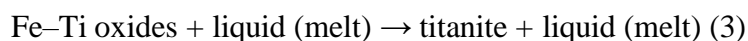
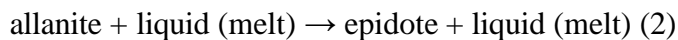
Feldspar deformation is strongly dependent on temperature (Tullis, 1983; Tullis & Yund, 1985, 1987). The microstructures identified in feldspars from these granitoids suggest that their dynamic recrystallization was controlled mainly by bulging (BLG) and SGR, followed by GBAR. Passchier & Trouw (2005) indicate that under medium-grade conditions ($450\text{--}600^{\circ}\text{C}$) dislocation climb is possible in feldspars; thus, recrystallization process may occur along their rims. Under these conditions, the main recrystallization mechanism is BLG and core-and-mantle microstructure develops. Dynamic recrystallization by SGR in feldspars is activated at temperatures above 600°C (Gapais, 1989; Tullis & Yund, 1991), which would be coherent to admit an ultimate deformation temperature above 500°C for the rocks under study (Fig. 16). At temperatures above 600°C myrmekite and intragranular microcracks are common, and core-and-mantle microstructures still occur (Kruse et al., 2001), indicating continuity between magmatic and state-solid deformation. Like quartz, the occurrence of GBAR in feldspars suggests post-deformation static recrystallization, which is consistent with the relatively high temperature at the end of the crystal-plastic deformation that affected these granitoids. In this case, or if a large amount of water was present along grain boundaries, recovery, recrystallization and GBAR processes can continue in the absence of deformation towards a lower internal energy configuration of the crystal (Passchier & Trouw, 2005).

The micas show abundant evidence of deformational accommodation mechanisms (Kronenberg et al., 1990; Wilson, 1980), but amphibole deformation remains poorly understood (Imon et al., 2004). Biotite is commonly recrystallized and behaves ductilely at temperatures above 250°C , whereas GBM recrystallization in biotite becomes significant at medium to high-grade conditions (Stesky, 1978; Bell, 1998). Due to its broad recrystallization temperature spectrum,

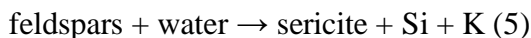
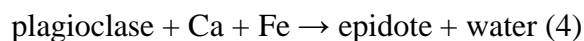
biotite is not a good mineral to estimate the deformation temperatures of Ourilândia do Norte granitoids (Fig. 16). Hornblende, if present, is deformed predominantly by microcracking, as well as the primary accessory minerals. These observations are consistent with amphibole deformation experiments, since at temperatures below 650–700 °C, it is deformed primarily by brittle mechanisms (Allison & LaTour, 1977; Imon et al., 2004). However, in Ourilândia amphibole-bearing granitoids, hornblende can occur with smooth undulatory extinction and subgrain formation, reinforcing the idea that these rocks started to deform at high temperatures.

6.2.2. Tardi- to post-magmatic transformations

Deformation of granitoid rocks involves grainsize reduction and foliation development, with recrystallization and neocrystallization associated with both processes (Vernon, 2004). In the Ourilândia do Norte area, all granitoids studied preserve various transformation microstructures related to the magmatic or subsolidus stages in which secondary mineralogy includes chlorite, muscovite, epidote, titanite and biotite (only when hornblende is present). Thus, the following microstructures occur: (i) calcium plagioclase partially transformed to sericite+epidote (saussuritization); (ii) K-feldspar to sericite (sericitization); (iii) K-feldspar replaced by vermicular intergrowth of quartz and sodic plagioclase (myrmekite); (iv) exsolution lamellae in alkali feldspar (perthite); (v) biotite partially transformed to chlorite+titanite; (vi) hornblende to biotite+quartz; (vii) hornblende to biotite+titanite+epidote, (viii) allanite to epidote; and (ix) Fe-Ti oxides to titanite. In addition, both intragranular and intergranular microfractures filled with quartz, quartz+feldspar, sericite+epidote or sericite+epidote+titanite can also occur. In this respect, transformation microstructures (vi), (viii) and (ix) can be formed in the magmatic stage from reequilibrium on the peritectic point and can be represented by general reactions (1), (2) and (3), respectively:



The transformation microstructures (i), (ii), (v) and (vii) may be formed in the presence of fluids in both tardi-magmatic and subsolidus stages (Hibbard, 1987; Best, 2003; Vernon, 2004). In addition to producing sericite and epidote, plagioclase saussuritization can also form calcite, if CO₂ fugacity is sufficiently high, and zoisite (Al analog of Fe-bearing epidote) (Vernon, 2004; Best, 2003). These transformations involve reactions of higher-T, primary magmatic mineral to lower-T, secondary, more hydrated subsolidus mineral or assemblage (Best, 2003). Thus, the aforementioned transformation microstructures can be represented by the general reactions (4), (5), (6) and (7), respectively:



Vernon (2004) undercores that these reactions are cyclic, whereby the chemical components released in one local reaction are used in another, without modifying whole rock chemicals. Although myrmekitic intergrowth can form in the tardi-magmatic stage (Hibbard, 1987), it is very common in deformed granitoids, and its origin is often attributed to solid-state replacement of K-feldspar accompanying deformation (Tsurumi et al., 2003; Paterson et al., 1989; Vernon, 2004). Albite exsolution lamellae are formed below the solvus curve by alkali feldspar

reequilibrium at lower temperatures. The widespread occurrence of these transformation microstructures in all Ourilândia do Norte granitoids, as well as in those of adjacent areas, indicate that the transformation microstructures (i, ii, iii, v, and vii) were formed in the tardigranitic/subsolidus stage, during the cooling these granitoids until the moderate deformation temperatures (above 500 °C). This hypothesis is reinforced by the presence of sericite on feldspar transformation, once at lower temperatures would be expected neocrystallization of clay minerals, instead of sericite (Best, 2003).

The water required for these transformations can have different sources. In closed magma systems, juvenile water exsolved from the crystallizing melt reacts at subsolidus temperatures with the primary magmatic minerals in a process where the rock effectively “stews in its own juices” during autometamorphism or deuterian alteration (Best, 2003). Oliveira et al. (2009, 2010) indicate that the sanukitoid affinity Rio Maria granodiorite magmas have high H₂O content, which suggests that the alteration of these rocks was controlled by juvenile fluids. In open magma systems, water may be drawn into a cooling dike from water-bearing wallrock and become a potential model to explain the fluid source in water-poor magma (e.g. Fig. 5f) (Best, 2003). As such, secondary mineral paragenesis analysis indicate that Ourilândia do Norte plutonic rocks were submitted to deuterian alteration under conditions compatible with lower amphibolite to higher greenschist facies.

6.3. Ascent and emplacement mechanisms and tectonic significance

The shape and internal structure study of plutons combined with the microstructural observations and country rock structural pattern can provide valuable information about the ascent and emplacement processes of granitic magmas. Granitoids are excellent tectonic markers and when emplaced in an orogenic system may register their different stages (pre-, syn- or post-collision), due to the narrow time span of the crystallization processes when compared to the total duration of the orogenesis. After complete crystallization, the granitoids show high deformation resistance, preserving in their fabrics the record of the tectonic processes that acted during their formation time (Paterson et al., 1989; Blenkinsop, 2000; Bitencourt & Nardi, 2000; Best, 2003; Moyen et al., 2003b; Vernon, 2004; Passchier & Trouw, 2005; Peternell et al., 2010; Neves, 2012; Florisbal, 2012). Paterson et al. (1989) report that a continuum likely exists between magmatic and solid-state processes operating during fabric development in orogenic granitoids. The authors divide this continuum into four types: (i) magmatic flow with less than 70% crystals and suspension-like behavior, without sufficient interference between crystals to cause plastic deformation; (ii) submagmatic flow with more than 70% crystals and plastic deformation of previously formed crystals; (iii) high-temperature solid-state flow; and (iv) moderate- to low-temperature solid-state flow. These supplemental information are coupled with field, photointerpretation and microstructural data and with the advancement of knowledge in the Ourilândia do Norte granitoid petrogenesis to suggest a tectono-magmatic model in which plutonism and regional deformation operated concurrently during the origin, ascent and emplacement of their magmas.

Field relationships indicate that the Mg-K granitoids are coeval to slightly older than Fe-K rocks, which allows to suggest a common deformation history for all the Ourilândia do Norte granitoids. In this regard, an integrated analysis of the data obtained in this research with those reported in previous works resulted in the following criteria aimed at inferring the interaction between magmatism and tectonism: (i) elongated or ellipsoidal shape of all batholiths and stocks studied; (ii) aligned pattern of these bodies, at regional-scale, with strips of EW-trending greenstone belt sequence, indicating that they were emplaced in a regional suture zone between Carajás and Rio Maria blocks; (iii) magmatic or mylonitic foliations showing subparallel direction with the main pluton trend, and a continuous arrangement with foliation in the country rocks; (iv) close relationship between these plutons and shear zones, where increasing higher strain domains toward their border zones, indicating that they are limited by large-scale shear zones; (v) microstructures

indicative of a continuum between magmatic and high-temperature solid-state processes during planar fabric development; (vi) evidence of oblique lineation and kinematic indicators which suggest a regime of high temperature sinistral transpression ([Araújo & Maia, 1991](#); [Pinheiro & Holdsworth, 1997](#)); (vii) all plutons studied went originated and emplaced within a narrow time span at 2875–2884 Ma (single-zircon Pb-evaporation ages of Mg-K granodiorite; [Santos et al., 2013a](#)); (viii) rocks of the EBGd group occur as lenses and show diffuse internal contacts with granites of the BMzG group, indicating that these batholiths were constructed by multiple magma pulses; (ix) petrogenetic evidence indicates that the origin of both Mg-K and Fe-K granitoids require syn-plutonic interaction of mantle- and crust-derived materials in a post-subduction setting; (x) U-Pb SHRIMP zircon dating of the enderbitic gneiss basement from Canaã dos Carajás area yielded ages of 3.0 Ga (cores) and 2.86 Ga (rims), in which the latter is attributed to granulite metamorphism and can be considered as the regional metamorphism peak of the Carajás province ([Pidgeon et al., 2000](#)); and (xi) trace element composition in granitoids are a function of their sources and melt crystallization history, where the tectonic environment is not a major determinant. Regarding the last criterion, it is important to note that in a tectonic setting discriminant diagrams (e.g. [Harris et al., 1986](#); Fig. 17), the Fe-K and Mg-K granitoids show ambiguous trace element signatures, with their samples concentrated in the boundary between the pre-collision and late- or post-collision fields. The coeval evidence and the different petrogenetic histories of these granitoids would be inconsistent with their generation in a pre-collision (subduction) setting.

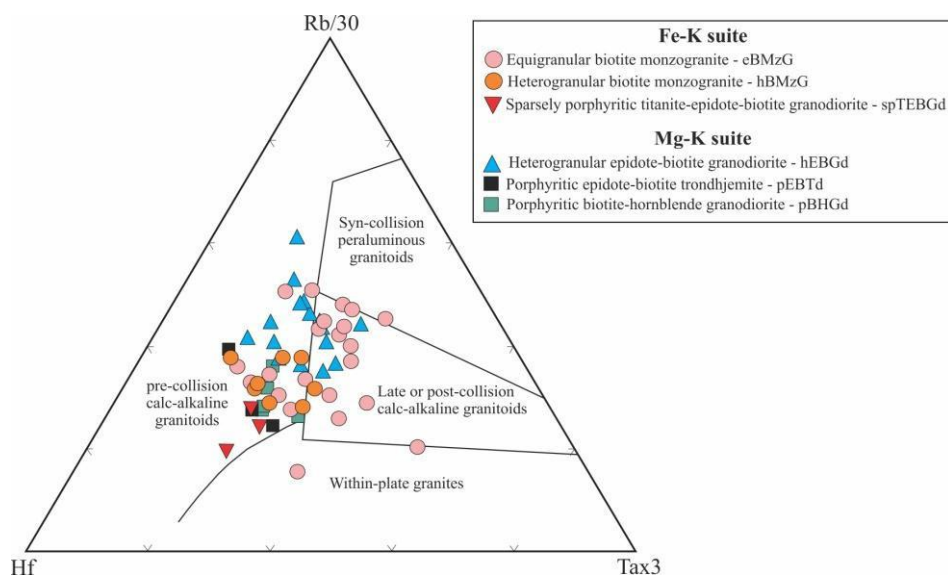


Figure 17 - Discriminant diagram of tectonic setting ([Harris et al., 1989](#)) showing ambiguous affinities for the Mg-K and Fe-K granitoids, with their samples concentrated in the boundary between the pre-collision and late- or post-collision fields.

The low viscosity contrast and mixing and/or mingling evidence indicate that Ourilândia Mesoarchean granitoids were emplaced near-synchronously at 2870 Ma, where these plutons might be at least 50 Ma younger than the older TTG basement from the Carajás province (~2.98–2.92 Ga). The previously described criteria indicate that the ascent and emplacement mechanisms of the magmas that gave rise to Ourilândia do Norte granitoids were controlled by tectonic processes and conditioned by trans-lithospheric shear zones in a sinistral transpressive tectonic regime. In this respect, the presence of pre-existing deep-reaching discontinuities combined with the occurrence of a voluminous crust-derived leucogranitic magmatism indicate that shear heating could contribute as heat source and crustal anatexis. [Hutton and Reavy \(1992\)](#) and [Ingram and Hutton \(1994\)](#) proposed that transpression in transcurrent or inverse shear zones can produce protuberances at the crust base.

These protuberances could be partially melted either because the crust is carried to deeper levels or because mantle-derived magmas would tend to remove these irregularities before causing large-scale crustal anatexis. Thus, such mechanism could collaborate as heat source, as well as for canalization and interaction of mantle- and crust-derived magmas. However, magma generation exclusively by tectonic control of local scale as shear heating is not sufficient to explain the heat source required to originate all granitoids studied, mainly those derived from the metassomatized mantle. It would also be inconsistent with the wide occurrence of analogous granitoids in the Carajás province.

Thus, in order to explain the formation of the voluminous and diversified Mesoarchean syntectonic Mg-K and Fe-K magmatism within a post-subduction setting is necessary to involve tectonic processes of regional amplitude scale capable of triggering a lithospheric reworking over a short interval of geologic time. Several models has been proposed to explain how a strong, short-lived external heat source could be responsible by granitoid formation in the final stages of the late-Archean geotectonic cycle (e.g. Moyen et al., 2003b; Heilimo et al., 2010; Almeida et al., 2011, 2013; Laurent et al., 2014a; 2014b): (i) breakoff of the subducted slab which causes an inflow of mantle asthenosphere beneath the orogenic prism, resulting in a thermal anomaly and partial melting of the metassomatized lithospheric mantle; (ii) crustal thickening developed by amalgamation of arcs or protocontinents; (iii) retreat (“rollback”) of the lithospheric mantle in the subducted slab; or (iv) delamination of the subcontinental lithospheric mantle beneath the upper plate. Almeida et al. (2011) indicate that in the RMD a thermal event related to slab breakoff and asthenosphere mantle upwelling induced the melting of the metasomatized mantle, generating sanukitoid magmas. This model seems to be coherent for the Ourilândia granitoids; however, it is worth highlighting that crustal thickening and deep-reaching shear zones filled by mantle-derived magmas may have contributed as heat source for crust-derived magma formation.

We propose that all the Mesoarchean granitoids from Ourilândia area were formed in the second stage of a two-stage tectono-magmatic model schematically illustrated in the flowchart of the Fig. 18. It summarizes the main mechanisms and processes involved in the origin and diversification of these rocks. Thus, according to this information, it can be inferred that, although Ourilândia granitoids are not cogenetic, they are syn- to tardi-tectonic and were emplaced in a collisional setting during lithospheric reworking (second stage; Fig. 18), where trans-lithospheric active shear zones acted as important conduits for magma transport and emplacement and were responsible for mantle decompression, reworking of pre-existing crustal sources and interaction between non-cogenetic magmas.

In orogenic setting, transport by tabular conduits is a important granitic magma ascent mechanism (D'Lemos et al., 1992; Brown and Solar, 1998; Weinberg, 1999; Rosenberg, 2004; Neves 2012). The previously listed criteria indicate that the ascent mechanisms of the magmas that gave rise to Ourilândia granitoids involved magma migration by penetrative flow during active deformation, through a pre-existing channel network, characterizing the crust segment studied as a multiple injection complex of mantle- and crust-derived magmas. Therefore, the accommodation of various mantle- and crust-derived magma pulses in a narrow time span built the studied batholiths. The space creation for the construction these batholiths could involve deformation and lateral translation of the country rocks, as a result of the injection of new pulses in the emplacement level (Cruden, 1998, 2006; Neves, 2012). Finally, according to aferementioned criteria, we can infer that the deformation history of the plutons studied transcends their magmatic history. Thus, high-temperature solid-state deformation continued as part of the same deformation event (D1; Fig.18) demonstrated by submagmatic microstructures down to moderate temperatures, above ~500 °C. As a result, the end of this ductile deformation at relatively high temperatures allowed the occurrence of static recrystallization observed in both the quartz and feldspars of all the granitoids studied. Superimposition of a second deformation event (D2) occasioned by reactivated shear zones due to the first inversion of the Carajas Basin (2.68-2.63 Ga; Tavares, 2015) and/or emplacement of

syntectonic Neoarchean granitoids (2.75 Ga; Barros et al., 2001; Feio et al., 2013) can be inferred for the Ourilândia do Norte area (Santos and Oliveira, 2016).

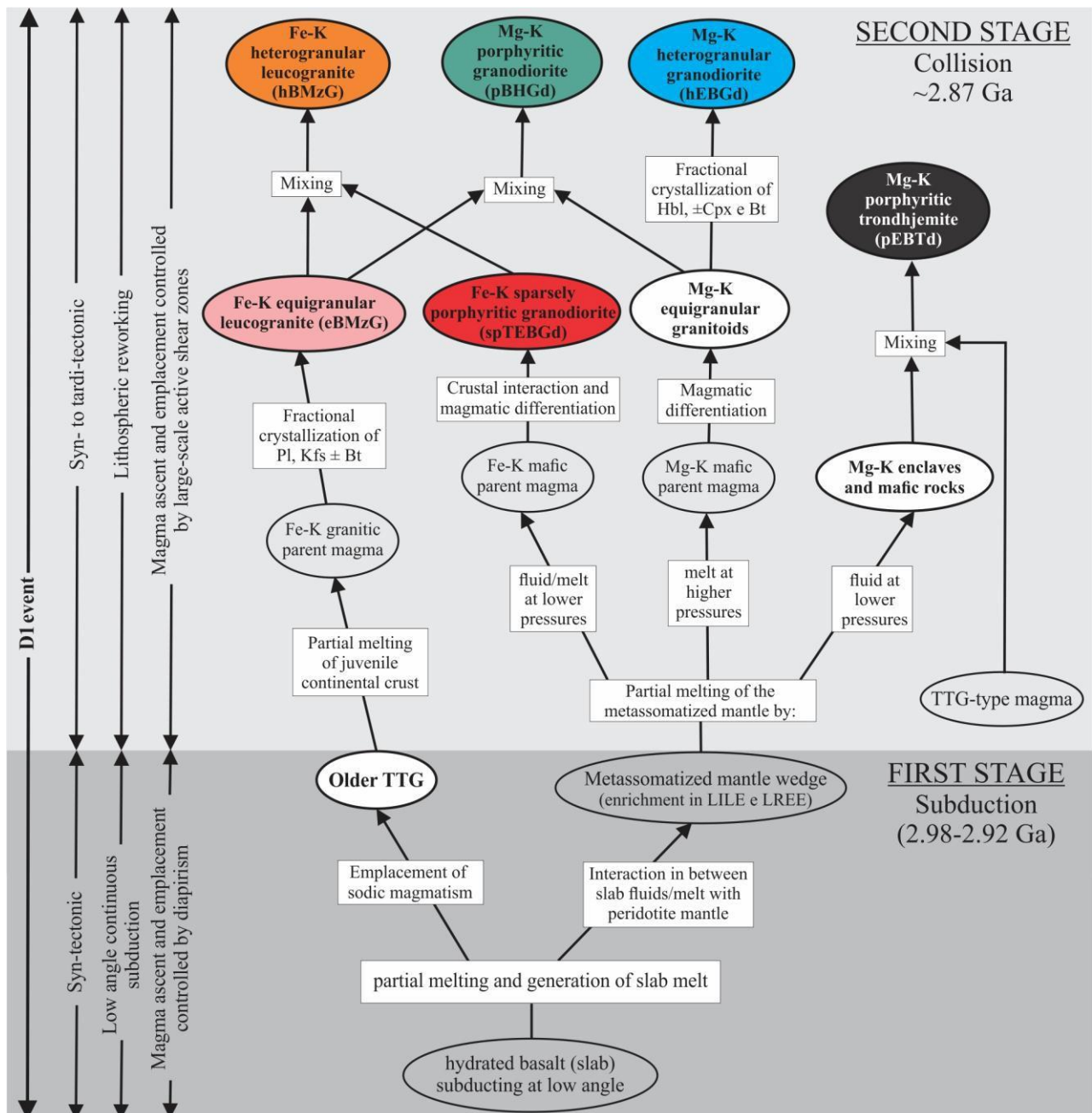


Figure 18 - Flowchart summarizing a two-stage tectono-magmatic model for the origin of the Ourilândia do Norte Mesoarchean Mg-K and Fe-K granitoids. First stage (2.98-2.92 Ga): low angle continuous subduction during basin closure, causing emplacement of sodium magmatism and mantle wedge metassomatism by slab melt/fluid. Second stage (~2.87 Ga): collision environment responsible for the origin of all granitoids studied, during lithospheric reworking induced by slab break off and crustal thickening. The former process causes an inflow of mantle asthenosphere beneath the orogenic prism, resulting a thermal anomaly and triggering the partial fusion of the previously enriched lithospheric mantle. Crustal melting, in turn, is favored by both mantle-derived magma underplating and crustal thickening. The magma ascent and emplacement process were controlled by deep-reaching and possibly trans-lithospheric active shear zones, which facilitated the interaction between mantle- and crustal-derived melts.

7. Conclusions

Mesoarchean Ourilândia do Norte plutons consist of granodiorites and monzogranites, with subordinate trondhjemites and (quartz) diorites (Santos & Oliveira 2016). New geological mapping data, obtained in this study, allowed to individualize three new groups of Mesoarchean granitoids: (i) biotite monzogranites (BMzG); (ii) epitote-biotite granodiorites (EBGd); and (iii) porphyritic granitoids (pGrt). The petrographic study showed that the granitoids of these groups are subdivided into two facies. The BMzG can be differentiated in equigranular (eBMzG) and heterogranular (hBMzG) facies, while the EBGd group is distinguished in heterogranular epitope-biotite granodiorite (hEBGd) and sparsely porphyritic titanite-epitote-biotite granodiorite (spTEBGd). These granitoids constitute two batholiths dominated by BMzG rocks, with less occurrence of EBGd lenses. The pGrt is individualized in porphyritic biotite-hornblende granodiorite (pBHGd) and porphyritic epidote-biotite trondhjemite (pEBTd), and occurs as smaller bodies, spatially associated with rocks of sanukitoid and BADR affinities, respectively. The mingling relationships established the contemporaneity between all the Ourilândia do Norte granitoids, including those of sanukitoid and BADR signatures.

These plutons were affected by heterogeneous deformation which are delimitated by large-scale shear zones. The meso- and microstructural data indicate that the rocks studied are syn-to late-tectonic and were affected by high temperature deformation ($> 500^{\circ}\text{C}$) and low differential stress, in a sinistral transpression regime, predominantly controlled by pure shear, indicating that the magmatic and solid-state fabrics are related to the same deformational event. Geochemically, except the EBtdp facies that has Mg-Na affinity, the Ourilândia do Norte granitoids can be grouped into two suites: (i) Fe-K suite that integrates the BMzG group and the spTEBGd facies; and (ii) Mg-K suite composed of granitoids (including hEBGd and pBHGd) and (quartz) diorites of sanukitoid and BADR affinities, respectively. Both groups are alkali-calcic to calc-alkaline and they differ on the basis of their FeO^t/MgO ratios, Al_2O_3 , K_2O and some trace elements (Sr, Ba, Rb). The origin of the eBMzG is attributed anatexis a 2.92-2.98 Ga old TTG crust. The hEBGd has sanukitoid affinity and could have been produced by intense fractionation of hornblende \pm clinopyroxene. The granitoids of spTEBGd, hBMzG, pBHGd and pEBTd facies show evidence of mingling and/or mixing between contrasting magmas, indicating that their origins require interaction between metassomatized mantle- and crustal derived magmas. Geochemical data and modeling were used to identify the different processes related to the origin and formation of these granitoids: (i) spTEBGd is enriched in HFSE (Ti, Zr and Y) and LILE (Ba and Sr) and was admitted as product of the partial melting of an enriched mantle source, with participation of crustal liquids, probably in a post-subduction setting; (ii) hBMzG is generated by the interaction between magmas of spTEBGd (60%) and eBMzG (40%) composition; (iii) pBHGd is formed by the hybridization between sanukitoid (80%) and leucomonzogranitic (20 %) magmas; and (iv) pEBTd is formed by an incomplete mixture between TTG signature trondhjemetic liquid (70-80%) and magma of BARD affinity (20-30%). Therefore, we can conclude that in ~ 2.87 Ga a significant crustal growth and reworking occurred in the final stages of stabilization of the first geotectonic cycle of the Carajás province. This leads us to suggest that all the Ourilândia do Norte Mesoarchean granitoids were emplacement during the second stage of a tectono-magmatic two-stage (subduction-collision) model: (i) first stage (2.98-2.92 Ga) - low-angle subduction with emplacement of slab-melt and consequent mantle wedge metasomatism; (ii) second stage (~ 2.87 Ga) - collisional environment where large-scale shear zones conditioned the rise and emplacement of magmas, acting as deep-reaching discontinuities and important conduit for transport and interaction between mantle- and crustal-derived magmas.

Acknowledgements

The authors thanks the members of the Research Group on Granitoids Petrology (RGGP) by support in the various stages of this work, especially Fernando Fernandes, Pablo Leite, Bhrenno Marangoanha, Eleison Garbriel, Jean Machado, Diwhemerson Sousa and Marcela Santos; and to the Post-Graduate Program in Geology and Geochemical (PPGG) of the Institute of Geosciences (IG) of the Federal University of Pará (UFPA) by ceded infrastructure. This research received financial support from CNPq (D. C. Oliveira - Grants – Proc. 485806/2013-4 and 311610/2012-9; M. N. S. Santos - scholarship - Proc. 133917/2013-4); Vale/FAPESPA (01/2010) and National Institute of Science and Technology-Geosciences in Amazon (INCT-GEOCIAM – CNPq/MCT/FAPESPA – Process nº 573733/2008-2).

References

- Allison, I., LaTour, T.E., 1977. Brittle deformation of hornblende in a mylonite: a direct geometrical analogue of ductile deformation by translation gliding. Canadian Journal of Earth Sciences, 14, 1953-1958.
- Almeida, F.F.M., Hasui, Y., Brito Neves, B.B., Fuck, R.A., 1981. Brazilian Structural Provinces: an introduction. Earth Science Review, 17, 1-29.
- Almeida, J.A.C., Dall'Agnol, R., Leite, A.A.S., 2013. Geochemistry and zircon geochronology of the Archean granite suites of the Rio Maria granite-greenstone terrane, Carajás Province, Brazil. Journal of South American Earth Sciences, 42, 103-126.
- Almeida, J.A.C., Dall'Agnol, R., Oliveira, M.A., Macambira, M.J.B., Pimentel, M.M., Rämö, O.T., Guimarães, F.V., Leite, A.A.S., 2011. Zircon geochronology, geochemistry and origin of the TTG suites of the Rio Maria granite-greenstone terrane: implications for the growth of the Archean crust of the Carajás Province, Brazil. Precambrian Research, 187, 201-221.
- Althoff, F.J., Barbey, P., Boullier, A. M., 2000. 2.8-3.0 Ga plutonism and deformation in the SE Amazonian craton: the Archean granitoids of Marajoara (Carajás Mineral province, Brazil). Precambrian Research, 104, 187-206.
- Araújo, O.J.B., Maia, R.G.N., 1991. Serra dos Carajás, Folha SB-22-Z-A. CPRM, Rio de Janeiro, 136p.(final report).
- Barbosa, A.A., Lafon, J.M., Neves, A.P., Vale, A.G., 1995. Geocronologia Rb-Sr e Pb-Pb do Granito Redenção, SE do Pará: implicações para a evolução do magmatismo proterozoico da região de Redenção. Boletim do Museu Paraense Emílio Goeldi. Série Ciências da Terra, 7, 147-164.
- Barker, F., 1979. Trondhjemites: definition, environment and hypotheses of origin. In: Barker, F. (Ed.) Trondhjemites, dacites and related rocks. Amsterdam, Elsevier, p.1-12.
- Barker, F., Arth, J.G., 1976. Generation of trondhjemite-tonalite liquids and Archean bimodal trondhjemite-basalt suites. Geology, 4, 596-600.
- Barros C.E.M., Sardinha A.S., Barbosa J.P.O., Krimski R., Macambira M.J. B. 2001. Pb-Pb and zircon ages of Archean sytectonic granites of the Carajás metallogenic province, Northern Brazil. In: Serviço Nacional de Geologia e Mineral, 3º Simpósio Sul-Americano de Geologia Isotópica, Resumos Expandidos, Pucon, Chile, 1 CD-ROM.
- Bell, T.H., 1998. Recrystallization of biotite by subgrain rotation. In: Snoke A, Tullis J, Todd VR (eds) Fault related rocks – a photographic atlas. Princeton University Press, New Jersey, pp 272-273.
- Belousova, E.A., Kostitsyn, Y.A., Griffin, W.L., Begg, G.C., O'Reilly, S.Y., Pearson, N.J. 2010. The growth of the continental crust: constraints from zircon Hf-isotope data. Lithos. 119 (3-4), 457-466.
- Best, M.G., 2003. Igneous and metamorphic petrology. Freeman, New York, 758 pp.

- Bitencourt, M.F., Nardi, L.V.S., 2000. Tectonic setting and sources of magmatism related to the Southern Brazilian shear Belt. *Revista Brasileira de Geociências*, 30, 186-189.
- Blenkinsop, T.G., 2000. *Defomation Microstructures and Mechanisms in Minerals and Rocks*. Kluwer Academic Publishers, Dordrecht, 150p.
- Bouchez, J.L., Delas, C., Gleizes, G., Nédélec, A., Cuney, M., 1992. Submagmatic microfractures in granites. *Geology*, 20, 35-38.
- Bowden, P., Batchelor, R.A., Chapell, B.W., Didier, J., Lameyre, J., 1984. Petrological, geochemical and source criteria for the classification of granitic rocks: a discussion. *Physics, Earth Planet Sciences*, 35, 1-11.
- Brown, M., Solar, G.S., 1998. Shear-zone system and melts: feedback relations and self-organization in orogenic belts. *Journal of Structural Geology*, 20, 1365-1393.
- Champion, D.C., Smithies, R.H., 2001. Archaean granites of the Yilgarn and Pilbara cratons, Western Australia. In: Cassidy K.F., Dunphy J.M., Van Kranendonk M.J. (Eds.), *Proceedings of the Fourth International Archaean Symposium*. AGSO-Geoscience Australia, Perth, Australia, 37, 134-136.
- Champion, D.C., Smithies, R.H., 2003. Archaean granites. In: Blevin P.L., Chappell B.W., Jones M. (Eds.), *Magmas to Mineralisation: The Ishihara Symposium*, AGSO-Geoscience Australia, 14, 19-24.
- Condie, K.C., 1981. Archaean greenstone belts. In: Windley, B.F. (Ed.), *Developments in Precambrian Geology*, 3, 434 pp.
- Condie, K.C., O'Neill, C., 2010. The Archean-Proterozoic boundary: 500 my of tectonic transition in Earth history. *American Journal of Science*, 310, 775-790.
- Cruden, A.R., 1998. On the emplacement of tabular granites. *Journal of the Geological Society*. London, 155, 835-862.
- Cruden, A.R., 2006. Emplacement and growth of plutons: implications for rates of melting and mass transfer in continental crust. In: Brown, M., Rushmer, T. (Eds.) *Evolution and Differentiation of the Continental Crust*. Cambridge University Press, 455-519.
- Cunha, I.R.V., Dall'Agnol, R., Feio, G.R.L., 2016. Mineral chemistry and magnetic petrology of the Archean Planalto Suite, Carajás Province – Amazonian Craton: implications for the evolution of ferroan Archean granites. *Journal of South American Earth Sciences*, 67, 100-121.
- D'Lemos, R.S., Bronw, M., Strachan, R.A., 1992. Granite magma generation and emplacement within a transpressional orogen. *Journal of the Geological Society*, London, 149, 487-490.
- Dall'Agnol, R., Oliveira, D.C., Guimarães, F.V., Gabriel, E.O., Feio, G.R.L., Lamarão, C.N., Althoff, F.J., Santos, P.A., Teixeira, M.F.B., Silva, A.C., Rodrigues, D.S., Santos, M.J.P., Silva, C.R.P., Santos, R.D., Santos, P.J.L., 2013. Geologia do Subdomínio de Transição do Domínio Carajás – Implicações para a Evolução Arqueana da Província Carajás – Pará. *Anais do 13º Simpósio de Geologia da Amazônia*, Belém.
- Dall'Agnol, R., Cunha, I.R.V., Guimarães, F.V., Oliveira, D.C., Teixeira, M.F.B., Feio, G.R.L., Lamarão, C.N., 2016. Mineralogy, geochemistry, and petrology of Neoarchean ferroan to magnesian granites of Carajás Province, Amazonian Craton: The origin of hydrated granites associated with charnockites. *Lithos*, 277, 3-32. <http://dx.doi.org/10.1016/j.lithos.2016.09.032>
- Debon, F., Le Fort, P., 1983. A chemical–mineralogical classification of common plutonic rocks and associations. *Transactions of the Royal Society of Edinburgh, Earth Sciences*, 73, 135-149.
- Dhuime, B., Hawkesworth, C.J., Cawood, P.A., Storey, C.D., 2011. A change in the geodynamics of continental growth 3 billion years ago. *Science*, 335, 1334-1336.
- Evensen, N.M., Hamilton, P.T., O'nions, R.K., 1978. Rare earth abundances in chondritic meteorites. *Geochimica ET Cosmochimica Acta*, 39, 55-64.
- Feio, G.R.L., Dall'Agnol, R., 2012. Geochemistry and petrogenesis of the Mesoarchean granites from the Canaã dos Carajás area, Carajás Province, Brazil: Implications for the origin of Archean granites. *Lithos*, 154, 33-52.

- Feio, G.R.L., Dall'Agnol, R., Dantas, E.L., Macambira, M.J.B., Gomes, A.C.B., Sardinha, A.S., Oliveira, D.C., Santos, R.D., Santos P.A., 2012. Geochemistry, geochronology, and origin of the Neoarchean Planalto Granite suite, Carajás, Amazonian craton: A-type or hydrated charnockitic granites? *Lithos*, 151, 57-73.
- Feio, G.R.L., Dall'Agnol, R., Dantas, E.L., Macambira, M.J.B., Santos, J.O.S., Althoff, F.J., Soares, J.E.B., 2013. Archean granitoid magmatism in the Canaã dos Carajás area: Implications for crustal evolution of the Carajás province, Amazonian craton, Brazil. *Precambrian Research*, 227, 157-185.
- Florisbal, L.M., 2012. Petrogênese de granitos sintectônicos em ambiente pós-colisional do escudo catarinense: estudo integrado de geologia estrutural, geoquímica elemental e isotópica Sr-Nd-Pb e geocronologia U-Pb em zircão. Tese de doutorado, Instituto de Geociências, Universidade de São Paulo, 218 p.
- Frost B.R., Barnes, C.G., Collins, W.J., Arculus, R.J., Ellis, D.J., Frost, C.D., 2001. A geochemical classification for granitic rocks. *Journal of Petrology*, 42, 2033-2048.
- Frost, C.D., Frost, B.R., Chamberlain, K.R., Hulsebosch, T.P., 1998. The Late Archean history of the Wyoming province as recorded by granitic magmatism in the Wind River Range, Wyoming. *Precambrian Research*, 89, 145-173.
- Gabriel, E.O., Oliveira, D.C., 2014. Geologia, petrografia e geoquímica dos granitoides arqueanos de alto magnésio da região de Água Azul do Norte, porção sul do Domínio Carajás, Pará. *Boletim do Museu Paraense Emílio Goeldi, Ciências Naturais*, 9(3):533-564.
- Gapais, D., 1989. Shear structures within deformed granites: mechanical and thermal indications. *Geology*, 17, 1144-1147.
- Gleason, G.C., Tullis J., 1995. A flow law for dislocation creep of quartz aggregates determined with the molten salt cell. *Tectonophysics*, 247, 1-23.
- Guitreau, M., Blichert-Toft, J., Martin, H., Mojzsis, S., Albarède, F., 2012. Hafnium isotope evidence from Archean granitic rocks for deep-mantle origin of continental crust. *Earth and Planetary Science Letters*, 337, 211–223.
- Harris, N.B.W., Pearce, A.J., Tindle, A.G., 1986. Geochemical characteristics of collision-zone magmatism. In: Coward, M.P., Ries, A.C. (Eds.), *Collision Tectonics*, Geological Society of America Special, 19, 115-158.
- Heilimo, E., Halla, J., Adersen, T., 2013. Neoarchean crustal recycling and mantle metasomatism: Hf-Nd-Pb-O isotope evidence from sanukitoids of the Fennoscandian shield. *Precambrian Research*, 228, 250-266.
- Heilimo, E., Halla, J., Hölttä, P., 2010. Discrimination and origin of the sanukitoid series: geochemical constraints from the Neoarchean western Karelian Province (Finland). *Lithos*, 115, 27-39.
- Hibbard, M.J., 1987. Deformation of incompletely crystallised magma systems: granitic gneisses and their tectonic implications. *J. Geol.*, 951, 543-561.
- Hirth, G., Tullis, J., 1992. Dislocation creep regimes in quartz aggregates. *J. Struct. Geol.*, 14, 145-159.
- Hutton, D.H.W., Reavy, R.J., 1992. Strick-slip tectonics and granite petrogenesis. *Tectonics*, 11 (5), 960-967.
- Imon, R., Okudaira, T., Kanagawa, K., 2004. Development of shape- and lattice-preferred orientations of amphibole grains during initial cataclastic deformation and subsequent deformation by dissolution, precipitation creep in amphibolites from the Ryoke metamorphic belt, SW Japan. *J Struct Geol.*, 26, 793-805.
- Ingran, G.M., Hutton, D.H.W., 1994. The Great Tonalite Sill: emplacement into a contractional shear zone and implications for late Cretaceous to early Eocene tectonics in southeastern Alaska and British Columbia. *Geological Society of America Bulletin*, 106, 715-728.

- Jayananda, M., Martin, H., Peucat, J.-J., Mahabaleswar, B., 1995. Late Archaean crust–mantle interactions: geochemistry of LREE-enriched mantle derived magmas. Example of the Closepet batholith, Southern India. *Contributions to Mineralogy and Petrology*, 199, 314–329.
- Kohlstedt, D.L., Evans, B., Mackwell, S.J., 1995. Strength of the lithosphere: constraints imposed by laboratory experiments. *J. Geophys. Res.*, 100, 17587–17602.
- Kramers, J.D., Tolstikhin, I.N., 1997. Two major terrestrial Pb isotope paradoxes, forward transport modeling, core formation and the history of the continental crust. *Chemical Geology*, 139, 75–110.
- Kronenberg, A.K., 1994. Hydrogen speciation and chemical weakening of quartz. In: Heaney P.J., Prewitt C.T., Gibbs G.V. (eds) *Silica: physical behavior, geochemistry, and materials applications*. Mineral Soc. Am. Rev. Mineral, 29, 123–176.
- Kronenberg, A.K., Kirby, S.H., Pikston, J.C., 1990. Basal slip and mechanical anisotropy of biotite. *J. Geophys. Res.*, 95, 19257–19278.
- Kruse, R., Stünitz, H., Kunze, K., 2001. Dynamic recrystallisation processes in plagioclase porphyroclasts. *J. Struct. Geol.*, 23, 1781–1802.
- Lameyre, J., Bowden, P., 1982. Plutonic rock type series: discrimination of various granitoid series and related rocks. *Journal of Volcanology and Geothermal Research*, 14, 169–186.
- Laurent, O., Martin, H., Moyen, J.F., Doucelance, R., 2014a. The diversity and evolution of late-Archean granitoids: evidence for the onset of “modern-style” plate tectonics between 3.0 and 2.5 Ga. *Lithos*, 205, 208–235.
- Laurent, O., Rapopo, M., Stevens, G., Moyen, J.F., Martin, H., Doucelance, R., Bosq, C., 2014b. Contrasting petrogenesis of Mg-K and Fe-K granitoids and implications for post-collisional magmatism: case study from the Late-Archean Matok pluton (Pietersburg block, South Africa). *Lithos*, 196–197, 131–149.
- Le Maitre, R.W., 2002. A classification of igneous rocks and glossary of terms. 2nd Edition, London, 193p.
- Leite, A.A.S., Dall’Agnol, R., Macambira, M.J.B., Althoff, F.J., 2004. Geologia e geocronologia dos granitóides arqueanos da região de Xinguara (PA) e suas implicações na evolução do terreno granito-greenstone de Rio Maria. *Revista Brasileira de Geociências*, 34, 447–458.
- Leite-Santos, P.J. and Oliveira, D.C., 2014. Trondjemitos da área de Nova Canadá: novas ocorrências de associações magnáticas tipo TTG no Domínio Carajás. *Boletim do Museu Paraense Emílio Goeldi, Ciências Naturais*, Belém, 9(3), 635–659.
- Leite-Santos, P.J., Oliveira, D.C., 2016. Geologia, petrografia e geoquímica das associações leucograníticas arqueanas da área de Nova Canadá – Província Carajás. *Boletim IG-USP – Série Científica*, 16 (2), 37–66.
- Luan, F.C., Paterson, M.S., 1992. Preparation and deformation of synthetic aggregates of quartz. *J. Geophys. Res.*, 97, 301–320.
- Martin, H., 1994. The Archean grey gneisses and the gneisses of continental crust. In: Condie K.C. (Ed.), *Developments in Precambrian Geology. Archean Crustal Evolution*. Elsevier, Amsterdam, 11, 205–259.
- Martin, H., Smithies, R., Rapp, R.P., Moyen, J.F., Champion, D., 2005. An overview of adakite, TTG, and sanukitoid: relationships and some implications for crustal evolution. *Lithos*, 79(1–2), 1–24.
- Moreto, C.P.N., Monteiro, L.V.S., Xavier, R.P., Amaral, W.S., Santos, T.J.S., Juliani, C., Souza, Filho, C.R., 2011. Mesoarchean (3.0 and 2.86 Ga) host rocks of the iron oxide-Cu-Au Bacaba deposit, Carajás Mineral Province: U-Pb geochronology and metallogenetic implications. *Mineralium Deposita* 46, 789–811.
- Moyen J.F., Nédélec A., Martin H., Jayananda M. 2003b. Syntectonic granite emplacement at different structural levels: the Closepet granite, South India. *Journal of Structural Geology* 25, 611–631.

- Moyen, J.F., Martin, H., Jayananda, M., Auvray, B., 2003a. Late Archaean granites: a typology based on the Dharwar Craton (India). *Precambrian Research*, 127, 103-123.
- Neves, S.P., 2012. Granitos orogênicos: da geração dos magmas à intrusão e deformação. Synergia, Rio de Janeiro, 147 p.
- Nockolds, S.R., Aleen, R., 1953. The geochemistry of some igneous rock series, Part I. *Geochemical Cosmochemical Acta*, 4, 105-142.
- O'Connor, J.T., 1965. A classification for quartz-rich igneous rocks based on feldspar ratios. US Geological Survey Professional Papers, 525B, 79-84.
- Oliveira, M.A., Dall'Agnol, R., Almeida, J.A.C., 2011. Petrology of the Mesoarchean Rio Maria suite: implications for the genesis of sanukitoid rocks. *J. Petrology*, 51(10), 2121-2148.
- Oliveira, M.A., Dall'Agnol, R., Althoff, F.J., Leite, A.A.S., 2009. Mesoarchean sanukitoid rocks of the Rio Maria Granite-Greenstone Terrane, Amazonian craton, Brazil. *Journal of South American Earth Sciences*, 27, 146-160.
- Oliveira, M.A., Dall'Agnol, R., Scaillet, B., 2010. Petrological constraints on crystallization conditions of Mesoarchean sanukitoid rocks, southeastern Amazonian Craton, Brazil. *Journal of Petrology*, 51, 2121-2148.
- Paiva, Jr. A.L., Lamarão, C.N., Lima, P.H.A., 2011. Geologia, Petrografia e Geoquímica do Batólito Seringa, Província Carajás, SSE do Pará. *Revista Brasileira de Geociências*, 41(2), 185-202.
- Passchier, C.W., Trouw, R.A.J., 2005. *Microtectonics*, 2nd ed., Germany, Springer-Verlag, 366 p.
- Paterson, S.R., Vernon, R.H., Tobisch, O.T., 1989. A review of criteria for the identification of magmatic and tectonic foliations in granitoids. *J. Struct. Geol.*, 11, 349-364.
- Peccerillo, A., Taylor, S.R., 1976. Geochemistry of Eocene calcalkaline volcanic rocks from the Kastamoru area, Northern Turkey. *Contributions to Mineralogy and Petrology*, 58, 63-81.
- Peternell, M., Bitencourt, M.F., Kruhl, J.H., Stäb, C., 2010. Macro and microstructures as indicators of the development of syntectonic granitoids and host rocks in the Camboriú region, Santa Catarina, Brazil. *Journal of South American Earth Sciences*, 29, 738-750.
- Pidgeon, R.T., Macambira, M.J.B., Lafon, J.M., 2000. Th-U-Pb isotopic systems and internal structures of complex zircons from the Pium complex, Carajás province, Brazil: evidence for the ages of the granulite facies metamorphism and the protolith of the enderbite. *Chemical Geology*, 166, 159-171.
- Pinheiro, R.V.L., Holdsworth, R.E., 1997. Reactivation of Archaean strike-slip fault systems, Amazon region, Brazil. *Journal of the Geological Society*, 154, 99-103.
- Post, A.D., Tullis, J., Yund, R.A., 1996. Effects of chemical environment on dislocation creep of quartzite. *J. Geophys. Res.* 101, 22143-22155.
- Rodrigues, D.S., Oliveira, D.C., Macambira, M.J.B., 2014. Geologia, geoquímica e geocronologia do Granito Mesoarqueano Boa Sorte, município de Água Azul do Norte, Pará – Província Carajás. *Boletim do Museu Paraense Emílio Goeldi, Ciências Naturais*, 9(3), 597-633.
- Rollinson, H. 1993. Using geochemical data: evaluation, presentation, interpretation, Zimbabwe, 344p.
- Ronaib, C.P.S., Oliveira, D.C., 2013. Geologia, petrografia e geoquímica das associações TTG e leucogranodioritos do extremo norte do Domínio Rio Maria, Província Carajás. *Boletim do Museu Paraense Emílio Goeldi, Ciências Naturais*, 8 (3): 383-415.
- Rosenberg, C.L., 2004. Sher zone and magma ascent: a model based on a review of the Tertiary magmatism in the Alps. *Tectonics*, 23(3).
- Santos, J.O.S., 2003. Geotectônica do Escudo das Guianas e Brasil-Central. In: Bizzi, L. A. et al. (Ed.). *Geologia, tectônica e recursos minerais do Brasil: texto, mapas e SIG*. Brasília. CPRM-Serviço Geológico do Brasil, 169-226p.
- Santos, M.J.P., Lamarão, C.N., Lima, P.H.A., Galarza, M.A., Mesquita, J.C.L., 2013a. Granitoides arqueanos da região de Água Azul do Norte, Província Carajás, sudeste do estado do Pará:

- petrografia, geoquímica e geocronologia. Boletim do Museu Paraense Emílio Goeldi. Ciências Naturais, 8(3), 325-354.
- Santos, M.N.S., Oliveira, D.C. 2016. Rio Maria granodiorite and associated rocks of Ourilândia do Norte - Carajás province: Petrography, geochemistry and implications for sanukitoid petrogenesis. *Journal of South American Earth Sciences*, 72, 279-301
- Santos, M.S., 2017. Granitoides TTG de Água Azul do Norte. MS thesis. Post-Graduate Program in Geology and Geochemical of the Institute of Geosciences of the Federal University of Pará (UFPA), Brazil, 64p.
- Santos, P.A., Teixeira, M.F.B., Dall'Agnoll, R., Guimarães, A.V., 2013b. Geologia, petrografia e geoquímica da associação Tonalito-Trondhjemito-Granodiorito (TTG) do extremo leste do Subdomínio de Transição, Província Carajás, Pará. Boletim do Museu Paraense Emílio Goeldi, Ciências Naturais, 8(3), 257-290.
- Santos, R.D., Galarza, M.A., Oliveira, D.C., 2013c. Geologia, geoquímica e geocronologia do Diopsídio-Norito Pium, Província Carajás. Boletim do Museu Paraense Emílio Goeldi, Ciências Naturais, 8(3), 355-382.
- Shand, S.J., 1943. The Eruptive Rocks, 2nd edn. (New York: John Wiley), 444p.
- Silva, A.C., Dall'Agnol, R., Guimarães, F.V., Oliveira, D.C., 2014. Geologia, petrografia e geoquímica de Associações Tonalíticas e Trondhjemíticas Arqueanas de Vila Jussara, Província Mineral de Carajás, Pará. Boletim do Museu Paraense Emílio Goeldi, Ciências Naturais, 9(1), 13-46.
- Souza, S.Z., Dall'Agnol, R., Althoff, F.J., Leite, A.A.S., Barros, C.E.M., 1996. Carajás mineral province: geological, geochronological and tectonic constraints on the Archean evolution of the Rio Maria granite-greenstone Terrain and the Carajás block. Extended abstracts. In: Simp. Arch. Terr. South Amer. Plataform, Brasília. SBG, Brasília, 31-32p.
- Souza, Z.S., Potrel, A., Lafon, J.M., Althoff, F.J., Pimentel, M.M., Dall'Agnol, R., Oliveira, C.G., 2001. Nd, Pb and Sr isotopes in the Identidade Belt, an Archean greenstone belt of Rio Maria region (Carajás Province, Brazil): implications for the geodynamic evolution of the Amazonian craton. *Precambrian Research*, 109, 293-315.
- Stesky, R.M., 1978. Mechanisms of high temperature frictional sliding in Westerly granite. *Can. J. Earth. Sci.*, 15, 361-375.
- Stipp, M., Stünitz, H., Heilbronner, R., Schmid, S.M., 2002. The eastern Tonale fault zone: a "natural laboratory" for crystal plastic deformation of quartz over a temperature range from 250 to 700 °C. *J. Struct. Geol.*, 24, 1861-1884.
- Sylvester, P.J., 1994. Archean granite plutons. In: CONDIE, K. C. (ed.). Archean crustal evolution. Developments in precambrian geology 11. Amsterdam, Elsevier. p. 261-314.
- Tassinari, C.C.G., Macambira, M.J.B., 2004. Evolução tectônica do Cráton Amazônico. In: Mantesso Neto, V., Bartorelli, A., Carneiro, C.D.R., Brito Neves, B.B. de (org). Geologia do continente Sul Americano. Evolução da obra de F.F.M. de Almeida. São Paulo BECA, 471-486p.
- Tavares F.M., 2015. Evolução geotectônica do nordeste da Província Carajás. Tese. Universidade Federal do Rio de Janeiro, Rio de Janeiro, 115p.
- Taylor, S.R., McLennan, S.M., 1985. The Continental Crust: Its Composition and Evolution. Backwell Scientific, Oxford. 321p.
- Taylor, S.R., McLennan, S.M., 1995. The geochemical evolution of the continental crust. *Reviews of Geophysics*. 33 (2), 241–265.
- Teixeira, M.F.B., Dall'Agnol, R., Silva, A.C., Santos, P.A., 2013. Geologia, petrografia e geoquímica do Leucogranodiorito Pantanal e dos leucogranitos arqueanos da área a norte de Sapucaia, Província Carajás, Pará: implicações petrogenéticas. Boletim do Museu Paraense Emílio Goeldi, Ciências Naturais, 8 (3), 291-323.

- Tsurumi, J., Hosonuma, H., Kanagawa, K., 2003. Strain localization due to a positive feedback of deformation and myrmekite-forming reaction in granite and aplite mylonites along the Hatagawa Shear Zone of NE Japan. *J. Struct. Geol.*, 25, 557-574.
- Tullis, J., 1983. Deformation of feldspars. In: Ribbe P.H. (ed) *Feldspar mineralogy*. Mineral Soc. Am. Rev. Mineral, 2, 297-323.
- Tullis, J., Yund, R.A., 1985. Dynamic recrystallisation of feldspar: a mechanism for ductile shear zone formation. *Geology*, 13, 238-241.
- Tullis, J., Yund, R.A., 1987. Transition from cataclastic flow to dislocation creep of feldspar: mechanisms and microstructures. *Geology*, 15, 606-609.
- Tullis, J., Yund, R.A., 1991. Diffusion creep in feldspar aggregates: experimental evidence. *J. Struct. Geol.*, 13, 987-1000.
- Vasquez, L.V., Rosa-Costa, L.R., Silva, C.G., Ricci, P.F., Barbosa, J.O., Klein, E.L., Lopes, E.S., Macambira, E.B., Chaves, C.L., Carvalho, J.M., Oliveira, J.G., Anjos, G.C., Silva, H.R., 2008. *Geologia e Recursos Minerais do Estado do Pará: Sistema de Informações Geográficas – SIG: texto explicativo dos mapas Geológico e Tectônico e de Recursos Minerais do Estado do Pará*. CPRM. Belém. 329 p.
- Vernon, R.H., 2004. A practical guide to rock microstructures. Cambridge University Press, 594p.
- Villemant, B., Jaffrezic, H., Joron, J.L., Treuil, M., 1981. Distribution coefficients of major and trace elements, fractional crystallisation in the alkali basalt series of Chaine des Puys (Massif Central, France). *Geochimica et Cosmochimica Acta*, 45, 1997-2016.
- Weinberg, R.F., 1999. Mesoscopic pervasive felsic magma migration: alternatives to diking. *Lithos*, 46, 393-410.
- Wilson, C.J.L., 1980. Shear zones in a pegmatite: a study of albite-mica-quartz deformation. *J. Struct. Geol.*, 2, 203-209.

Appendix A. Analytical procedures

All the 56 samples were processed in the Rock Processing Laboratory of the Federal University of Pará. They had their weathered rims removed and were previously squashed and comminuted to millimeter-size ($90\% < 200$ mesh). These rock hand specimens were crushed by stainless steel jaw crusher and then pulverized in stainless steel bowl. This material was sent to ACME ANALYTICAL LABORATORIES LTD and used for major, minor and trace elements analyses, according to total whole rock characterization with AQ200 (GROUP LF202). The information regarding the description of the methods applied and the detection limits are available in laboratory website http://acmelab.com/pdfs/Acme_Price_Brochure.pdf. Major and minor elements concentrations were determined using ICP-ES (Inductively Coupled Plasma - Emission Spectrometry) whiles the trace elements and Rare Earth Elements were analyzed by ICP-MS (Inductively Coupled Plasma - Mass Spectrometry).

CAPÍTULO 3 - CONSIDERAÇÕES FINAIS

Trabalhos de mapeamento geológico realizados na área de Ourilândia do Norte, pelo Grupo de Pesquisa Petrologia de Granitoides, mostraram que esse segmento de crosta é formado predominantemente por granitoides mesoarqueanos de afinidade sanukitoide (~2,87 Ga), (quartzo) dioritos de afinidade BADR (basalto-andesito-dacito-riolito) e domínios com ocorrência de leucogranitos indiferenciados (Santos *et al.* 2013a, Santos & Oliveira 2016). Além de monzogranitos com clinopiroxênio, cortando os demais granitoides. Novos dados de mapeamento geológico obtidos neste estudo permitiram definir a natureza e aspectos deformacionais dos leucogranitos até então indiferenciados, levando a individualização de três novos grupos de granitoides, classificados como: (i) biotita monzogranitos (BMzG); (ii) epidoto-biotita granodioritos (EBGd); e (iii) granitoides porfiríticos (Grtp).

O estudo petrográfico mostrou que os granitoides de cada grupo são subdivididos em duas fácies. As rochas do grupo BMzG são diferenciadas em fácies biotita monzogranito equigranular (BMzGe) e biotita monzogranito heterograngular (BMzGh) e as do grupo EBGd em epidoto-biotita granodiorito heterograngular (EBGdh) e titanita-epidoto-biotita granodiorito esparsamente porfirítico (TEBGdep). Esses granitoides compõem dois batólitos separados por uma faixa, de *trend* ENE-WSW, formada por sanukitoides e rochas de afinidade BADR. O batólito situado na porção central da área mostra uma forma elipsoidal, com maior eixo orientado na direção ENE-WSW; e o outro, localizado a sudeste, tem uma forma de arco. Ambos são amplamente dominados por granitos do grupo BMzG, com menor ocorrência de lentes formadas por rochas do grupo EBGd. Os granitoides do grupo Grtp são separados em fácies biotita-horblenda granodiorito porfirítico (BHGdp) e epidoto-biotita trondjemito porfirítico (EBTdp) e ocorrem como corpos menores, espacialmente associados com as rochas de afinidade sanukitoide e BADR, respectivamente. As relações de *mingling* estabeleceram a contemporaneidade entre todos os granitoides de Ourilândia do Norte, incluindo os de assinatura sanukitoide e BADR.

Em termos de geologia estrutural, esses plútôns foram afetados por deformação heterogênea, suas porções centrais representam domínios de menor *strain* e frequentemente mostram foliação magnética de direção principal ENE-WSW e mergulho subvertical, definida pela orientação preferencial de fenocristais euédricos de feldspato e fases máficas, comumente superposta por fraca deformação em estado sólido. Enquanto as bordas desses plútôns são marcadas por zonas de cisalhamento de grande escala, mostrando uma geometria

anastomosada, onde foliações miloníticas são tipicamente desenvolvidas. Os dados meso- e microestruturais indicam que as rochas estudadas são sin- a tardi-tectônicas e foram afetadas por deformação de alta temperatura ($> 500 ^\circ\text{C}$), sob baixo esforço diferencial e taxa de deformação, em regime de transpressão sinistral (Araújo & Maia 1991, Pinheiro & Holdsworth 1997), controlado predominantemente por cisalhamento puro, indicando que as tramas magmáticas e de estado sólido estão relacionadas a um mesmo evento deformacional.

Os dados de geoquímica em rocha total indicam que com exceção dos trondjemitos de fácies EBTdp que têm afinidade Mg-Na, os demais granitoides de Ourilândia do Norte podem ser agrupados em duas suítes: (i) suíte Fe-K que integra os leuco- a biotita monzogranitos do grupo BMzG e as rochas de fácies TEBGdep; e (ii) suíte Mg-K composta por granitoides de afinidade sanukitoide (incluindo os granodioritos de fácies EBGdh e BHGdp) e (quartzo) dioritos de afinidade BADR. Ambos os grupos são cálcico-alcalinos a alcalino-cálcicos e diferem entre si com base em suas relações $\text{FeO}^\text{t}/\text{MgO}$, Al_2O_3 , K_2O e alguns elementos traços (Sr, Ba, Rb). Em termos petrogenéticos, a origem dos BMzGe é atribuída à anatexia crustal durante retrabalhamento de uma crosta TTG (2,92-2,98 Ga). O EBGdh tem afinidade sanukitoide e pode ser produzido por intenso fracionamento de hornblenda \pm clinopiroxênio. Os granitoides de fácies TEBGdep, BMzGh, BHGdp e EBTdp mostram evidências de *mingling* entre magmas contrastantes, indicando que sua origem requer interação entre magmas derivados da fusão parcial do manto metassomatizado e da crosta. Dados geoquímicos e modelagem foram utilizados para identificar os diferentes processos relacionados à origem e formação destes granitoides: (i) As rochas de fácies TEBGdep são enriquecidas em HFSE (Ti, Zr e Y) e LILE (Ba e Sr) e foram formadas por fusão parcial de uma fonte mantélica enriquecida, provavelmente em um ambiente de pós-subducção, com participação de líquidos anatéticos crustais; (ii) os granitos do BMzGh são gerados pela interação entre magmas de composição TEBGdep (60%) e eBMzG (40%); (iii) as granodioritos de fácies BHGdp são formadas pela interação entre magmas sanukitoide (80%) e leucomonzogranítico (20%); e (iv) as rochas de EBTdp são originadas por uma mistura incompleta entre líquido trondjemítico de assinatura TTG (70-80%) e magma derivado do manto metassomatizado por fluidos (20-30%).

Portanto, podemos concluir que no final do Mesoarqueano, em $\sim 2,87$ Ga, ocorreu um significativo crescimento e retrabalhamento crustal, nas fases finais de estabilização do primeiro ciclo geotectônico registrado na Província Carajás. Nos levando a sugerir que todos os granitoides mesoarqueanos de Ourilândia do Norte foram alojados durante a segunda etapa de um modelo tectono-magmático de dois estágios (subducção-colisão): (i) primeiro estágio

(2,98-2,92 Ga) - subducção contínua de baixo ângulo com geração e colocação de *slab-melt* e consequente metassomatismo da cunha mantélica; (ii) segundo estágio (~2,87 Ga) – pequeno intervalo de tempo em que todos os granitoides estudados foram posicionados, em um ambiente colisional, durante retrabalhamento litosférico, onde zonas de cisalhamento translitosféricas, em regime transpressivo sinistral, condicionaram a ascensão e colocação dos magmas, servindo como condutos para o transporte e interação entre magmas não cogenéticos.

Os mecanismos de ascensão dos magmas que deram origem aos granitoides de Ourilândia do Norte envolveram migração de magma por fluxo penetrativo durante deformação ativa, através de uma rede de canais pré-existentes, caracterizando o segmento de crosta estudado como um complexo de múltiplas injeções de magma (D'Lemos *et al.* 1992, Weinberg 1999, Neves 2012). A construção desses plútuns requer a injeções de vários pulsos derivados do manto e da crosta, em um curto intervalo de tempo geológico. Assim, a criação do espaço ocorreu via deformação e translação lateral das rochas encaixantes, como resultado da injeção de novos pulsos no nível de alojamento (Cruden 2006, Neves 2012).

A história de deformação desses plútuns transcende no tempo suas histórias magmáticas. Assim, deformação de estado sólido em alta temperatura continuou como parte do mesmo evento de deformação (D1) demonstrado pelas microestruturas submagmáticas e pode ter atingido temperaturas moderadas de até ~500 °C. Como resultado, o fim desta deformação dúctil em temperaturas relativamente elevadas permitiu a ocorrência de recristalização estática observada nos cristais de quartzo e feldspato de todos os granitoides estudados.

Para a área de Ourilândia do Norte, pode ser inferido a superposição de um segundo evento de deformação (D2) ocasionado pela reativação de zonas de cisalhamento durante a colocação de granitoides neoarqueanos sintectônicos (2,75 Ga; Barros *et al.* 2001, Feio *et al.* 2013, Dall'Agnol *et al.* 2017) e/ou a primeira inversão da Bacia Carajás (2,68-2,63 Ga; Tavares 2015). Neste contexto, estudos futuros sobre os granitos com clinopiroxênio, integrando dados de petrologia e geologia estrutural, são de fundamental importância para uma melhor compreensão de como o evento D2 afetou a área estudada.

O nível de erosão dos granitoides estudados está provavelmente nas proximidades da fronteira entre os ambientes mesozonal e catazonal. Por outro lado, além dos eventos de deformação dúctil D1 e D2, essas rochas são afetadas por pelo menos dois eventos de deformação rúptil mais jovens, em níveis progressivamente mais rasos. O primeiro evento, representado por uma família de lineamentos NW-SE, os quais são interpretados como falhas

normais relacionadas à ascensão e colocação de magmatismo intraplaca paleoproterozóico (por exemplo, granito Seringa) – Oliveira *et al.* (2008). O segundo evento, evidenciado por uma família de lineamentos N-S a NNE-SSW, os quais são interpretados como falhas inversas ou de cavalgamento relacionadas à amalgamação do cinturão Araguaia no Neoproterozóico (Marangoanha & Oliveira 2014). Essas inferências refletem os processos de exumação e evolução do nível de erosão da área de Ourilândia do Norte, uma vez que, para um mesmo nível de erosão, os plútões estudados, que foram posicionados em um ambiente dúctil mais profundo, foram afetados por deformação rúptil em menores profundidades após um longo intervalo de tempo a partir de suas colocações.

Finalmente, baseado nas informações obtidas para a área de Ourilândia do Norte podemos concluir que a ocorrência do Granodiorito Rio Maria nessa região indica que a mesma faz parte do Domínio Rio Maria (Oliveira *et al.* 2009). No entanto, a presença de intrusões mais jovens de monzogranitos com clinopiroxênio sugere que o segmento de crosta compreendido pela área de Ourilândia seria melhor interpretado como fazendo parte do Subdomínio Sapucaia, definido como uma extensão do Domínio Rio Maria afetado pelos eventos neoarqueanos que deram origem à Bacia Carajás (Dall’Agnol *et al.* 2013). Por outro lado, a ampla ocorrência de granitoides alto-K e a ausência de rochas representativas do embasamento TTG apontam que essa região sofreu intenso retrabalhamento crustal, semelhante ao que foi atribuído ao Subdomínio Canaã dos Carajás (Feio & Dall’Agnol 2012, Dall’Agnol *et al.* 2013). Nesse contexto, o atual estágio do conhecimento nos permite interpretar que, ao invés de um limite entre domínios distintos, o segmento de crosta compreendido pela área de Ourilândia do Norte seria melhor interpretado como uma zona de interferência entre domínios tectônicos, em que o alojamento de um volumoso e diversificado magmatismo cárlico-alcalino alto-K (suítes Mg-K e Fe-K) marca a “zona de sutura”.

REFERÊNCIAS

- Almeida F.F.M., Hasui Y., Brito Neves B.B., Fuck R.A. 1981. Brazilian structural Provinces: an introduction. *Earth Science Review*, **17** (1-2): 1-29.
- Almeida J.A.C., Dall'Agnol R., Dias S.B., Althoff F.J. 2010. Origin of the Archean leucogranodiorite-granite suites: evidence from the Rio Maria terrane and implications for the granite magmatism in the Archean. *Lithos*, **120** (3): 235-257.
- Almeida J.A.C., Dall'Agnol R., Leite A.A.S. 2013. Geochemistry and zircon geochronology of the Archean granite suites of the Rio Maria granite-greenstone terrane, Carajás Province, Brazil. *Journal of South American Earth Sciences*, **42**:103-126.
- Almeida J.A.C., Dall'Agnol R., Oliveira M.A., Macambira M.J.B., Pimentel M.M., Rämö O.T., Guimarães F.V., Leite A.A.S. 2011. Zircon geochronology, geochemistry and origin of the TTG suites of the Rio Maria granite-greenstone terrane: implications for the growth of the Archean crust of the Carajás Province, Brazil. *Precambrian Research*, **187**: 201-221.
- Almeida J.A.C., Oliveira M.A., Dall'Agnol R., Althoff, F.J., Borges R.M.K. 2008. *Relatório de mapeamento geológico na escala 1:100.000 da Folha Marajoara (SB-22-ZC V)*. Belém, CPRM – Serviço Geológico do Brasil, 147 p. (Programa Geobrasil).
- Althoff F.J., Barbey P., Boullier A. M. 2000. 2.8-3.0 Ga plutonism and deformation in the SE Amazonian craton: the Archean granitoids of Marajoara (Carajás Mineral Province, Brazil). *Precambrian Research*, **104**: 187-206.
- Araújo O.J.B., Maia R.G.N. 1991. *Serra dos Carajás, Folha SB-22-Z-A*. CPRM, Rio de Janeiro, 136p.(Relatório Final).
- Avelar, V.G. 1996. *Geocronologia Pb-Pb por evaporação em monocrystal de zircão do magmatismo da região de Tucumã, SE do estado do Pará, Amazônia Oriental*. MS Dissertation, Programa de Pós-graduação em Geologia e Geoquímica, Instituto de Geociências, Universidade Federal do Pará, Belém, 149p.
- Barker F. 1979. Trondhjemites: definition, environment and hypotheses of origin. In: Barker F. (ed.). *Trondhjemites, dacites and related rocks*. Amsterdam, Elsevier, p.1-12.
- Barker F., Arth J.G. 1976. Generation of trondhjemite-tonalite liquids and Archean bimodal trondhjemite-basalt suites. *Geology*, **4** (10): 596-600.
- Barros C.E.M., Sardinha A.S., Barbosa J.P.O., Krimski R., Macambira M.J. B. 2001. Pb-Pb and zircon ages of Archean sytectonic granites of the Carajás metallogenic province, Northern Brazil. In: Serviço Nacional de Geologia e Mineral, 3º Simpósio Sul-Americano de Geologia Isotópica, *Resumos Expandidos*, Pucon, Chile, 1 CD-ROM.
- Best M.G. 2003. *Igneous and metamorphic petrology*. New York, Freeman, 758 p.
- Blenkinsop T.G. 2000. *Defomation microstructures and mechanisms in minerals and rocks*. Dordrecht, Kluwer Academic Publishers, 150p.

- Champion D.C., Smithies R.H. 2001. Archaean granites of the Yilgarn and Pilbara cratons, Western Australia. In: Cassidy K.F., Dunphy J.M., Van Kranendonk M.J. (eds.). Fourth International Archaean Symposium. *Proceedings...* AGSO-Geoscience Australia, Perth, Australia, **37**: 134-136.
- Champion D.C., Smithies R.H. 2003. Archaean granites. In: Blevin P.L., Chappell B.W., Jones M. (eds.). *Magmas to mineralisation: the Ishihara Symposium*, Australia, AGSO-Geoscience, **14**: 19-24.
- Chayes F. 1956. *Petrographic modal analysis*. New York, John Wiley e Sons, 113p.
- Condie K.C. 1993. Chemical composition and evolution of the upper continental crust: contrasting results from surface samples and shales. *Chemical Geology*, **104** (1-4): 1-37.
- Costa J.B.S., Araújo J.B., Santos A., Jorge João X.S., Macambira M.J.B., Lafon J.M. 1995. A Província Mineral de Carajás: aspectos tectono-estruturais, estratigráficos e geocronológicos. *Boletim Museu Paraense Emílio Goeldi*, Série Ciências da Terra, Belém, **7**: 199-235.
- Cruden A.R. 2006. Emplacement and growth of plutons: implications for rates of melting and mass transfer in continental crust. In: Brown M., Rushmer T. (ed.). *Evolution and Differentiation of the Continental Crust*. Cambridge University Press, p. 455-519.
- D'Lemos R.S., Bronw M., Strachan R.A. 1992. Granite magma generation and emplacement within a transpressional orogen. *Journal of the Geological Society*, London, **149**: 487-490.
- Dall'Agnol R., Oliveira D.C., Guimarães F.V., Gabriel E.O., Feio G.R.L., Lamarão C.N., Althoff F.J., Santos P.A., Teixeira M.F.B., Silva A.C., Rodrigues D.S., Santos M.J.P., Silva C.R.P., Santos R.D., Santos P.J.L. 2013. Geologia do subdomínio de transição do Domínio Carajás – implicações para a evolução Arqueana da Província Carajás – Pará. In: 13º Simpósio de Geologia da Amazônia, Belém, *Anais...*, p.00-00.
- Dall'Agnol R., Oliveira M.A., Almeida J.A.C., Althoff F.J., Leite A.A.S., Oliveira D.C., Barros C.E.M. 2006. Archean and Paleoproterozoic granitoids of the Carajás metallogenic province, eastern Amazonian craton. In: Dall'Agnol R., Rosa-Costa L.T., Klein E.L. (eds.). *Symposium on Magmatism, Crustal Evolution, and Metallogenesis of the Amazonian Craton. Abstracts volume and Field Trips Guide*. Belém, PRONEX-UFPA/SBG-NO, **150p. ou p. 150**
- Dall'Agnol R., Teixeira N.P., Rämo O.T., Moura C.A.V., Macambira M.J.B., Oliveira D.C. 2005. Petrogenesis of the Paleoproterozoic rapakivi A-type granites of the Archean Carajás metallogenic province. *Lithos*, Brazil, **80**: 101-129.
- Dall'Agnol R., Cunha I.R.V., Guimarães F.V., Oliveira D.C., Teixeira M.F.B., Feio G.R.L., Lamarão C.N. 2016. Mineralogy, geochemistry, and petrology of Neoarchean ferroan to magnesian granites of Carajás Province, Amazonian Craton: The origin of hydrated granites associated charnockites. *Lithos*, **277**: 3-32.
- Dall'Agnol R., Oliveira D.C. 2007. Oxidized, magnetite-series, rapakivi-type granites of Carajás, Brazil: implications for classification and petrogenesis of A-type granites. *Lithos*, **93** (3): 215-233.

- Debon F., Le Fort P. 1983. A chemical-mineralogical classification of common plutonic rocks and associations. *Earth and Environmental Science Transactions of The Royal Society of Edinburgh*, **73** (3): 135-149.
- Docegeo E. D. A. 1988. Revisão litoestratigráfica da Província Mineral de Carajás. In: 35º Congresso Brasileiro de Geologia, CVRD, Belém. *Anais....* p.10-54.
- Evensen N.M., Hamilton P.T., O’Nions R.K. 1978. Rare earth abundances in chondritic meteorites. *Geochimica ET Cosmochimica Acta*, **42** (8): 1199-1212.
- Feio G.R.L., Dall’Agnol R. 2012. Geochemistry and petrogenesis of the Mesoarchean granites from the Canaã dos Carajás area, Carajás Province, Brazil: implications for the origin of Archean granites, *Lithos*, **154**:33-52.
- Feio G.R.L., Dall’Agnol R., Dantas E.L., Macambira M.J.B., Gomes A.C.B., Sardinha A.S., Oliveira D.C., Santos R.D., Santos P.A. 2012. Geochemistry, geochronology, and origin of the Neoarchean Planalto Granite suite, Carajás, Amazonian craton: A-type or hydrated charnockitic granites? *Lithos*, **151**: 57-73.
- Feio G.R.L., Dall’Agnol R., Dantas E.L., Macambira M.J.B., Santos J.O.S., Althoff F.J., Soares J.E.B. 2013. Archean granitoid magmatism in the Canaã dos Carajás area: Implications for crustal evolution of the Carajás province, Amazonian craton, Brazil, *Precambrian Research*, **227**: 157-185.
- Florisbal L.M. 2012. *Petrogênese de granitos sintectônicos em ambiente pós-colisional do escudo catarinense: estudo integrado de geologia estrutural, geoquímica elemental e isotópica Sr-Nd-Pb e geocronologia U-Pb em zircão*. PhD Thesis, Instituto de Geociências, Universidade de São Paulo, São Paulo, 218 p.
- Fossen H., tradução: Andrade, R.D.F. 2012. *Geologia estrutural*. São Paulo, Editora Oficina de Textos, 584p.
- Frost B.R., Barnes C.G., Collins W.J., Arculus R.J., Ellis D.J., Frost C.D. 2001. A geochemical classification for granitic rocks. *Journal of Petrology*, **42**: 2033-2048.
- Frost C.D., Frost B.R., Chamberlain K.R., Hulsebosch T.P. 1998. The Late Archean history of the Wyoming province as recorded by granitic magmatism in the Wind River Range, Wyoming. *Precambrian Research*, **89** (3-4): 145-173.
- Gabriel E.O., Oliveira D.C. 2014. Geologia, petrografia e geoquímica dos granitoides arqueanos de alto magnésio da região de Água Azul do Norte, porção Sul do Domínio Carajás, Pará. Belém, *Boletim do Museu Paraense Emílio Goeldi, Ciências Naturais*, **9** (3): 533-564.
- Gill R. 2010. *Igneous rocks and processes: a practical guide*. [S.l.], Wiley-Blackwell. 472p.
- Heilimo E., Halla J., Hölttä P. 2010. Discrimination and origin of the sanukitoid series: geochemical constraints from the Neoarchean western Karelian Province (Finland). *Lithos*, **115**: 27-39.
- Hibbard M.J. 1987. Deformation of incompletely crystallised magma systems: granitic gneisses and their tectonic implications. *J. Geol.*, **951**: 543-561.

Hutchison C.S. 1974. *Laboratory handbook of petrography techniques*. London, John Wiley e Sons, 527p.

Lafon J.M., Macambira M.J.B., Pidgeon R.T. 2000. Zircon U-Pb SHRIMP dating of Neoarchean magmatism in the southwestern part of the Carajás Province (eastern Amazonian Craton, Brazil). In: SBG, 31º International Geological Congress, *Abstracts*, Rio de Janeiro, 1 CD-ROM.

Lafon J.M., Rodrigues E., Duarte K.D. 1994. Le granite Mata Surrão: un magmatisme monzogranitique contemporain des associations tonalitiques trondhjemíticas-granodioríticas archéennes de la région de Rio Maria (Amazonie Orientale, Brésil). *Comptes Rendus de la Académie de Sciences de Paris*, **318**(5): 643–649.

Laurent O., Martin H., Moyen J.F., Doucelance R. 2014a. The diversity and evolution of late-Archean granitoids: evidence for the onset of “modern-style” plate tectonics between 3.0 and 2.5 Ga. *Lithos*, **205**: 208-235.

Laurent O., Rapopo M., Stevens G., Moyen J.F., Martin H., Doucelance R., Bosq C. 2014b. Contrasting petrogenesis of Mg-K and Fe-K granitoids and implications for post-collisional magmatism: case study from the Late-Archean Matok pluton (Pietersburg block, South Africa). *Lithos*, **196**: 131-149.

Le Maitre R.W. 2002. *A classification of igneous rocks and glossary of terms*. 2nd Edition, London, 193p.

Leite-Santos P.J. Oliveira D.C. 2014. Trondjemitos da área de Nova Canadá: novas ocorrências de associações magnéticas tipo TTG no Domínio Carajás. *Boletim do Museu Paraense Emílio Goeldi, Ciências Naturais*, Belém, **9**(3): 635-659.

Leite-Santos P.J., Oliveira D.C. 2016. Geologia, petrografia e geoquímica das associações leucograníticas arqueanas da área de Nova Canadá – Província Carajás. *Boletim IG-USP – Série Científica*, Belém, **16** (2): 37-66.

Macambira M.J.B., Lafon J.M. 1995. Geocronologia da Província Mineral de Carajás; síntese dos dados e novos desafios. *Boletim do Museu Paraense Emílio Goeldi*, Belém, **7**: 263-288.

Macambira M.J.B., Lancelot J. 1991. Em busca do embasamento arqueano da região de Rio Maria, sudeste do Estado do Pará. In: RBG, Simpósio de Geologia da Amazônia, 3, *Resumos Expandidos*, Belém, 49-58.

Macambira M.J.B., Lancelot J. 1996. Time constraints for the formation of the Archean Rio Maria crust, southeastern Amazonian Craton, Brazil. *International Geology Review*, **38** (12):1134-1142.

Mackenzie W.S., Donaldson C.H., Guilford C. 1982. *Atlas de igneous rocks and their textures*. Harlow Essex, England, Longman Group Ltda, 148p.

Marangoanha B., Oliveira D.C. 2014. Diabásios e anfibolitos da área de Nova Canadá: natureza e implicações tectônicas para a Província Carajás. *Boletim do Museu Paraense Emílio Goeldi, Ciências Naturais*, Belém, **9** (3): 565-596.

- Martin H. 1994. The Archean grey gneisses and the gneisses of continental crust. In: Condie K.C. (ed.), *Developments in precambrian geology*. Archean crustal evolution. Amsterdam, Elsevier, **11**: 205-259.
- Medeiros H., Dall'Agnol R. 1988. Petrologia da porção leste do Batólito Granodiorítico Rio Maria, Sudeste do Pará. In: 35º Congresso Brasileiro de Geologia, *Anais de Congresso Brasileiro de Geologia*, **3**: 1488-1499.
- Moyen J.F., Martin H., Jayananda M., Auvray B. 2003a. Late Archaean granites: a typology based on the Dharwar Craton (India). *Precambrian Research*, **127**: 103-123.
- Moyen J.F., Nédélec A., Martin H., Jayananda M. 2003b. Syntectonic granite emplacement at different structural levels: the Closepet granite, South India. *Journal of Structural Geology*, **25**: 611-631.
- Neves S.P. 2012. *Granitos orogênicos: da geração dos magmas à intrusão e deformação*. Synergia, Rio de Janeiro, 147 p.
- Nockolds S.R., Aleen R. 1953. The geochemistry of some igneous rock series, Part I. *Geochemical Cosmochemical Acta*, **4**:105-142.
- O'Connor J.T. 1965. A classification for quartz-rich igneous rocks based on feldspar ratios. *US Geological Survey Professional Papers B*, **525**:79-84.
- Oliveira D.C. Gabriel E.O., Santos P.J.L., Silva C.R.P., Rodrigues D.S., Santos R.D., Galarza M.A., Marangoanha B., Santos M.S., Souza D.B. 2014. Geologia da região de Água Azul do Norte (PA) - Implicações para a compartimentação tectônica do Domínio Carajás. In: 47º Congresso Brasileiro de Geologia, Salvador. *Anais...* 1 CD-ROM.
- Oliveira D.C., Dall'Agnol R., Silva J.B.C., Almeida J.A.C. 2008. Gravimetric, radiometric, and magnetic susceptibility study of the Paleoproterozoic Redenção and Bannach plutons: implications for architecture and zoning of A-type granites. *Journal of South American Earth Sciences*, **25** (1): 100-115.
- Oliveira M.A., Dall'Agnol R., Almeida J.A.C. 2011. Petrology of the mesoarchean Rio Maria suite: implications for the genesis of sanukitoid rocks. *J. Petrology*, **51**(10): 2121-2148.
- Oliveira M.A., Dall'Agnol R., Althoff F.J., Leite A.A.S. 2009. Mesoarchean sanukitoid rocks of the Rio Maria Granite-Greenstone Terrane, Amazonian craton, Brazil. *Journal of South American Earth Sciences*, **27** (2):146-160.
- Oliveira M.A., Dall'Agnol R., Scaillet B. 2010. Petrological constraints on crystallization conditions of Mesoarchean sanukitoid rocks, southeastern Amazonian Craton, Brazil. *Journal of Petrology*, **51**:2121-2148.
- Passchier C.W., Trouw R.A.J. 2005. *Microtectonics*, 2nd ed., Germany, Springer-Verlag, 366 p.
- Paterson S.R., Vernon R.H., Tobisch O.T. 1989. A review of criteria for the identification of magmatic and tectonic foliations in granitoids. *Journal of Structural Geology*, **11**: 349-364.

- Peccerillo A., Taylor S.R. 1976. Geochemistry of Eocene calcalkaline volcanic rocks from the Kastamoru area, Northern Turkey. *Contributions to Mineralogy and Petrology*, **58**: 63-81.
- Pimentel M.M., Machado N. 1994. Geocronologia U-Pb dos Terrenos Granito-Greenstone de Rio Maria, Pará. In: 38º Congresso Brasileiro de Geologia, *Resumos Expandidos*, Camboriú, p.390-391.
- Pinheiro R.V.L., Holdsworth R.E. 1997. Reactivation of Archaean strike-slip fault systems, Amazon region, Brazil. *Journal of the Geological Society*, **154**: 99-103.
- Ragland P.C. 1989. *Basic analytical petrology*. New York, Oxford University Press.
- Rivalenti G., Mazzuchelli M., Girardi V.A.V., Cavazzini G., Finatti C., Barbieri M.A., Teixeira W. 1998. Petrogenesis of the Paleoproterozoic basaltic-andesite-rhyolite dyke association in the Carajás region, Amazonian craton. *Lithos*, **43**: 235-265.
- Rodrigues D.S., Oliveira D.C., Macambira M.J.B. 2014. Geologia, geoquímica e geocronologia do Granito Mesoarqueano Boa Sorte, município de Água Azul do Norte, Pará – Província Carajás. *Boletim do Museu Paraense Emílio Goeldi*, Ciências Naturais, Belém, **9** (3): 597-633.
- Rolando A.P., Macambira M.J.B. 2003. Archean crust formation in Inajá range area, SSE of Amazonian Craton, Brazil, based on zircon ages and Nd isotopes. In: South American Symposium on Isotope Geology, 4, *Expanded Abstracts*, Salvador, 1 CD-ROM.
- Rollinson H. 1993. *Using geochemical data: evaluation, presentation, interpretation*, Zimbabwe, [s.n], 344p.
- Ronaib C.P.S., Oliveira D.C. 2013. Geologia, petrografia e geoquímica das associações TTG e leucogranodioritos do extremo norte do Domínio Rio Maria, Província Carajás. *Boletim do Museu Paraense Emílio Goeldi*, Ciências Naturais, **8** (3): 383-415.
- Santos J.O.S. 2003. Geotectônica do Escudo das Guianas e Brasil-Central. In: Bizzi, L. A. et al. (ed.). *Geologia, tectônica e recursos minerais do Brasil*: texto, mapas e SIG. Brasília. CPRM- Serviço Geológico do Brasil, 169-226p.
- Santos M.J.P., Lamarão C.N., Lima P.H.A., Galarza M.A., Mesquita J.C.L. 2013a. Granitoides arqueanos da região de Água Azul do Norte, Província Carajás, sudeste do estado do Pará: petrografia, geoquímica e geocronologia. *Boletim do Museu Paraense Emílio Goeldi*. Ciências Naturais, **8** (3): 325-354.
- Santos M.N.S., Oliveira D.C. 2016. Rio Maria granodiorite and associated rocks of Ourilândia do Norte - Carajás province: Petrography, geochemistry and implications for sanukitoid petrogenesis. *Journal of South American Earth Sciences*, **72**: 279-301
- Santos M.S. 2017. *Granitoides TTG de Água Azul do Norte*. MS Dissertation, Programa de Pós-Graduação em Geologia e Geoquímica, Instituto de Geociências, Universidade Federal do Pará, Belém, 64p.

- Santos P.A., Teixeira M.F.B., Dall'Agnol R., Guimarães A.V. 2013b. Geologia, petrografia e geoquímica da associação Tonalito-Trondjemito-Granodiorito (TTG) do extremo leste do Subdomínio de Transição, Província Carajás, Pará. *Boletim do Museu Paraense Emílio Goeldi, Ciências Naturais*, Belém, **8** (3): 257-290.
- Santos R.D., Galarza M.A., Oliveira D.C. 2013c. Geologia, geoquímica e geocronologia do Diopsídio-Norito Pium, Província Carajás. *Boletim do Museu Paraense Emílio Goeldi, Ciências Naturais*, Belém, **8** (3): 355-382.
- Shand S.J. 1943. *The eruptive rocks*, 2nd edn. New York, John Wiley, 444p.
- Silva A.C., Dall'Agnol R., Guimarães F.V., Oliveira D.C. 2014. Geologia, petrografia e geoquímica de Associações Tonalíticas e Trondjemíticas Arqueanas de Vila Jussara, Província Mineral de Carajás, Pará. *Boletim do Museu Paraense Emílio Goeldi, Ciências Naturais*, Belém, **9** (1): 13-46.
- Silva F.F., Oliveira D.C., Antonio P.J., D'Agrella Filho M.S., Lamarão C.N. 2016. Bimodal magmatism of the Tucumã area, Carajás province: U-Pb geochronology, classification and processes. *Journal of South American Earth Sciences*, **72**: 95-114.
- Silva G.G., Lima M.I.C., Andrade A.R.F., Issler R.S., Guimarães G. 1974. Folha SB-22 Araguaia e parte da SC-22 Tocantins. Geologia. In: BRASIL-MME. Projeto RADAM BRASIL. *Folhas SC-22 Tocantins. Geologia, geomorfologia, pedologia, vegetação e uso potencial da terra*. DNPM, Rio de Janeiro, **4**: 1-143.
- Silva Jr., R.O., Dall'Agnol R., Oliveira E.P. 1999. Geologia, petrografia e geoquímica dos diques proterozoicos da região de Rio Maria, sudeste do Pará. *Geochim. Bras.* **13**(2): 163-181.
- Souza S.Z., Dall'Agnol R., Althoff F.J., Leite A.A.S., Barros C.E.M. 1996. Carajás mineral province: geological, geochronological and tectonic constraints on the Archean evolution of the Rio Maria granite-greenstone Terrain and the Carajás block. Extended abstracts. In: Symposium on Archean Terranes of South America Platform, Brasília, *Extended abstracts*, 31-32p.
- Souza Z.S., Potrel A., Lafon J.M., Althoff F.J., Pimentel M.M., Dall'Agnol R., Oliveira C.G. 2001. Nd, Pb and Sr isotopes in the Identidade Belt, an Archean greenstone belt of Rio Maria region (Carajás Province, Brazil): implications for the geodynamic evolution of the Amazonian craton. *Precambrian Research*, **109**: 293-315.
- Streckeisen A. 1976. To each plutonic rock its proper name. *Earth-Science Reviews*, **12**:1-13.
- Sylvester P.J. 1994. Archean granite plutons. In: Condie, K. C. (ed.). *Archean crustal evolution. Developments in precambrian geology*, Amsterdam, Elsevier, 261-314p.
- Tassinari C.C.G., Macambira M.J.B. 2004. Evolução tectônica do Cráton Amazônico. In: Mantesso Neto, V., Bartorelli, A., Carneiro, C.D.R., Brito Neves, B.B. de (org). *Geologia do continente Sul Americano. Evolução da obra de F.F.M. de Almeida*. São Paulo BECA, 471-486p.
- Tavares F.M. 2015. *Evolução geotectônica do nordeste da Província Carajás*. TS Doutorado, Universidade Federal do Rio de Janeiro, Rio de Janeiro, 115p.

- Taylor S.R., McLennan S.M. 1985. *The continental crust: its composition and evolution.* Oxford, Backwell Scientific, 321p.
- Teixeira M.F.B., Dall'Agnol R., Silva A.C., Santos P.A. 2013. Geologia, petrografia e geoquímica do Leucogranodiorito Pantanal e dos leucogranitos arqueanos da área a norte de Sapucaia, Província Carajás, Pará: implicações petrogenéticas. *Boletim do Museu Paraense Emílio Goeldi, Ciências Naturais*, Belém, **8** (3): 291-323.
- Throw A.J.R., Passchier C.W., Wiersma D.J. 2010. *Atlas of mylonites and related microstructures.* [S.I.], Springer, 322p.
- Vasquez L.V., Rosa-Costa L.R., Silva C.G., Ricc, P.F., Barbosa J.O., Klein E.L., Lopes E.S., Macambira E.B., Chaves C.L., Carvalho J.M., Oliveira J.G., Anjos G.C., Silva H.R. 2008. *Geologia e recursos minerais do estado do Pará: Sistema de Informações Geográficas.* texto explicativo dos mapas Geológico e Tectônico e de Recursos Minerais do Estado do Pará. CPRM, Belém, 329p.
- Vernon R.H. 2004. *A practical guide to rock microstructures.* Cambridge, Cambridge University Press, 594p.
- Weinberg R.F. 1999. Mesoscopic pervasive felsic magma migration: alternatives to diking. *Lithos*, **46**: 393-410.